Robust Rotordynamics

Andrew Iain James Rix

December 2016

Thesis submitted to the University of Nottingham

for the degree of Doctor of Philosophy

Supervisor: Prof. Seamus Garvey

Thesis Summary

Vibration generated from main rotor unbalance has a major impact on the aerospace gas turbine industry. It impacts the engine structural design and weight in a range of ways. For example, the engine must be able to manage and withstand the loads from a major event such as the release of a fan blade, and at the other end of the scale the engine design must minimise the orbit of a rotor due to “normal operation” unbalance that will influence blade tip and seal clearances which will significantly affect fuel efficiency. The variability in vibration responses from engines is also a significant problem. A design and production solution that does not cater for unbalance in a robust and repeatable manner causes significant costs to the business in the form of rejects from pre-delivery engine vibration tests (and therefore engine rebuilds), and reliability costs in service.

A combination of logistical and technological drivers differentiate aerospace gas turbines and their derivatives from other types of gas turbines with respect to the approach for managing vibration, leading to a bespoke approach for the design, build, and balancing. The key drivers are: limited accessibility to rotors within the engine, the requirement for exchangeable modules (sub-assemblies) of major parts of the rotor without rebalancing, the use of only low-speed balancing on pseudo-rigid rotors with bladed assemblies, very low vibration limits leading to very tight balancing limits, extreme weight limits for design solutions, and the need for highly accurate, repeatable, and stable rotor joints.

The overall aim of this study is to create a system that ensures the most cost-effective and robust engine design solution with respect to managing vibration. In order for such a system to deliver value into the engine design, the process and tools must be extremely fast and

flexible because the timescales of a proposed new engine programme are such that many design decisions are made in the very early stages of the design process that significantly constrain the engines architectural parameters. Based on these parameters there is a snowballing effect of parallel analysis and design streams that make further design decisions relating to the myriad of requirements that the engine must satisfy. Therefore the fundamental design of the engine becomes rapidly more difficult to change, even in the early design stages. The consequence of this situation is that if the structural design of an engine is to be influenced for the purpose of improved control of vibration, this information is required very early in the design process.

This study proposes a novel and rapid robust design system herein named “Robust Rotordynamics” that has been created to deal with the unique challenges that are faced in the aerospace gas turbine industry. However it has many elements that can be read across to other rotating machinery business sectors. The system comprises an overarching process and a set of novel tools and methods that have been created to support the process. These tools comprise an Unbalance Response Function (URF) design method that effectively delivers a preliminary design assessment and a very fast Monte-Carlo simulation and comparison method with supporting software for comparing and improving build and balance design solutions. Also developed is a novel set of criteria for determining when a design is acceptable to move forward from the preliminary stages with minimum risk of expensive vibration management steps, or fundamental redesign needing to be taken late in the design process. The aim of the overall process is to generate a system that identifies and controls critical parameters, and alleviates time wasted controlling non-critical parameters. The target outcome is therefore the most cost effective, predictable and repeatable solution with respect to rotor generated vibration (i.e. robust).

Also introduced in this study are practical methods of improving the outcome of build and balance. Rotor build alignment methods are discussed in some detail and explored with simulations that produced some new and significant findings regarding the key parameters for selecting the most effective build methods. Two novel methods of informing and improving the outcome of the low-speed balancing process using extra information available about the rotor are introduced. These methods comprise the use of the covariance matrix to use manufacture and build data to inform the balance process, and the use of a dual mass balancing simulator to improve the effectiveness of the use of mass simulators in rotors that have a significant degree of flexibility.

During these studies there have been some innovations/discoveries that do not align closely with the core theme, but are of some relevance so have been included in the thesis. One such finding is the identification of a mechanism for the coupling of the first and second harmonic rotor order amplitudes due to the bearing misalignment angle caused by rotor bending. Another is the invention of a novel fan blade off fusing mechanism that can be used to increase and tune the gyroscopic moments present following a fan blade-off and mechanical fusing event. This fuse has a much more open design space than traditional mechanical fuses, thereby enabling post-fused dynamic tuning to reduce the loads from unbalance that the engine and supporting structures have to tolerate, potentially leading to a significant weight saving.

Acknowledgements

Firstly I would like to thank my supervisor Professor Seamus Garvey for his endless patience, wisdom (both technical and general), and humour.

Secondly I would like to thank my wife Clare for her support during this foolhardy endeavour.

I would also like to thank all at Rolls-Royce who had an influence in this work both in supporting and encouraging me to complete these studies.

Table of Contents

List of Figures

Nomenclature

i) Acronyms and terms

Field Balancing	See Trim Balancing
GT	Gas Turbine
HP	High Pressure Rotor
IP	Intermediate Pressure Rotor
LP	Low Pressure Rotor
ODS	Operational Deflection Shape
PoT	Pass-off Test (Pre-delivery engine test performed on a stationary test stand, vibration is one of the parameters measured and checked)
RR	Rolls-Royce
SFD	Squeeze Film Damper
SSFR	Steady-state Forced Response
Trim Balancing	Balancing of the rotor in its operational stator.
URF	Unbalance Response Function
WEMM	Whole Engine Mechanical (Finite Element) Model

ii) Definitions

Couple Unbalance	Equal magnitude unbalance vectors in two axially displaced locations on the rotor opposing by 180° (see ISO1925, 2001 (3.8) for a complete defintion)
Curvic Coupling	A toothed rotor joint type which has a tooth profile form similar to a bevel gear.
Diametral or Transverse Moment of Inertia	Moment of inertia about an axis 90° to the rotor centreline.
Dynamic Unbalance	Any combination of Static and Couple unbalances detected in two axial planes of

	the rotor (see ISO1925, 2001 (3.9) for a complete defintion)
n^{th} Engine Order	Same as rotor order (n^{th} multiple of the rotor rotational frequency).
Intermodular Joint	A joint that provides connection between mating modules.
Intramodular Joint	A joint that is inside a module, therefore is not disturbed during module replacement
Long Mandrel	A piece of balancing tooling that connects from a joint face of the engine component being balanced to a bearing support that is same relative axial location as the operational rotor support bearing.
Low-speed-balancing	Rotor balancing operations that are performed at speeds well below the flexible modes of the rotor so that the rotor can be said to be performing in a rigid-body state.
Module	A rotor sub-assembly that is intended to be interchangeable without the need to rebalance the rotor.
n^{th} Rotor Order	n^{th} multiple of the rotor rotational frequency.
Short Mandrel	A piece of balancing tooling that connects from a joint face of the engine component being balanced to a bearing support that is a short as possible providing bearing support location close to the component joint.
Spigot	Associated with flange bolted joints, it a protrusion of a ring of material on one side of the joint at the inner or outer diameter that provides radial location across the joint.
Static Unbalance	Total unbalance measured in a single plane. (see ISO1925, 2001 (3.6) for a complete defintion)

Swash	A small angular error on a rotor dimension that is intended to be perpendicular to the rotor axis e.g. a swash error of a joint face.
Trim Balancing	Balancing of the rotor in the engine at its operating speed.
Unbalance Response Function (URF)	A set of responses to a fixed unbalance quantity at a number of rotor locations, measured at a single sensor.

iii) Mathematical Notation

- Scalar variables are italic e.g. '*n*'
- Vector quantities are in bold lower case, and a subscript in brackets refers to an element of a vector, e.g. '$\mathbf{x}_{(n)}$'
- Matrix quantities are in bold upper case, and subscripts in brackets refer to an element of the matrix by row then column, e.g. '$\mathbf{C}_{(n,m)}$'
- Complex quantities are indicated by a tilde, e.g. $\tilde{u}$

Symbol	Description
AF	Amplification Factor (American Petroleum Institute, 1998)
a	real valued amplitude of dynamic response.
a_{error}	real valued amplitude of dynamic response due to residual unbalance.
α_{ω}	sensitivity of the engine to arising unbalance and inter-modular joint repeatability at rotor speed ω.
BM	bending moment
$b, \tilde{b}$	real or complex valued slope of a linear function.
$c, \tilde{c}$	real or complex intercept of a linear function.
$e_n, \tilde{e}_n$	eccentricity, the radial distance between the center of gravity and the center of rotation of the rotating mass. If subscripted, n refers to the component or sub assembly reference number. If complex, the eccentric error is a vector in a radial plane of the rotor.
e_2	the size of the second Fourier component of the profile of a shaft surface measured as an eccentricity.
e_{dyn}	dynamic eccentricity.

e_{per}	permissible final unbalance eccentricity (as defined by (ISO1940-1, 2003).
E	Young’s modulus
F	force.
f_n, $\tilde{f}_n$	front (left side) unbalance correction of the rotor. If real valued then it is unbalance magnitude, if complex it is defining unbalance as a single plane vector quantity. When used as a subscript, the element of the set corresponding to the front balance plane location. When subscripted with a c or t it is referring to a compressor or turbine front correction plane respectively.
G	balance grade (as defined by (ISO1940-1, 2003).
$\tilde{\mathbf{g}}_b$	is a complex vector, that represents the force response due to the unbalance induced rotor bending only measured at bearing b.
$\mathbf{h}$	is a vector, the same length as $\mathbf{x}$, which represents the initial (inherent) unbalance (before assembly balance) of each significant mass in the rotor. An example of a significant mass would be one bladed disc stage. Ideally this should be calculated using a stochastic simulation method.
h_{max}, h_{min}	the maximum and minimum dimensions of an ellipse.
I	second moment of area.
I_p	polar moment of inertia.
I_d	diametral or transverse moment of inertia (moment of inertia about an axis at 90° to the rotor centreline).
$\tilde{\mathbf{j}}_{s,n}$, $\tilde{\mathbf{j}}_{e,n}$	are complex column vectors of joint face swash and eccentricity values respectively. Each value represents a vector quantity on an axial plane. If used, n denotes that the vector is a subset only relating to component or sub assembly n.
$\tilde{\mathbf{k}}_c$	an unbalance response function, similar to $\tilde{\mathbf{k}}_u$, where the values are generated from unit point couple unbalances.

$\tilde{\mathbf{k}}_e$	an unbalance response function (similar to $\tilde{\mathbf{k}}_u$) but the responses are driven by unit joint eccentricity values that cause and unbalance distribution along the rotor.
$\tilde{\mathbf{k}}_{hs}$	an unbalance response function where the values are not a linear function of $\mathbf{x}$
$\tilde{\mathbf{k}}_L$	is a special case of $\tilde{\mathbf{k}}_u$ where the the values are a linear function of $\mathbf{x}$
$\tilde{\mathbf{k}}_s$	an unbalance response function (similar to $\tilde{\mathbf{k}}_u$) but the responses are driven by unit joint swash values that cause and unbalance distribution along the rotor.
$\tilde{\mathbf{k}}_{u,b}$	is the same as $\tilde{\mathbf{k}}_u$ but measured at bearing b.
$\tilde{\mathbf{k}}_u$	is a column vector, with q elements, of complex dynamic responses to static unit unbalances applied at the major masses (an unbalance response function).
L	length of rotor between bearings.
M	is the total mass of the rotor ($M = \lvert\mathbf{m}\rvert$).
$\mathbf{m}$	is a vector of real numbers, with q elements, which contains the mass of each major component of the rotor.
m_n	is the mass of the component or sub assembly denoted n.
Q	Q factor - a measure of damping.
q	is a single valued real variable indicating the number of elements in the vector $\mathbf{x}$
$r_n, \tilde{r}_n$	rear (right side) unbalance correction plane of the rotor. If real valued then it is unbalance magnitude, if complex it is defining unbalance as a single plane vector quantity. When used as a subscript, it means the element of the set corresponding to the rear balance plane location.
$\tilde{\mathbf{R}}_c$	is a concatenation of $\tilde{\mathbf{k}}_c$ vectors for multiple rotor speed increments, therefore each column represents a $\tilde{\mathbf{k}}_c$ vector at

	each speed increment and each row represents the axial station along the rotor with the axial location of these stations defined in the vector $\mathbf{x}$.
$\tilde{\mathbf{R}}_u$	is a concatenation of $\tilde{\mathbf{k}}_u$ vectors for multiple rotor speed increments, therefore each column represents a $\tilde{\mathbf{k}}_u$ vector at each speed increment and each row represents the axial station along the rotor with the axial location of these stations defined in the vector $\mathbf{x}$.
SM	Separation Margin (American Petroleum Institute, 1998), how far a resonance occurs from the operational speed range.
$\tilde{\mathbf{s}}_b$	is a complex vector, the same length as $\mathbf{x}_b$,that represents radial forced response measured at bearing b, to unit unbalances applied at each bearing in turn (from 1 to q)
T_g	unbalance magnitude at the turbine module centre of gravity.
t	time (s).
$\mathbf{u}, \tilde{\mathbf{u}}$	is a real or complex column vector comprising static unbalance distribution along a rotor with q elements, with the elements corresponding to the axial stations defined in $\mathbf{x}$.
$\tilde{\mathbf{u}}_b$	a complex column vector, similar to $\tilde{\mathbf{u}}$, which includes applied unbalance corrections at the balancing correction planes.
$u_c, \tilde{u}_c$	couple unbalance, if complex indicates a vector quantity.
$\tilde{\mathbf{u}}_{corr,n}$	a complex column vector containing unbalance corrections. It has elements to represent the whole rotor (or a module of the rotor if n is used), but only the balance correction stations have non zero values.
$\tilde{u}_{c,m(i)}$	a complex couple unbalance vector that arises due to errors within the module number "i".
$\tilde{\mathbf{u}}_{c,b,\omega}$	a complex vector, which is a calculated response assuming the unbalance forces were transferred to the bearings via a rigid rotor.

$\tilde{\mathbf{u}}_{c,m}$	a column vector of the values of $\tilde{u}_{c,m(i)}$ comprising couple unbalances of all modules in the rotor.
U_{per}	real valued permissible residual unbalance.
$\tilde{u}_s$	a complex static unbalance vector.
$\tilde{u}_{s,m(i)}$	a complex static unbalance vector that arises due to errors within the module number "i".
$\tilde{\mathbf{u}}_{s,m}$	a column vector of the values of $\tilde{u}_{s,m(i)}$ comprising static unbalances of all modules in the rotor
$\tilde{\mathbf{u}}_{s,m,\theta}$, $\tilde{\mathbf{u}}_{s,t,\theta}$	complex valued column vectors comprising the values of $\tilde{u}_{s,m,\theta(i)}, \tilde{u}_{s,t,\theta(i)}$ respectively for all values of "i". If subscripted with an "m" it represents all unbalances in the module being balanced. If subscripted with a "t" it represents all unbalances in the balancing simulator tooling.
$\tilde{u}_{s,m,\theta(i)}, \tilde{u}_{s,t,\theta(i)}$	complex valued point couple unbalance at axial location "i", being caused by a swash joint error θ. If subscripted with an "m" it is in the module being balanced. If it is in the balance tooling it is subscripted with a "t".
v	the total number of bearings on the rotor.
$\mathbf{x}$	a column vector of real numbers containing the axial location of each unit unbalance at the significant masses.
$\mathbf{x}_b$	a vector of real numbers containing the axial location of the bearings for the rotor.
x_n	values of axial location along the rotor measured from the front (left hand) bearing location. Subscripts are described locally.
$\mathbf{z}$	a temporary column vector of real valued ones.
α	is the sensitivity of the engine to arising unbalance and inter-modular joint repeatability at rotor speed ω.
β	is the sensitivity of the engine to inherent unbalance at rotor speed ω. Inherent unbalance is described in section 7.4.
ε_r	strain in the rotor.

ε_S	strain in the stator.
ζ	damping ratio.
θ_n	swash angle of a joint face relative to the component centerline. The subscript refers to the component.
μ	roller bearing contact angle.
ϕ_n	Inclination of component inertial axis of component n to geometric centreline.
ψ	angle by which a component or sub assembly will be rotated as part of an aligned build process.
ω	rotor speed (radians/second).

1 Introduction

1.1 Chapter Aim

The chapter will introduce the background and motivation for this study looking into the relationship between Rotor Balancing and Rotor-Dynamics primarily from the perspective of the Aerospace industry. It will also introduce the objectives and layout of the thesis.

1.2 Industry Motivation

Engine vibration is becoming increasingly significant in terms of aerospace engine manufacturer profits and engine sales. In the Civil Aerospace market vibration is a key parameter for airlines when choosing engines. This is due to a requirement of reduced cabin noise to increase passenger comfort. In the Military Aerospace market the focus is on low vibration to prevent pass-off test failures and in-flight vibration warnings that will affect mission readiness. In the Energy business, where contracts are generally based on “power by the hour” and vibration deterioration in service is very significant, it has been shown that the lower the vibration that can be achieved on pass-off, the longer the life will be in service before vibration limits are reached. In the Aerospace industry, the cost of failing a pass-off test is likely to be a significant profit impact to the manufacturer. The technical challenge and associated risk of significant cost penalties is further exacerbated by the requirement, particularly in the small engine civil markets, that each new engine design will operate with lower vibration than the previous engine design.

This study focusses on the rotordynamic issues associated with Aerospace gas turbine design, but as the derivatives of these engines are used in the Energy / Oil and Gas / Marine sector also, some read across is appropriate.

1.3 Rotor Balancing Drivers/Challenges Specific to the Aerospace Gas Turbine Industry

It is a combination of requirements and drivers that makes the rotordynamics and balancing of aerospace gas turbines and their derivatives particularly challenging. These are described in detail below.

1.3.1 Accessibility of Rotors

The design constraints of aerospace gas turbines dictate that the engine must be assembled from access to the ends of the engine (for strength and weight reasons, casings are joined axially). Therefore it must be possible to disassemble the rotor after balancing. The only rotor that can be readily accessed for balancing without significant disassembly is the LP rotor, where it is sometimes possible to apply balance weights to the front and/or rear of the rotor for the purposes of trim balancing (i.e. balancing in the final stator). This is very different to many land based gas turbines where the casings can often be separated longitudinally allowing access to the rotor without having to break any rotor joints. The consequences of the aerospace gas turbine arrangement is that the unbalance distribution along the rotor is slightly different each time the rotor is accessed due to the rotor joint build repeatability. The relative rotor bearing alignments through the casing also vary which can change the engine response. Therefore, performing back to back tests where access to the rotor is required is very expensive due to the time taken to strip and rebuild the engine plus the vibration measurement results tend to contain significant scatter, therefore making definitive conclusions from a limited number of tests is very difficult.

1.3.2 Customer Modularity Requirements

It is required that any Major Repairable Assembly (MRA) is replaceable without selectivity of the MRAs available (i.e. random selection) or trim balancing of the engine. The MRAs are sometimes referred to as modules. *Figure 1* below shows the normal breakdown of modules for a typical large civil engine.

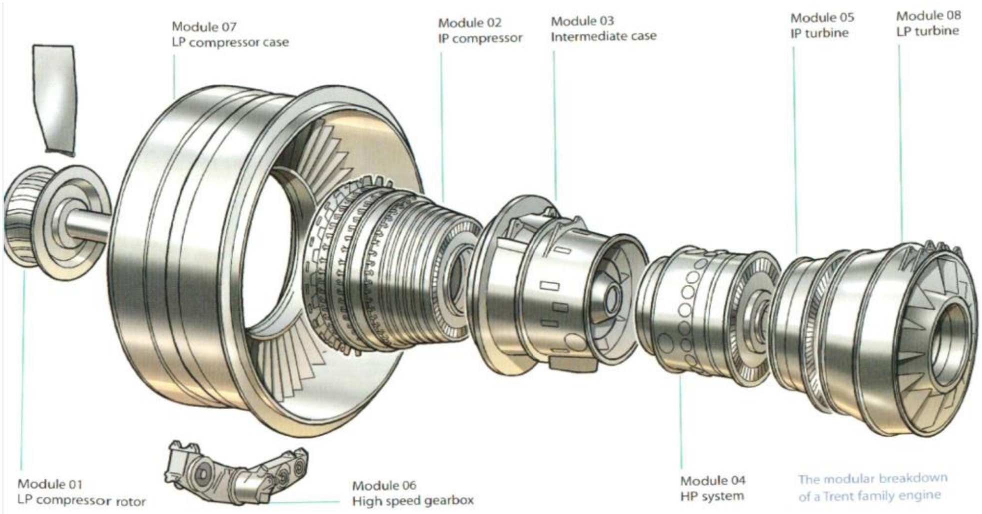

Figure 1: The Modular Breakdown of a Rolls-Royce Trent Family Large Civil Engine (source: The Jet Engine – ©Rolls-Royce plc.)

This requirement is very challenging with respect to managing unbalance and vibration. This is because the repeatability of rotor joints becomes a critical design driver, and the whole dynamic system must not be sensitive to the unbalance distribution in large sections of the rotor being changed.

1.3.3 Low-speed Balancing

Aerospace gas turbine modules are serviced and built all over the world at a variety of facilities. For example, military engines are sometimes overhauled by the military customer themselves. Civil engines are sometimes overhauled at airline operated facilities. This means that a large number of balancing machines of various sizes are employed around the world to balance gas turbine MRA’s for aero engine manufacturers. If a bladed part of a rotor were to be balanced at its operating speed outside of the engine, this would cause a number of problems. Due to the air pressure on the blades, the power needed to rotate it would be significant, a significant amount of noise would be generated, and the forces that would need to be reacted to constrain the “thrust” from the rotor would be large which can negatively influence balancing results. Furthermore, the health and safety requirements for the containment of high energy debris in a workshop would be a significant undertaking. It is possible to get around some of these issues by using a vacuum chamber around the balancing machine, but it is a very costly and time consuming process, especially when the global number of machines is taken into account. The other major reason not to balance at high operating speeds is the modularity requirement; the benefits of high speed (i.e. flexible rotor) balancing would be reduced and likely negated due to the change in unbalance distribution caused by changing the adjoining MRA.

1.3.4 Balance Tolerance Requirements

Because of the nature of aerospace gas turbine rotors, a very fine balancing tolerance is required. The current balancing standard for rigid rotors (ISO1940-1, 2003, pp. 9-12) describes the determination of balancing tolerances. For convenience, the process of determining balancing tolerances is described briefly here. Initially the balancing grade (G grade) desired is determined based on the type of machinery being balanced. For example, aerospace gas turbine rotors are generally categorised at G of 6.3, whereas cars (including wheels, crankshafts, etc.) are balanced at a G of 40. The G values are are intended to represent the vibration magnitude (in mm/s) that will arise if the rotor is balanced to this grade; therefore a typical vibration level for an aerospace gas turbine will be 6.3mm/s and for a car it will be 40mm/s. The balance tolerance (permissible unbalance (U_{per}) is then determined using the following formula from (ISO1940-1, 2003, p. 10):

$$U_{per} = 1000 \cdot \frac{G.M}{\omega} \tag{1.1}$$

where

U_{per} is the numerical value of the permissible residual unbalance (g.mm).

G is the balance grade (mm/s)

M is the rotor mass (kg)

ω is the rotor speed (radians/s).

Note that the ISO uses the most practical units rather than SI.

Once U_{per} is determined, the permissible distance between the centre of rotation and the centre of gravity, denoted e_{per}, can be determined by

$$e_{per} = \frac{U_{per}}{m} = \frac{1000.G}{\omega} \tag{1.2}$$

which produces a distance in μm.

Although the stated balancing grade of 6.3 is the target for an aerospace gas turbine rotor, because the rotor contains many joints between components and a number of MRA's, in order to achieve this level each component and MRA is actually balanced to a G of around 2.5. Generally this means that aerospace gas turbine rotors are balanced to an extremely fine limit, with a centre of gravity eccentricity of less than 2μm.

1.3.5 Vibration Level Inconsistencies/Scatter

There are two categories of vibration inconsistencies to consider, one is engine “run to run” variability on the same engine, the other is “engine to engine” variability. They are briefly outlined as a) and b) below.

a) Due to the complex nature of the gas turbine engine, some engines display variations in vibration from one run to the next, even when the operating conditions have been made as similar as possible. This makes the task of optimising to a moving target very difficult, especially in operations such as trim balancing. These inconsistancies are believed to be principally from the squeeze film dampers, which are being investigated in a separate study.

b) Engine to engine variability is the key focus of this study, because this is the more significant contributor to pre-delivery test vibration issues. To manage this issue, all variations possible in arising unbalance need to be effectivley and consistantly controlled. Measuring the size of this variability is confounded by the variability from (a). However, this is demonstrable because vibration pass-off test rejects can usually be sufficiently improved by stripping, rebalancing and rebuilding. Therefore producing a robust method of building and balancing rotors is clearly the main requirement.

1.3.6 Weight Requirements

The stringent weight requirements that necessarily drive every part of aerospace gas turbine design have a significant influence on rotordynamics. Rotors are frequently required to operate near to, or even to pass through, resonant conditions. This is because the change of stiffness or addtion of mass to move a resonance away from the speed range would make an engine unfeasible or uncompetitive. Therefore, the drive to minimise vibration forcing levels from the rotor through tuning the manufacturing tolerances, balancing methods, build practices and smart underlying design is very strong.

1.4 The Technical Motivation for This Study

Over the last twenty years, the drivers for certain balancing methods and those methods within the aerospace sector have remained remarkably unchanged. However, a few factors have changed significantly, that have not been fully addressed or utilised.

1. Aerospace gas turbine rotors have become lighter and faster, bringing more flexible modes into the running speed range so that the compromises that are made in low-speed modular balancing (3.6.1) have become more evident.
2. The advent of accessible dynamic FE models of gas turbine engines (known as Whole Engine Mechanical Models (WEMM) see section 1.1), with fast solvers, that have been adequately validated has made dynamic analysis significantly more accurate and practical.
3. Manufacturing and measurement advances have become such that much more can be known and controlled about rotor component manufacturing.

Due to very low vibration limits, a number of engines fail to consistently achieve low enough vibration at Pass-off Test (PoT), which shows that the current methods can be inadequate. A few exercises have been done to utilise the WEMM in informing the balancing process (sometimes performed too late in the design process to change the design, leading to expensive build and balance process fixes), but there is no clear and defined method available to decide when to depart from the traditional methods, or exactly how the WEMM can be used to inform the design of the gas turbine or the balancing and build methods.

Alongside the above motivation, there are a number of known issues with the current methods detailed in section 3.6 which are briefly outlined below.

a) Low-speed modular balancing using simulators (outlined in 3.6.1) generates large internal bending moments due to the fact that adjoining modules (and therefore the associated simulators) tend to be significantly axially displaced from the balancing correction planes that are necessarily mounted on the module being balanced. This concept is described in section 5.10 and pictured in Figure 28, where the bending moment induced by the simulator unbalance and the subsequent balancing is represented.

b) The bending moments generated from the low-speed balancing are not a problem if the rotor is rigid enough, when rotating at its operating speed in the real engine. However, when the reduction in dynamic stiffness in the rotor is significant enough that bending will occur, then vibration can result. This is a key point, because some very expensive and time consuming balancing processes can actually make the vibration higher than it would have been without any balancing at all.

c) The use of balancing mass simulators has historically been an assumed requirement if the adjoining component was of significant mass compared to the component being balanced. The use of balancing mass simulators incurs significant cost both in the design and purchase of the simulators, followed by the operating cost involved in regular calibration, and the time cost in the balancing process; during the process the simulator may have to be reconnected to the module being balanced up to three times. It can take several hours per reconnection due to the size and weight of the components to be maneuvered, the number of bolts on a rotor joint, the complex multi-step torque tightening procedures, and bolt access issues. It can be shown that, for the same reasons stated in a) and b) above, lower or similar vibration may be achievable by having no mass simulator at all, giving a significant cost and time saving benefit together with a potential reduction in vibration levels and the associated costs. This is discussed in more detail in chapter 5.

d) Current methods do not predict when the rotor is sufficiently rigid for low-speed balancing to be adequate to balance a gas turbine rotor. Most of the literature suggests that this must be determined by trial and error on rotor hardware. This is not an option on an aerospace gas turbine due to the accessibility of rotors (1.3.1) which leads to a very high cost of engine rebuild, and the late design stage in which this would be discovered (i.e. if hardware is available, the fundamental design is fixed unless significant cost and delays to the design program are incurred). Furthermore, high speed balancing cannot be considered as a fallback position for a bladed MRA for the reasons stated in section 1.3.3. Rotordynamic design acceptance criteria and the rigidity of rotors for balancing is considered in chapter 7.

e) The dynamics of any rotor in a multi rotor aerospace gas turbine cannot be considered in isolation. Aerospace gas turbines have very light supporting structures and rely on the inertias and forces in the other rotors for some stability. Therefore any rotor balancing solution that depends on modal response corrections must factor in the modal behavior in the engine which includes other engine rotors. This is a significant contrast to many other industries that use gas turbines, where only one rotor is present and/or the supporting structure is extremely heavy and stiff.

f) Although a lot of time and expense has gone into creating highly repeatable rotor joints for inter-modular joint locations (the need for which is briefly described in section 3.6.2) these joints remain a primary source of vibration pass-off test rejects. This is because they take a very significant amount of time and care to clean to the required level, they are not always assembled under ideal (clean room) conditions, requiring multiple torqueing steps and sequential tightening, often in very difficult to access areas (e.g. through the rotor bore), they are susceptible to damage when the very heavy components are being brought together or being moved around. It is also not normal practice to use anti-corrosion coatings on the mating surfaces because of the required repeatability. This could lead to corrosion of the surfaces and significant reworking required in maintenance. It can be shown that not all inter-modular joints contribute equal sensitivity to vibration; therefore before a highly expensive joint type is selected for the purpose of minimising vibration, an assessment of the sensitivity should be conducted. The cost impact on an engine production program is significant over its lifetime.

g) The process of building a rotor sometimes involves a scheme to align the measured dimensional component imperfections (within tolerance) to achieve a specific goal. This is to achieve a rotor that has the straightest possible alignment to the rotor running centerline for various reasons i.e. engine performance and/or vibration. Other schemes of rotor alignment have also been devised. These schemes incur significant build costs due to the need to measure every major rotor component in detail. A method to determine whether straight build methods are required to achieve acceptable vibration is needed, together with feedback into the early design of an engine, which may result in the process being avoided. The topic of aligned rotor build is discussed in section 3.5.

1.5 Thesis Objectives

An up to date set of design methods for rotordynamics and rotor balancing are required to move the industry towards a much more cost-effective and data informed solution.

It is the aim of this study to create these methods, and ensure that they are practical (fast and simple enough) for use in the early design stages of a real aerospace gas turbine, when the fundamental design can be influenced at minimum cost.

The objectives of these studies can be summarised in the following points:

i. Capture the current state-of-the-art methodologies and technology employed in modular low-speed balancing. Identify any gaps between the state-of-the-art and the requirements of the Aerospace industry.

ii. Develop and demonstrate a methodology whereby an engine design is developed with vibration performance requirements as one of the primary objectives whilst recognising manufacturing, balancing, and build limitations and requirements. This methodology should also allow the maximum design space for the fundamental engine design requirements (i.e. performance, weight and cost).

iii. An overarching requirement of objective (ii) is that the methodology must be able to deliver results that can influence design quickly. Early engine designs move quickly, design influencing results must be delivered within a few days of effort, ideally hours.

iv. It is not always possible to influence engine designs in their early stages, for example, in the case of existing products. Developing methods to improve the outcome of low speed modular methodologies is a key requirement for these products, as well as expanding the effective options available for new designs in the most cost effective manner.

1.6 Thesis Description and Layout

Chapters 2 and 3 of this thesis are the “Literature Review” and “Sources and Control of Rotor Ordered Vibration in Gas Turbines” respectively. These chapters are aimed at objective (i) describing the current state-of-the-art and the challenges that the Aerospace industry currently faces.

In response to objectives (ii) and (iii), Chapter 4 proposes a Rotordynamic Design *System* that comprises a Rotordynamic Design *Process* together with some demonstrated design assessment methods and supporting software. The principal design method proposed is the Unbalance Response Function (URF) methodology that is detailed in Chapter 5 and the supporting software is the "Robust Rotordynamics Monte-Carlo Software" described in chapter 6. Particularly in support of objective (iii), chapter 7 proposes new Rotordynamic Criteria for assessment of the likely robustness of a new rotor design that takes into account the manufacturing capabilities and limitations as well as in-service unbalance degradation. It aims to achieve this whilst improving the design space limitations imposed by the existing criteria in use today.

Chapter 0 introduces methods to improve the outcome of the low-speed balancing processes that are a requirement of the aerospace industry. In the first part of this chapter, the Unbalance Co-variance Matrix is introduced to determine the most likely unbalance distribution along a rotor based on the low-speed balancing data together with knowledge of the rotor manufacturing/build process. In the second part of this chapter, the "dual mass simulator" is proposed as a practical invention to implement the three plane modular balancing techniques proposed by (Schneider, 2000) without adding significant time to the balancing process.

The thesis concludes and proposes areas for further work in chapter 0.

Presented in the appendix is a novel fan blade-off fusing mechanism that was developed during these studies.

2 Literature Review

2.1 Literature Discussion

A wide range of literature is currently available in the field of rotor balancing, addressing various aspects of the subject. Low-speed rotor balancing is a very mature subject area, with very little being produced in the last ten years. An account of the historical development of balancing is given in the review by Foiles et al. (Foiles, Allaire, & Gunter, 1998), where more than 160 references on previous work are cited; some date back as early as the 1920s. An older review by Parkinson (Parkinson, 1991) provides more detailed explanations on various aspects of rotor balancing including more than 60 references on the subject prior to 1990. Influence Coefficient Balancing and Modal Balancing are two of the most popular methods of balancing for rotors that have significant flexibility.

Influence coefficient balancing assumes that the rotor response is a linear function of unbalance. The correction weights are calculated from an over-determined system of equations because the total number of vibration measurements almost always exceeds the number of available balance planes. The most common solution approach is the use of the least-squares method (Goodman, 1964). In its most common form, a number of test runs are performed to determine the response of trial weights in multiple correction planes at different speeds.

The modal balancing method is a stepwise mode-by-mode balancing method (Lund & Tonnesen, 1972). Orthogonal sets of weights are calculated and applied for balancing each modal component whilst not influencing the previous balance at lower modes. Literature on Modal Balancing includes methods of balancing flexible rotor systems without test runs (Gneilka, 1983), and simultaneous balancing of the first and second flexural modes whilst running the rotor at a speed between these speeds (Xu & Qu, 2001). In the latter, an obvious advantage is that the rotor need not be run at either of these critical speeds, thus eliminating the necessity to operate the rotor under these high vibration conditions.

A very comprehensive text on the low-speed balancing of rigid rotors is the International Standards Organisation papers (ISO1940-1, 2003) and (ISO1940-2, 1997). The most notable contribution is the definition of the international balance grade system, whereby a permissible residual unbalance is defined depending on vibration requirements, rotor mass and rotor speed. This system is globally adopted in the rotating machinery industries, including aerospace. Flexible rotors are dealt with in (ISO11342, 1998) which it is recommended is considered in parallel to the ISO1940 documents. Unfortunately the definition of whether a rotor should be considered as rigid or flexible is not really addressed. Aerospace industry rotors generally fall into a category that has been termed “pseudo-rigid” (first reference found in (Schneider, 2000)). This is because the typical mode shape of an aerospace gas turbine engine has a significant amount of strain energy in the static structure. This tends to morph a classical rotor bend mode which would be considered purely a “rotor mode” in a rigid stator where all the strain energy is in the rotor, into a composite mode shape of stator and rotor strain. Importantly for this study the low-speed balancing of flexible rotors is discussed, although a methodology is not defined. The main comments about the low-speed balancing are quoted here because they are very pertinent to this thesis:

“The process of balancing a flexible rotor in a low-speed balancing machine is an approximate one. The magnitude and distribution of initial unbalance are major factors determining the degree of success that can be expected. For rotors in which the axial distribution of initial unbalance is known and appropriate correction planes are available, the permissible initial unbalance is limited only by the amount of correction possible in the correction planes. For rotors in which the actual distribution of the initial unbalance is not known, there are no generally applicable low-speed balancing methods. However, sometimes the magnitude can be controlled by the pre-balancing of individual components. In these cases the low-speed initial unbalance can be used as a measure of the distribution of unbalance."

Annex B of (ISO11342, 1998) is titled "Optimum planes balancing — Low-speed three-plane balancing". It states that if certain conditions are met in the geometry of the rotor and knowledge of the modes and likely unbalance distributions relative to the unbalance measured at low-speed are known, then a third plane of balancing correction can be calculated from the low-speed balancing information. In (Ehrich, 1990) this is developed into a much more complex system, dealing with more complex mode shapes and any number of balance lands. In (Schneider, Exchangeability of rotor modules - a new balancing procedure for rotors in a flexible state, 2000) the extension of multiplane balancing at low-speeds for flexible rotors is extended to low-speed balancing with exchangeable modules. In this paper more than one configuration of the module (or sub-assembly) being balanced is utilized on the balancing machine to gain information about the geometric errors of the module. Along with the mode shape function, this information is then used to inform the three plane balance of the module to account for flexibility and perform the usual rigid body corrections. This is discussed further in section 8.3.

In the paper (Smith, 2000), it is concluded that balancing considerations should commence in the design office. This is a very valuable point and a key principle behind the methods proposed in this thesis. In the detail Smith is really talking about the practicalities of balancing i.e. where/how should the rotor be supported for rigid balancing, and what balancing machine tooling shall be used; how facilitating this using the design of the rotor/machine itself. In this thesis, these fundamentals are assumed as a given, as the practicalities of rigid balancing to ISO standards are typically taken into account in aerospace gas turbine design. However, in this thesis the principle is extended in that for rotors with any appreciable degree of flexibility, dynamic modelling of the effects balancing and build process should begin in the design office, and should be a fundamental part of the design criteria. This information will guide all of the rotor dynamic design considerations, from balancing land locations and rotor balancing tooling, down to manufacturing tolerances of joint faces, and repeatability performance of particular types of joints.

Robustness of balancing is discussed in (Garvey, Friswell, Williams, Lees, & Care, 2001), where the authors emphasise that the rotor should not only be balanced for multiple speeds, but also for a multiplicity of other parameters in general. This work addresses the uncertainty associated with such parameters, and suggests how this can be counted for in determining a robust balance correction; particularly considering the balancing of rotors in balancing machines that are not dynamically similar to the stators in which these rotors will ultimately be deployed. Another aspect presented in the paper is the determination of a near optimal set of balance planes required for a satisfactory balancing operation. The paper by (Ehrich, 1990) describes a method having some commonality with what is presented in this paper - namely to achieve the results approaching those attainable from a high speed balancing operation at the low speeds of a balancing machine. Information on a particular rotor's dynamic behaviour is combined with data on the particular rotor's generic patterns of unbalance to achieve this. However, neither the unbalance co-variance matrix (presented in section 8.2) nor any other statistical measure is implemented to estimate the most likely state of unbalance in the procedure.

A relatively new development being applied to the process of flexible rotor balancing is the use of the “Holospectrum” presented in (Liu, 2005). The Holospectrum is a measurement/analysis technique that is used here for trial unbalance weight runs. The Holospectrum is a 3D measurement of the motion of the entire rotor, therefore the method proposed utilises this information to optimise to a whole rotor minimum response. The primary goal of the method presented in this paper is that the first two modal components of unbalance can be balanced simultaneously at the speed below the first critical speed. The main aims of the method as presented are time/cost saving and safety. Artificial neural networks are being applied in rotor balancing [(Stephenson, Grogan, Rost, Alleman, & Brown, 1992), (Wang, Zhang, Zhang, & Ma, 1998)], further extending the range of activities falling under the general description of rotor balancing.

Another area of key interest for these studies is the subject of Rotor Dynamic Acceptance Criteria. These are a key part of the process of designing a gas turbine, as they give a confidence measure that a design concept can be made to operate under the normal conditions of an aero gas turbine. A great deal of time and money is spent between a design concept and having a first engine to test, so the risk of whether it will be able to operate satisfactorily carries high consequences. Changes that can bring rotor dynamics from an unacceptable position to an acceptable one can be fundamental enough to require starting the whole engine design from the beginning. The only published set of criteria found is from (American Petroleum Institute, 1998) which are based on the predicted damping factor of resonances, and percentage operational speed separation margins that are dependent on those margins. The normal criteria used in aerospace are based on proportional strain energy distribution between the rotor and the stator. Both of these approaches are discussed in detail in chapter 7 of this thesis.

In (Werner, 2011) the analysis of large flexible induction rotors is demonstrated. The paper discusses optimization of the rotor design, trading the tolerances of single sided rotor core windings and the negative stiffness effects that can be tolerated verses rotor stiffness. In similarity to this thesis, the aim is to low speed balance a flexible rotor, and rotor design and manufacturing tolerances are discussed as key influences. However, the design of an induction rotor is significantly different to that of an aerospace gas turbine with very different design requirements and constraints.

2.2 Chapter Conclusion

There are only a few examples of literature that directly contributes to the key issues faced by the aerospace gas turbine industry. Low-speed balancing is a cost-effective incumbent constraint on gas turbine turbomachinery, and low-speed balancing technology relating to pseudo-rigid rotors has not advanced significantly. An area that has moved on significantly in this period is the ability to create accessible finite element models of whole engines, however the capability of these models has not been significantly utilised in the areas of build and balance and the related rotor design issues.

The few literature examples that do exist in this area focus on improving the low-speed balancing outcome, but fail to address the fundamental design considerations as a holistic “System Design” problem. The gas turbine engine needs to be designed with vibration performance requirements as part of the primary objectives whilst recognising the manufacturing, balancing, and build requirements and limitations. Also, unlike rigid rotors, pseudo-rigid rotors in flexible structures do not have an established published criterion for acceptable balance or design.

3 Sources and Control of Rotor Ordered Vibration in Gas Turbines

3.1 Chapter Introduction and Aims

In accordance with thesis objective (i) from section 1.5, the aim of this chapter is to describe the current normal practices of rotor balancing in the aerospace industry, and typical sources of unbalance together with the approaches taken to minimise them or their effects. This chapter also introduces the identification of a mechanism for the coupling of the first and second integer harmonic rotor order amplitudes due to the bearing misalignment angle when influenced by rotor bending. Note the term “rotor order” is used to describe the rotor rotational frequency.

3.2 Balancing Definitions

For reference in the rest of this document, static unbalance is defined as

$$u_s = m \times e, \tag{3.1}$$

where m is the mass which is offset from the centre of rotation, e is the eccentricity of that mass, and u is the unbalance with typical units of (g.mm) in the UK metric aerospace gas turbine industry.

Couple unbalance is defined as

$$u_c = \phi \times (I_p - I_d) \tag{3.2}$$

where ϕ is the angle of inclination of the mass, I_p and I_d are the polar and diametral moments of inertia respectively; u_c is the unbalance couple which is equivalent to two static unbalances of equal and opposite magnitudes separated by a distance and has typical units of (g.mm^2).

3.3 Bearing Alignment

If a thrust bearing is swashed (on the rotating side) there are three likely scenarios which can happen by degrees in combination, or individually:

1. When the thrust is applied it will be large enough to lift the weight of the rotor into square alignment with the thrust bearing swash, thereby forcing the bearing and squeeze film damper clearance at the other end of the rotor to become pushed over to one side affecting the performance of the damper.
2. When the thrust is applied, the rotor will bend to accommodate the misalignment causing deflection of the rotor centre line and therefore unbalance (if the misalignment is on the rotating track of the bearing).
3. The thrust is not great enough to lift the weight of the rotor or cause it to bend, therefore the rotor loads one side of the bearing more than the other, and at very low thrust the bearing sits loosely in its clearance, giving the bearing a non-linear stiffness. This stiffness would be characterised by high stiffness downwards and low stiffness upwards, with very complex behaviour at lateral angles. It should be noted that axial load on the thrust bearing is <u>not</u> always proportional to engine thrust, at operational speeds thrust on bearings can often be very low and can even reverse direction.

Figure 2 shows three situations of the bearing alignment under axial loads:

(a) Shows the straight bearing in full “square” contact which is the design condition.

(b) Shows the thrust bearing under an axial load which is insufficient to bend the rotor so that it is square to the bearing.

(c) Shows the effects where the axial load is large enough to overcome the mass and stiffness of the rotor and the squeeze film stiffness, which are effects that can happen independently or in combination.

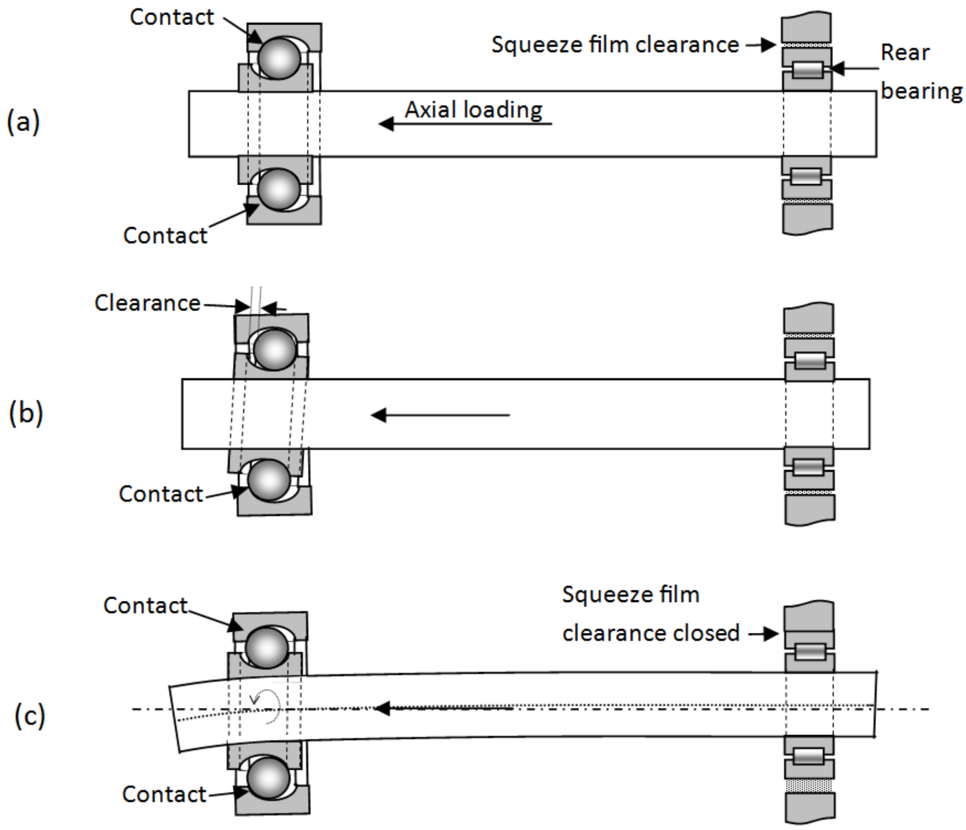

Figure 2: Angular misalignment in a rolling element “thrust” bearing. (a) shows the bearing in full contact, (b) shows the thrust bearing under low axial load, and (c) shows the axial load overcoming the rotor and squeeze film stiffness.

During the investigations conducted in this study, an engine demonstrated significant sensitivity to the alignment of the front bearing of the HP rotor. A modelling study was conducted using a WEMM to quantify the effect. Only a linear WEMM was available and this particular rotor showed that, even at idling speed, the thrust on this bearing would be large enough to lift the rotor and force the bearing into square alignment (scenario (1)) and on this particular bearing the axial load on the bearing would increase with engine speed. The misalignment measured was great enough to completely close the squeeze film damper gap at the rear bearing therefore the situation was now dominated by scenario (2) above (what is the effect of the bending of the rotor), the effect of which needed to be quantified. This combination of scenarios is shown in *Figure 2*(c).

The actual loading condition is non-linear due to the fact that the thrust applies a “straightening” moment to the thrust bearing (calculated from the axial load multiplied by the bearing radius) which will be amplitude limited because once the rotor bends and therefore the bearing tracks are straight relative to each other, the clearance gap in *Figure 2*(b) will close. Once the clearance is closed further increases in axial load do not impart more moment because the load is now reacted on both sides of the bearing (as per design intent).

Only a linear WEMM was available, so the following approach was adopted. The bearing straightening force moment (rotating with the speed of the rotor) was applied to the rotor. This moment was a constant value based on the axial load at idle representing a minimum value for an idle to maximum speed analysis on this particular rotor. The vibration levels from the WEMM were measured together with angular displacement of the rotor at the bearing location. The following scaling logic was then applied to the vibration results at all speed points analysed between idle and maximum:

i. If the predicted angular displacement of the rotor (WEMM_displacement) at the bearing location was less than the angle required to close the bearing clearance measured from a real engine (engine_displacement), the results were not factored.
ii. If the predicted angular displacement of the rotor at the bearing location was sufficient to close the bearing clearance measured from a real engine, then the predicted vibration was factored down by the ratio of the datum to the angular displacement calculated, that is:

$$Vibration(factored) = WEMM\_Vibration \times \left(\frac{engine\_displacement}{WEMM\_displacement} \right)$$

(where WEMM_displacement > engine_displacement).

The results of this analysis are given below, where it can be seen that 60% of the vibration limit is consumed by this one error. No other unbalance or vibration source was included in the model.

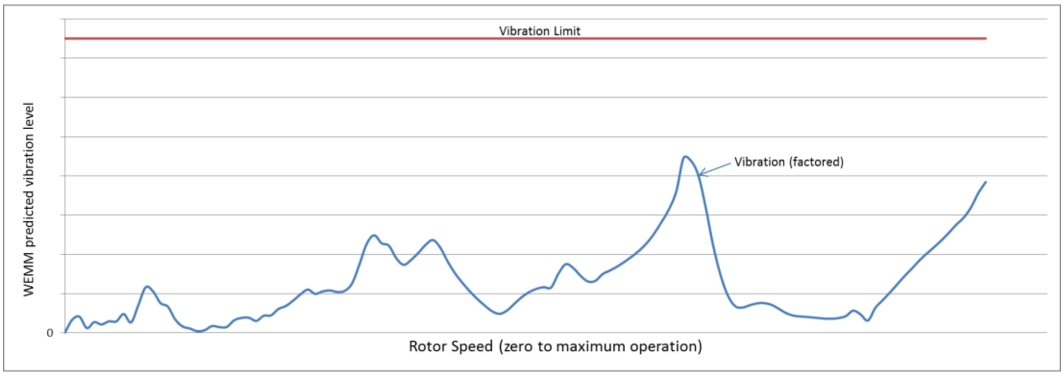

Figure 3: Predicted vibration response to a real measured bearing alignment error.

It is clear from this result that bearing swash can be a very significant contributor to engine vibration levels, and therefore needs to be considered as a key parameter in rotor alignment decisions.

3.4 The Coupling of First and Second Rotor Orders Through Shaft Bending and Bearing Angular Misalignment

Another finding in this study is the identification of a mechanism for the coupling of the first and second integer harmonic engine order amplitudes due to the bearing misalignment angle when influenced by rotor bending. In this section the mechanism is firstly explored on a simple idealised knife-edge bearing, and later the influence of a ball-bearing geometry is explored.

A bent rotor is pictured in *Figure 4*. When this rotor is operating, the bent shape will orbit around the horizontal rotor centre line. A key parameter to note in the figure is the bearing angular displacement (ϕ).

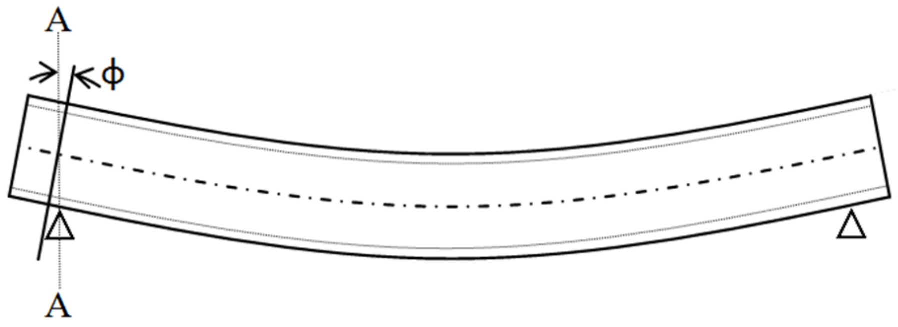

Figure 4: Rotor bending causing angular misalignment at the bearings

The cross section labelled AA is drawn in *Figure 5* below.

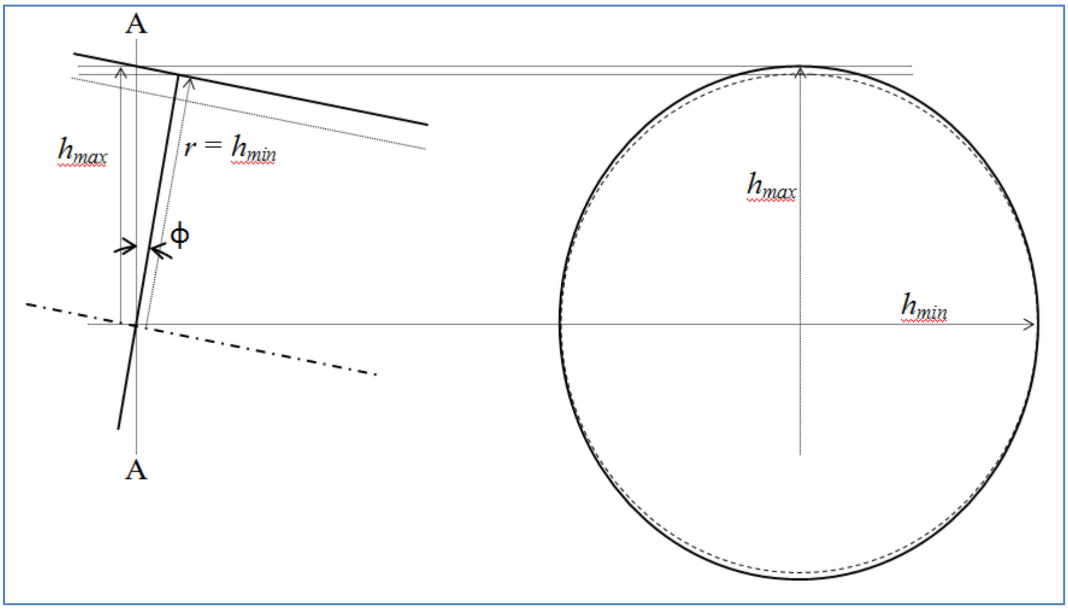

Figure 5: Rotor cross-section AA, ellipse generated by the swash angle (ϕ)

The rotor is circular when viewed in a cross-sectional plane perpendicular to its axis; the axis is shown as a dash-dot line. Due to the bend of the rotor, the angle ϕ will be generated at the bearing location. If the rotor remains bent in the rotating frame of the rotor (i.e. the bend rotates synchronously with the rotor), the bearing contact on the rotor will be at the axial position marked as A-A in the figure. The presence of the inclining angle ϕ causes the bearing contact cross-section to become elliptical. The axes of the ellipse can be seen labelled h_{max} and h_{min}, with the outer radius of the rotor (r). It is clear from the diagram that the minimum axis of the ellipse is equal to the outer radius of the rotor ($h_{min} = r$). The amplitude of the major axis of the ellipse h_{max} relates to r by the equation:

$$h_{\max} = \frac{h_{\min}}{\cos\phi} = \frac{r}{\cos\phi} \quad . \tag{3.3}$$

Because a rotor with an elliptical cross section will generate a twice per revolution (second order) displacement sine wave ($d_{0\text{-}pk}$):

$$d_{o-pk}(t) = e_2 \sin 2\omega t \ , \tag{3.4}$$

where 't' is time and 'ω' is the rotor speed, and e_2 can be described as the second order eccentricity and is defined as:

$$e_2 = \frac{h_{\max} - h_{\min}}{2} = \frac{\left(\dfrac{r}{\cos\phi} - r\right)}{2} = \frac{\left(r\left(1 + \dfrac{\phi^2}{2} + \dfrac{\phi}{24}^4 + \ldots\right) - r\right)}{2} \quad . \tag{3.5}$$

Differentiating eq. 3.4 twice with respect to time, the acceleration due to the second order is determined by:

$$\frac{d^2(d_{0-pk})}{dt^2} = -4\omega^2 e_2 \sin 2\omega t \ . \tag{3.6}$$

Then by Newton's second law and assuming that the rotor is rigid, the second order force generated at the bearing (F_2) due to the supported mass of the rotor at the bearing m can be calculated from:

$$F_2 = -4\omega^2 m e_2 \sin 2\omega t \ . \tag{3.7}$$

For comparison, the centrifugal force generated by first order unbalance can be represented by:

$$F_1 = m e \omega^2 \sin \omega t \tag{3.8}$$

where "$m.e$" is defined (in eq. 3.1) as the unbalance u.

Comparison of equations 3.7 and 3.8 shows that the second order force is four times more sensitive to the eccentricity term than the first order force. As shown in section 1.3.4, the balance tolerance requirements can be determined in terms of permissible eccentricity (e_{per}). An average e_{per} for aerospace gas turbine rotor components would be 2μm, and would be expected to result in a vibration level of around 2mm/s. A level of 0.5mm/s is easily detectable from the engine vibration transducer; therefore a detectable eccentricity of the first engine order (e) would be 0.5μm (2μmx0.5mm.s^{-1}/2mm.s^{-1}=0.5μm). Furthermore, because the e_2 is 4 times more sensitive than e it is reasonable to conclude that an e_2 of around 0.1μm would be detectable.

The eccentricity comparison here relates only to the mass eccentricity at the bearing. The question remains whether is it likely that an e_2 of greater than 0.1μm will be generated on a real engine, which is dependent on ϕ. Therefore, using some values taken from the WEMM analysis of a real engine architecture, the following architecture is assumed:

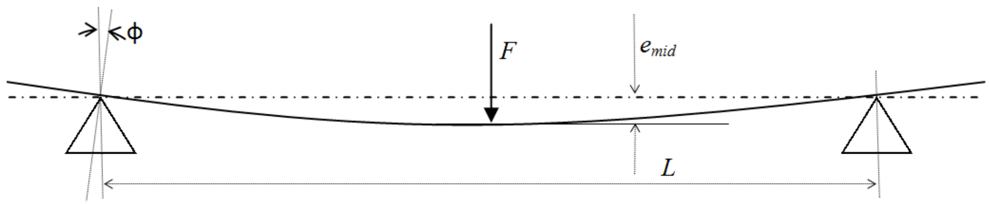

Figure 6: Dynamic deflection of a rotor during running

The bearing radius (r) is 100mm and the rotor length (L) is 1.5m for this rotor. The predicted dynamic deflection at the mid span (e_{mid}) is 0.25mm. In order to find a relationship between e_{mid} and ϕ, a uniform stiffness of rotor is assumed, and the relationship is derived below.

The relationship between bending moment (BM), Young's modulus (E) and the Second moment of area (I) and the bending of the beam is well known and defined as:

$$\frac{BM}{E \cdot I} = \frac{d^2x}{dy^2} \tag{3.9}$$

and rearranging gives:

$$BM = E \cdot I \frac{d^2x}{dy^2}. \tag{3.10}$$

The slope at the ends of the beam is defined by:

$$\frac{dy}{dx} = \pm \frac{F \cdot L^2}{16 \cdot E \cdot I}. \tag{3.11}$$

And the standard equation for deflection at the centre of a simply supported beam is:

$$y = -\frac{F \cdot L^3}{48 \cdot E \cdot I}. \tag{3.12}$$

Assuming a positive on eq. 3.11, and dividing by eq. 3.12 gives:

$$\frac{\left(\frac{dy}{dx}\right)}{y} = \frac{\left(\frac{F \cdot L^2}{16 \cdot E \cdot I}\right)}{-\left(\frac{F \cdot L^3}{48 \cdot E \cdot I}\right)}. \tag{3.13}$$

Rearranging and cancelling gives:

$$\frac{dy}{dx} = \frac{-3 \cdot y}{L}. \tag{3.14}$$

The bearing misalignment angle ϕ can then be calculated from:

$$\tan(\phi) = \frac{dy}{dx}. \tag{3.15}$$

Therefore, using the values for this rotor (e_{mid}=0.25mm and L=1.5m) and equations 3.14, 3.15 and 3.5, e_2 is determined to be equal to 6.25x10^{-3} µm, which is well below the detectable level previously defined as 0.1 µm. However if the geometry of the thrust bearing is considered, as shown in *Figure 7*, under an axial thrust load the contact angle of the bearing µ is close to 45°. Therefore the sensitivity can be redefined assuming the angle ϕ causes the bearing contact to move along the tangent of the contact angle μ.

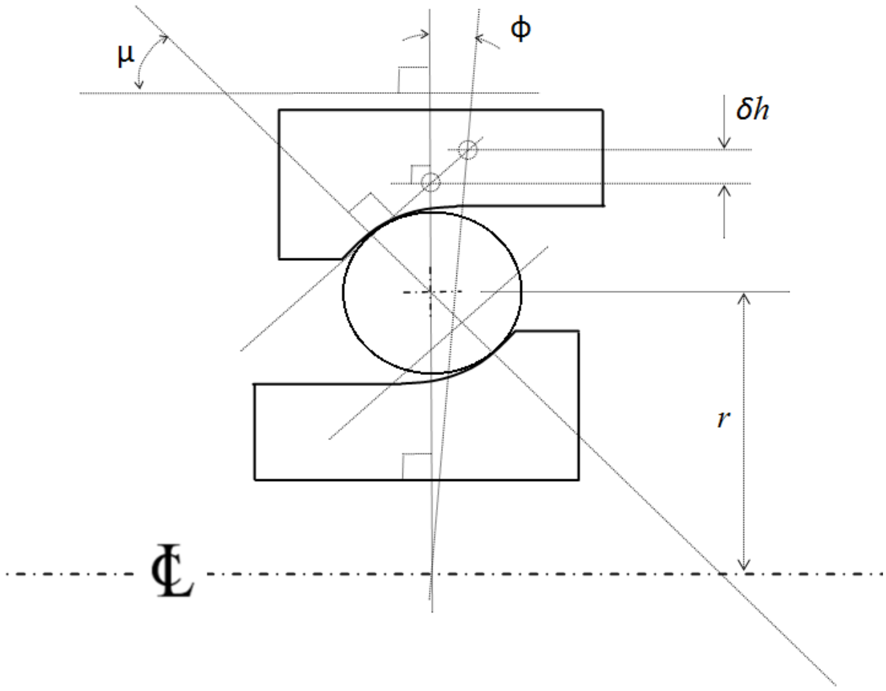

Figure 7: Thrust bearing contact angle

From this geometry, the difference between h_{max} and h_{min} can be determined from the following equation:

$$\partial h = h_{\max} - h_{\min} = \frac{r \sin\phi}{\sin(\mu+\phi)} \sin\mu \qquad (3.16)$$

Recalculating e_2 based on the subject rotor once more using equations 3.16 and 3.5, e_2 becomes 0.425μm, which puts the second engine order well above the detectability level of 0.1μm. Therefore shaft bending due to unbalance can lead to the generation of a second order vibration signal that will be proportional to the deflection of the shaft and therefore the unbalance.

Other sources of significant misalignment will naturally cause the same effect, rotor alignment (or misalignment) due to component tolerances is covered in section 3.5, where the effect of a small swash error in a joint is described in detail and pictured in *Figure 8* (b).

3.5 Rotor Alignment

The alignment of the geometric centre of rotor components and the unbalance that they generate is a surprisingly complex topic. The dynamic sensitivity of a rotor to a particular alignment error depends on a number of issues, such as where the tolerance error occurs on the rotor relative to the bearings, what type of tolerance error it is (i.e. a swash or eccentricity) and the distribution of mass properties along the rotor and the nature of those properties.

A rotor with two types of error featuring on one of its components in shown in the following figures. The rotor itself is made up of two major components, which will be referred to as modules for consistency with other parts of this study. In *Figure 8* there is a swash error in the left hand module, indicated by the the angle θ.

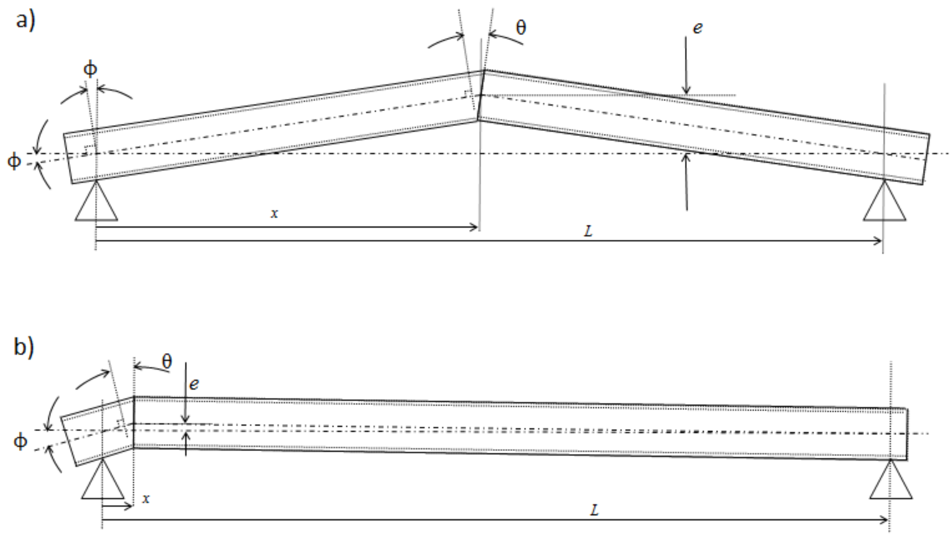

Figure 8: Simple rotor with a swash alignment error in the middle (a) and near the bearing (b)

With reference to *Figure 8*, the angle ϕ due to the joint swash θ (assuming small angles) can be found from

$$\phi = \theta \frac{L - x}{L} \quad , \tag{3.17}$$

and the value of 'e' at the joint due to θ can be found from

$$e = x\phi \, . \tag{3.18}$$

The key points to note from these equations and the effects of the swash errors shown in *Figure 8* are:

1. The maximum eccentricity of the rotor 'e' is greatest when the error is half way between the between the bearings as shown in (a). In diagram (b) where the error is very near the bearing, 'e' is minimised.

2. The angle of inclination ϕ is much increased on the shorter component when the joint is close to the bearing. In the limit where the joint is on top of the closest bearing (i.e. x is zero), ϕ becomes equal to θ.

It should also be noted that the equivalent angle of inclination for the right hand module is negligible.

In terms of rotor unbalance, point 1 is significant for when large masses are positioned near the centre of the rotor where they would generate significant unbalance due to this large offset. Point 2 is important for discs of significant mass, discs tend to have a large difference in their polar and transverse inertias and therefore cause significant point couple unbalances when rotating on an inclined axis (reference eq. 3.2).

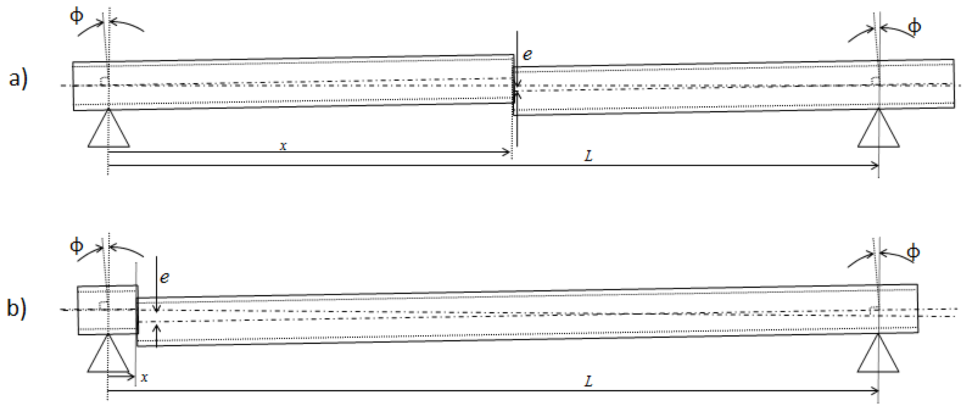

Figure 9: Simple rotor with an eccentric alignment error in the middle (a) and near the bearing (b)

Figure 9 shows the same rotor but with and eccentric error at a joint in the centre (a) and near the end (b). The key points to note are:

1. The maximum eccentricity of the rotor ‘e’ is minimised when the error is half way between the between the bearings as shown in (a) and maximised in diagram (b) where the error is very near the bearing.
2. The angle of inclination ϕ due to ‘e’ is constant regardless of the location of the joint between the bearings (‘x’). This can be seen from equation 3.19 below.

$$\sin\phi = \frac{e\left(\frac{L-x}{L}\right)}{L-x} = \frac{e}{L} \tag{3.19}$$

When a rotor with many component interfaces is considered, each with its own geometric error, and each with its own mass and inertia properties, the resulting unbalance distribution is very complex.

When a scheme for alignment of a rotor is created, vibration is not the only consideration; the “straightness” of the rotor also directly impacts the turbomachinery blade tip clearances, the minimisation of which is a critical parameter to maintain the performance of the engine.

Figure 10 and *Figure 11* are straight build alignment schemes with the rotor in vertical (build) orientation on the left hand side, and the same rotor supported on its two bearing locations on the right hand side.

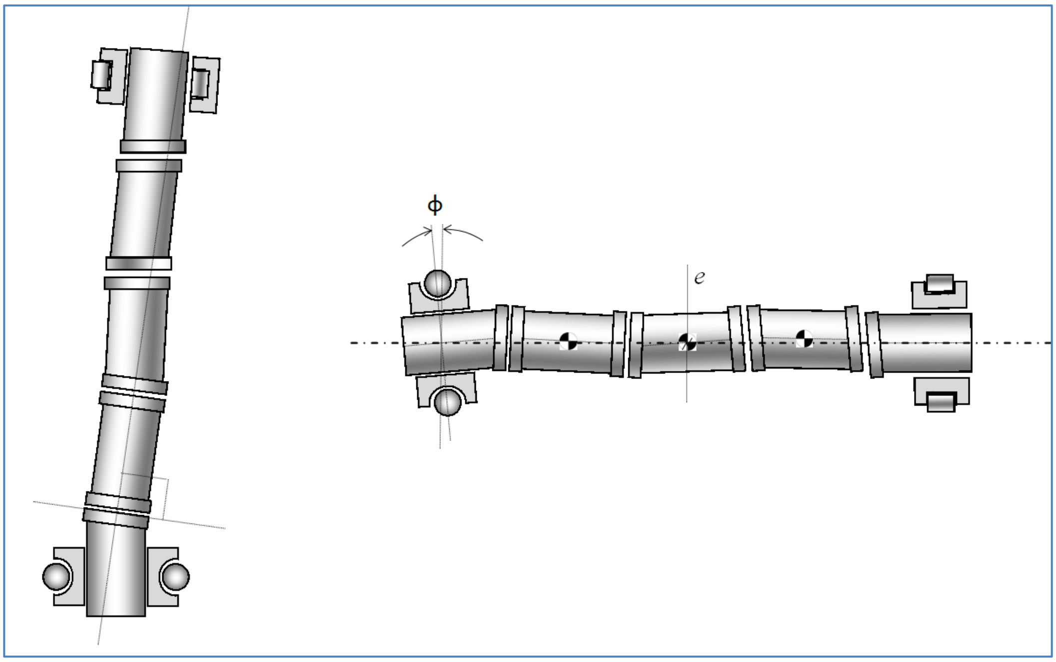

Figure 10: Rotor alignment to maximise rotor "straightness"

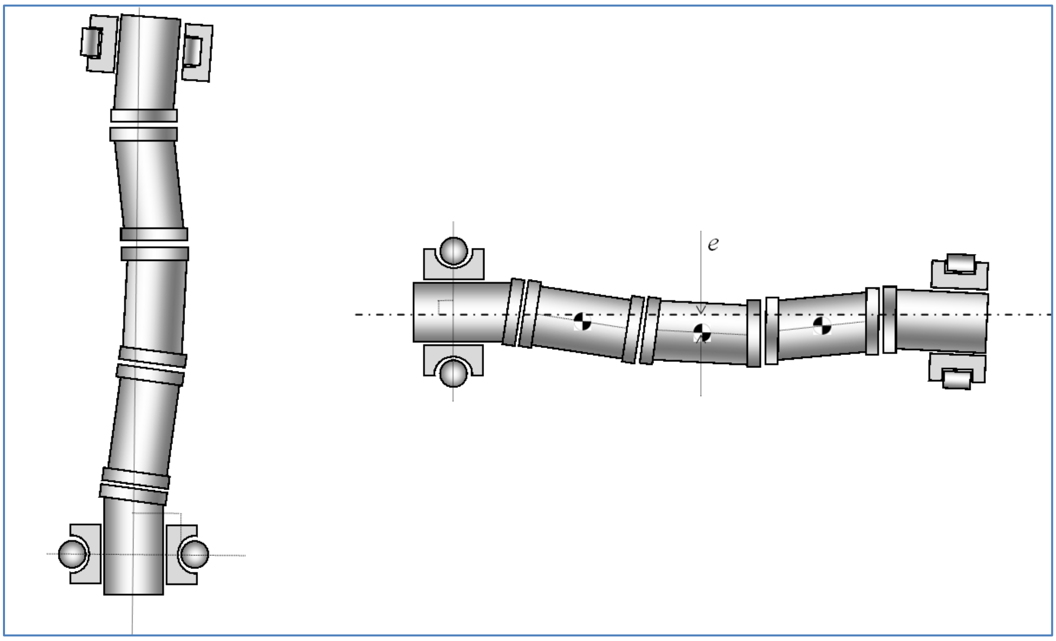

Figure 11: Rotor alignment to minimise bearing misalignment

In *Figure 10* the target has been to build the rotor to minimise the eccentricities (e) of all of the components along the rotor. The approach here is to project an imaginary line (shown) perpendicular from the face of the component which holds the axial location bearing (ball bearing), along the length of the rotor to the rear bearing location. The optimisation target of this build alignment method is to minimise the radial distance (w.r.t. the rotor centreline) between the projected line and the actual rear bearing location of the rotor. In *Figure 11*, the target has been to align the bearings as best as possible, therefore the imaginary projection line is drawn perpendicular to the front bearing plane. Comparing these figures, it is clear to see that these two targets produce two very different rotor shapes from the same set of components. In *Figure 10* the straightness has been maximised, at the detriment of the bearing alignment angle ϕ, which will introduce vibration via the mechanism described in section 3.3, but it will minimise the internal bending moments introduced during the low speed balancing process, and produce the best blade tip alignments. In *Figure 11* the bearing alignment has been optimised, at the expense of the straightness of the rotor. In reality, the situation is much more complicated than these simple global targets would demonstrate (although they are commonly used). For example, the low speed modular balance process causes large bending moments to be generated due to the rotor joint errors at the intermodular joints, therefore it may be optimal for vibration to target the alignment of a particular joint face. The process proposed in this thesis for determining this is discussed in more detail in section 6.3.

It should be noted that the above discussion focusses on geometric errors that relate to the manufacturing tolerances of components, superimposed on these errors are the variations due to joint build repeatability, which can only be influenced through the joint design and build practices.

3.6 Current Balancing Methods Specific to the Aerospace Gas Turbine Industry

Because of the drivers and requirements listed in section 1.3, the Aerospace gas turbine Industry has over many years developed a method of operation that uses low-speed-balancing to achieve its aims. The generally accepted definition of Low-speed-balancing is balancing operations that are performed at speeds well below the flexible modes of the rotor so that the rotor can be said to be performing in a rigid-body state. The methods are described briefly below.

3.6.1 Low Speed Balancing Using Mass Simulators

The use of balancing mass simulators is common within the aerospace gas turbine industry. If the module being balanced supports any other parts of the rotor that are not within the module, then the alignment errors (tolerances) in the module being balanced will cause the mass of the part being supported to generate some unbalance. The modularity requirement (1.3.2) dictates that parts outside of the module must be totally interchangeable without rebalance. Therefore it is clear that the unbalance correction applied to the module must correct for the offset/alignment errors that the module causes in the mass that it supports, even if the actual component that it will support cannot be present on the balancing machine. This is achieved through the use of tooling which is used during the balancing process to represent the adjoining mass, known as a balancing mass simulator. This is illustrated in *Figure 12*.

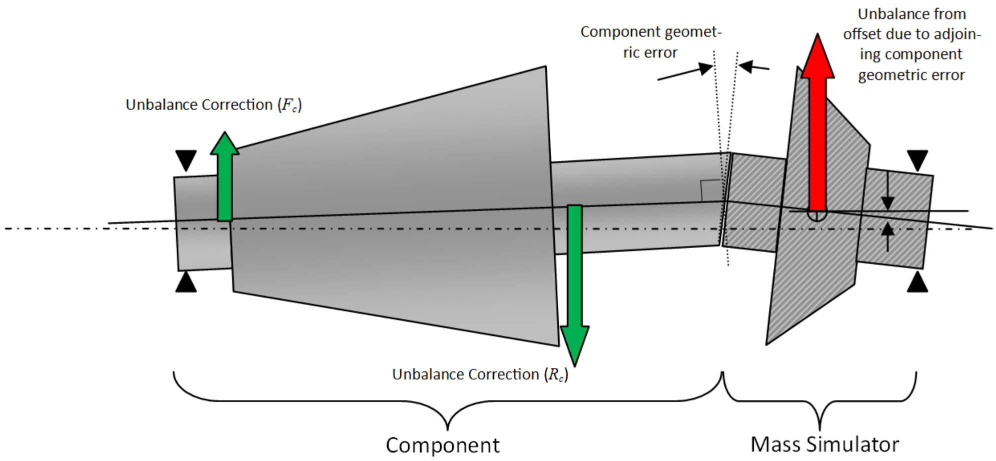

Figure 12: Illustration of Low Speed Modular Balancing using Simulators

The adjoining part of the rotor must be balanced in its own right for any misalignment that it causes on its own mass to be offset from its location features. Furthermore, adjoining modules often have an interdependent alignment relationship with their adjoining modules; this can also be seen in *Figure 12* where the joint in the centre of the rotor controls the position of the mass to the left and the right of the joint. In this case both of the modules must be balanced with the appropriate simulator.

Using this method described, providing the rotor is sufficiently rigid at all running speeds, the rotor can be sufficiently balanced.

3.6.2 High Quality Rotor Joints

Because of the modularity requirements, the balancing tolerance requirements and the use of the balancing process described in the previous section, there is an underlying requirement for a joint between different rotor modules that has an assembly repeatability of within 1μm. These joints also have to be maintained on the balancing mass simulator tooling which will be used thousands of times but must not lose repeatability due to wear. A joint commonly used to fulfill this function is the curvic coupling. The effects of repeatability and alignment errors in joints are discussed in section 3.5.

3.7 Unbalance relationships between adjoining components

For the convenience of this study, the geometric features of rotors that cause unbalance through offsetting the centre of gravity of the components of the rotor away from the rotational centre-line can be divided into three categories:

A. Rotor components which have geometry that controls the position of other components.

B. Rotor components which have geometry that *only* controls the position of its own mass.

C. Rotor components which have specific geometric features that simultaneously control the position itself and of other components.

Examples of each the 3 categories are given in *Figure 13* to *Figure 15* respectively. The traditional method for dealing with each of these unbalance types is described in following subsections.

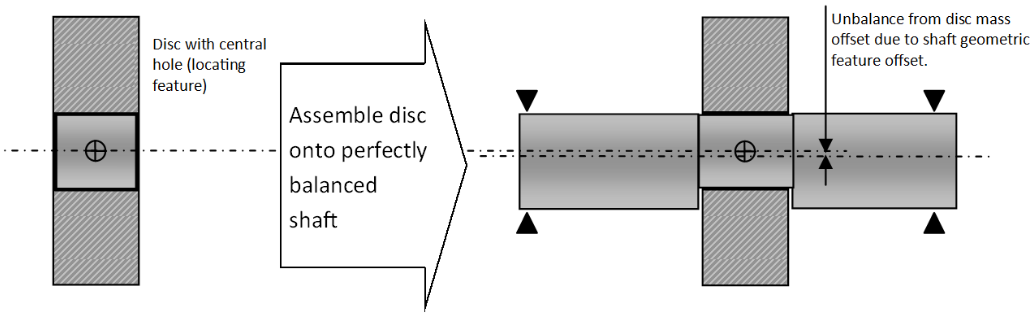

Figure 13: Example of a (Category A) type rotor component (shaft) that has geometry that controls the position of other components.

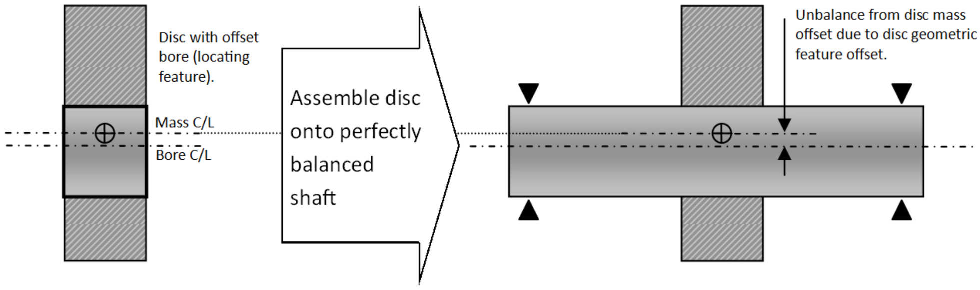

Figure 14: Example of a (Category B) type rotor component (disc) that only controls the position of its own mass.

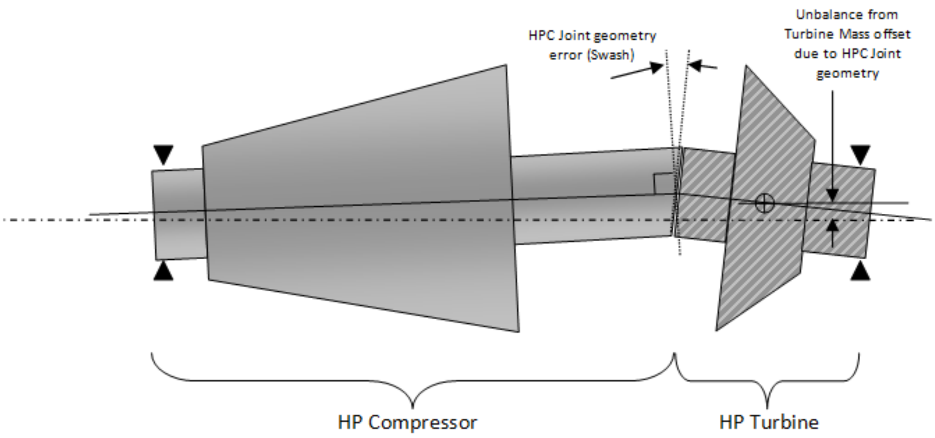

Figure 15: Example of a (Category C) type rotor component (HP Compressor Module) that has geometry features that control the position of its own mass and the position of other components.

3.8 Balancing Methods for Category 'A' Geometric Errors.

When balancing a component that has features that control the position of mating components, but those same features do not control the position of the component being balanced, the mass and inertia of the mating components should be represented on the balancing machine. This can be done in two ways, either by simply including the mating components on the balancing machine or, if it is not desirable to have the other components (for reasons explained below) a mass simulator can be used which normally has the same mass properties as the component it represents.

Some reasons for using mass simulators instead of the actual mating components are listed below:

1. Modularity: if the mating components are to be replaceable without rebalancing the rotor.
2. Delicate components: handling the components can cause them to be damaged, especially if they are delicate (i.e. the blades on a bladed disc).
3. Bladed assemblies: turbomachinery can cause issues due to air pressure developed by the blades. It can be difficult to drive the rotor with enough power, and it also creates pressure or "thrust" that must be reacted by the balancing machine which can cause inaccuracies. Also the noise can become prohibitive in a workshop environment.

3.9 Balancing Methods for Category 'B' Geometric Errors.

If a component being balanced has a location feature that only controls its own mass, it should be mounted from that same aligning feature when balancing. It is a common mistake to balance a component to a location feature that is not its assembly location feature when balancing to fine tolerances; this is because during balancing the centre of gravity will become aligned to the balancing location feature which will have a different axis to the assembly feature, resulting in unbalance in the assembly.

3.10 Balancing Methods for Category ‘C’ Geometric Errors.

Figure 15 shows the usual situation with a gas turbine rotor which has multiple parts. Here we can see that the swash error in the joint face at the right hand end of the HP Compressor causes the mass centres of both the compressor and the HP turbine modules to be offset from the geometric centreline. In this situation, similarly to category ‘A’ balancing, the mating component(s) should be represented on the balancing machine. If the rotor is to be modular so that any HPC can be fitted to any HPT, a mass simulator is commonly used. This is because the HPC must only be balanced for the unbalance that its geometric errors have caused, and not any unbalance in the adjoining turbine module that is due to some geometric error in only that particular turbine. However when this is done the engine dynamics of the rotor need to be carefully considered, because the unbalance correction is being applied at a significant axial distance from the portion of the unbalance that arises in the mating component, therefore a bending moment is generated that can lead to vibration (see section 5.10)

3.11 Chapter Conclusion

This chapter introduced the concepts of low-speed modular balancing, and the common sources of unbalance within the rotor, together with the concepts that are in common use today to achieve a balanced rotor. The areas of rotor build alignment and bearing alignment have a significant influence on vibration and are complex and interlinked but are not usually specifically addressed in today’s methods. A hypothesis for a mechanism for a rotor with a bend in it combined with a location bearing to cause detectable vibration at the frequency of the second harmonic of the rotational speed was also discussed.

4 Robust Rotordynamics Design System

4.1 Background and motivation

In accordance with thesis objective (ii) from section 1.5, the aim of this chapter is to describe the method that has been developed as part of these studies that identifies the most cost-effective and robust engine design solution that is able to adequately manage rotor ordered vibration. In order for such a system to deliver value into the engine design, the process and tools must be extremely fast and flexible because the timescales of a proposed new engine programme are such that many design decisions are made very early stages of the design process that fix many of the engines architectural parameters. Based on these parameters there is a very rapid snowballing effect of parallel analysis and design streams that make further design decisions relating to the myriad of requirements that the engine must satisfy. Therefore the fundamental design of the engine rapidly becomes more expensive/difficult to change, even in the early design stages. The consequence of this situation is that if the structural design of an engine is to be influenced for the purpose of improved control of vibration, this information is required very early in the design process.

There is very little guidance on modular balancing in publicly available literature. Low speed modular balancing processes have had layers of complexity added to them over many years to manage vibration problems that have occurred during engine development/service, which are read across to the next engine design. Alongside this, expensive design, manufacturing, and build techniques (such as “straight” build and balancing of every component in an assembly that will also be balanced as an assembly) have been found to alleviate vibration issues historically so these are also read across. These issues are further elaborated in section 1.4 and chapter 3. The main problem has been that the issue of rotordynamics and balancing has so many interacting variables that the modelling of the entire system with all its variables has not been feasible within the timescales of a commercial engine design project. There are two main reasons for this, firstly the complexity of the model to introduce all of the unbalance driving errors (also detailed in chapter 3). Secondly, if such a model was created using the normal WEMM methods, the time it would take to run would be prohibitive if a statistically significant population of rotors was to be considered.

This issue is further compounded because the number of balancing options available to the Engineer is almost limitless, so very large numbers of different balancing and build processes have to be tested. Furthermore, the processes to be tested are not created by any specified quantitative method, but either read across from previous methods, or created by the Engineer using experience and judgement. Initially “Robust Design” and “Design of Experiments” methods were explored to attempt to minimise the number of calculation sequences (“runs”) of the WEMM that were required. However, even with reduced model runs to explore the design space, the time to set up the model and the solution time was prohibitive for the timescales of early design.

The uncertainties above have driven the requirements for a simple, fast, and robust process to be developed as part of this study. These requirements are summarised below:

1. A method to quickly determine the most likely successful balancing, build, and design solutions that can employ the experienced Engineer’s knowledge of previous methods and understanding of practicalities of build

and balancing.

2. A modelling method that can accommodate the key drivers for rotor dynamic design and model the balancing process to compare the effectiveness of each method, on a statistically significant population of rotors (target solution time less than 1 hour).

3. A measure of “goodness” for each method.

The following sections describe the process and associated tools and methods that have been developed to meet these requirements.

4.2 Description of the Robust Rotordynamics Design Process

Figure 16 shows a flowchart of the Robust Rotordynamics Design Process, together with the key outputs described in each step. Note that the Robust Rotordynamics Design *Process*, when grouped with the technical toolset and methods that have been developed, is referred to as the Robust Rotordynamics Design *System*. A more complete description of each step of the process is given in the following text.

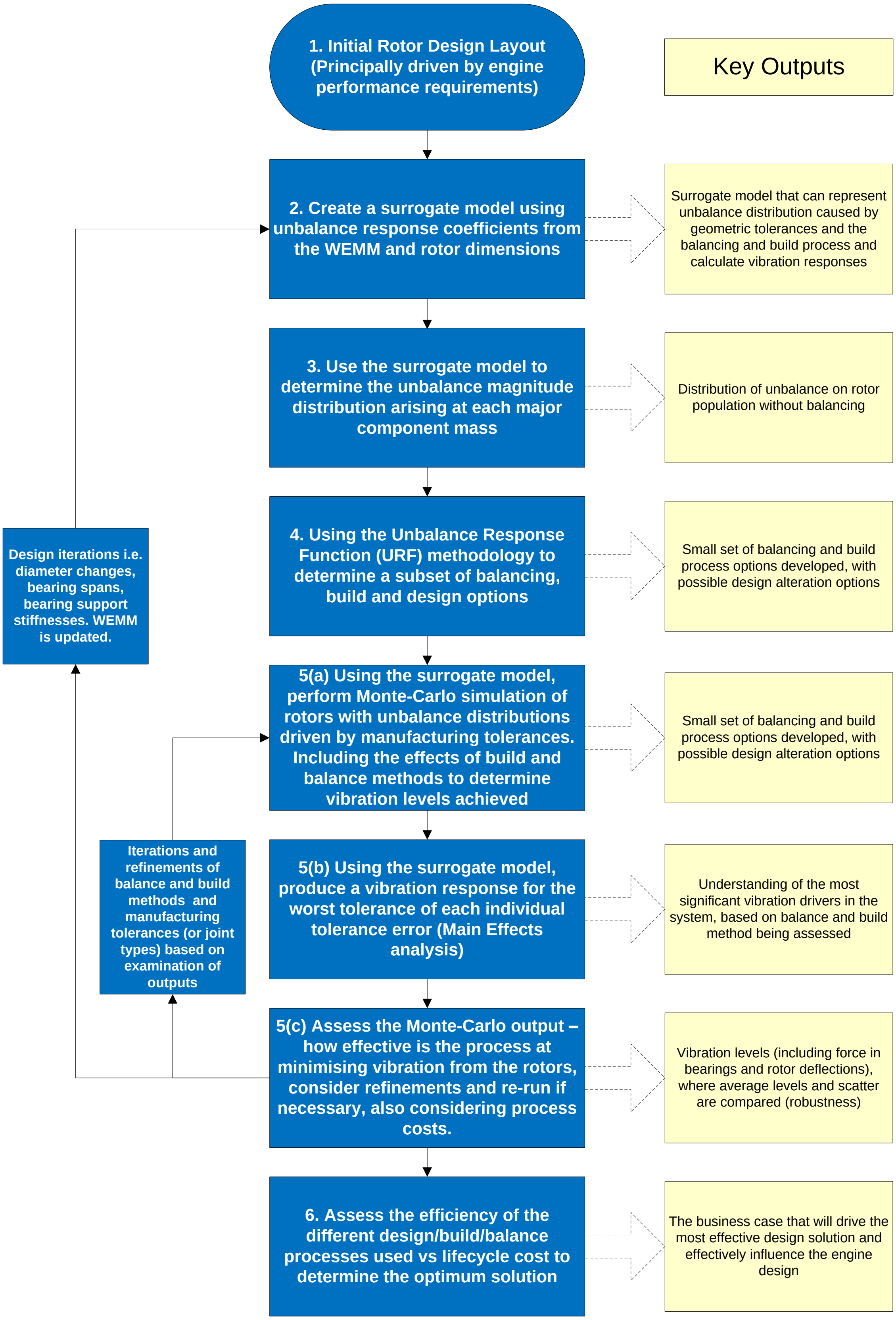

Figure 16: The Robust Rotordynamics Design Process

1. The initial fundamental requirements for an engine begin with the amount of thrust it must produce. Therefore the number of rotors, the number of stages for each compressor and turbine, the area of the gas path, and the size of the combustor, are mostly determined by the performance requirements in the first instance. Very early on, the rotors are assessed to ensure there are no major modes in the operating speed range, but after this point, changing the fundamentals of the engine structure (i.e. rotor length or diameter) is prohibitively expensive). Despite the design restrictions on the engine's fundamental layout, the Engineer can still do a lot to influence the design of the engine, such as changing the bearing support stiffness's and implementing changes to bearing locations and types, additional bearings, adding squeeze film dampers, rotor profiles, influencing manufacturing tolerances, balancing methods and build practices.

2. The "surrogate model" is a simplified model of the rotor that is used to calculate unbalance distribution along the rotor and the vibration that arises from them. It basically consists of a rigid stick model of the geometry of the rotor and associated component mass properties, which can have manufacturing tolerance effects imposed (i.e. on rotor joints) to determine the static rotor deflections that will occur. The dynamic response coefficients to unbalances placed at various points along the rotor are generated using the Whole Engine Mechanical Model (WEMM) and input into the surrogate model (Note that a WEMM is produced for other reasons than just rotor dynamic design, therefore it is assumed to exist and is available for rotor dynamic analysis). The surrogate model basically works in three steps:

i. It calculates the unbalance distribution along the rotor due to the geometry and manufacturing tolerance errors, including the effects of the build process adopted (i.e. the relative rotational alignment between components).

ii. From (i) it simulates the low speed balancing operation on that unbalance distribution.

iii. From the output of (ii) it uses the WEMM dynamic coefficients and the principle of linear superposition to calculate the total dynamic response.

The surrogate model coding has been packaged into a Monte-Carlo facility with specifically developed post processing capabilities. The fully packaged developed code has been called the Robust Rotordynamics Monte-Carlo Software, and is described more fully in section 6.

3. Before any balancing or build practices are determined, it is important to understand what the unbalance distribution and vibration response range from a population of rotors would be, if the rotor was just simply (and most cheaply) put together randomly without any balancing. The unbalance distribution information is used principally for the *Unbalance Response Function* analysis in step 4. The vibration response levels help to datum the whole analysis to determine the total benefit that the balancing and vibration specific build processes introduce. It has been found that some low speed balancing processes have made the vibration worse than it would have been had the rotor not been balanced at all.

4. The *Unbalance Response Function* graphing and analysis method has been developed to allow the Engineer to use their knowledge of practical balance and build methods and previous experience to build an appreciation of which possibilities are likely to produce the best solutions when low speed modular balancing is used. From the information in the graphs and applying the rules developed, for a typical rotor the Engineer is likely to come up with several competing solutions which should all be captured and passed onto the next step in the process. The key pieces of information that the analyst will derive will be: the most appropriate positions for balance lands, modular break locations, whether balancing mass simulators should be used, if so should they be full or scaled mass, whether some kind of build alignment is likely to be required, which components will need individual balancing and which can be balanced only as part of the assembly. The *Unbalance Response Function* graphing and analysis method development was a major part of this study and is described in detail in chapter 5.

5. Because step 5 is an iterative loop it is divided into three sus-steps. All the sub-steps of this part of the process are conducted using the Robust Rotordynamics Monte-Carlo Software which is described in detail in section 6, but briefly summarised here for convenience.

5 (a) The candidate balancing and build solutions identified from the URF process in step 4 are entered into the Monte-Carlo simulation software running the surrogate model. The resulting dynamic response levels from the engine operating speed range identified are output as a measure of the effectiveness of the process. These can be compared to the results from step 3 to show the full benefit of the process.

5 (b) The Main Effects analysis calculates the dynamic response of the engine to the effects of each individual tolerance error applied in turn (i.e. maximum eccentricity at each individual joint face). Individual critical joint tolerances can be identified which can drive decisions on the type of joint chosen for that location, and build methodology decisions i.e. “straight build should be performed to minimise swash at joint x”.

5 (c) The results from the above steps can be analysed on a simple level comparing the vibration average and scatter in the population of rotors. It should be noted that low scatter is preferable to low average vibration in most scenarios, so both must be considered. However, it is also possible to use the tools developed for reviewing the results to look at individual cases in the Monte-Carlo. An obvious example use of this is to analyse what the major contributor was to the worst case in the Monte-Carlo, and what can be done about it. Clearly this leads to re-iteration of the Monte-Carlo analysis (from 5 (a)) as build and balance options are refined. This is also where information about the cost of processes and their practical implications is required. For example, implementing a straight build step will require straight build machinery to be available at all sites where engines are overhauled, therefore it may be better to have a number of extra balancing steps instead, and the effectiveness of

alternatives can be assessed in these iterations. It can also lead to realisations that fundamental design issues of the dynamic system will cause issues and a redesign significant enough to change the rotor profile is required. In this case the reiteration will be from the beginning of the rotor dynamic design process as the WEMM and the surrogate model will need to be updated to reflect any structural changes.

6. In the final step, when all approaches to build and balance have been analysed for effectiveness with respect to controlling vibration, they must be compared for effectiveness vs cost over the lifecycle of the engine.

4.3 The Whole Engine Mechanical Model

For the purposes of the mechanical design and integration of a gas turbine engine, a finite element Whole Engine Mechanical Model (WEMM) is produced. Throughout this thesis, a number of different WEMMs are used that cannot be described in detail due to intellectual property restrictions. Therefore a generic description of a WEMM is given in this section for background purposes. It should be noted that throughout the design cycle of an engine the model starts in a very simple form, but is constantly developed through the design cycle improving in detail and fidelity. The WEMM as referenced in this thesis is often first conceived as rotors on simple springs, which is quickly updated to represent simple casings and eventually to full complexity and validation. References to the WEMM in this thesis may refer to any of these states. The general recommendation is that the best fidelity model available is used at all times and results are confirmed when the updated and validated model becomes available.

In its developed state the WEMM comprises the nacelle, major accessories, core engine casings, bearing support structures and main rotating shafts. It is then attached to a model of the pylon, wing and occasionally the aircraft. A general illustration is given in *Figure 17*.

For this study, the main interest in the model is an accurate representation of the dynamic behaviour of the engine under vibratory loads driven from the rotor. However, the model is used for a wide range of other purposes, such as calculating the loads through the engine during aircraft operations such as manoeuvres and landings. The WEMMs referred to in this study are linear models.

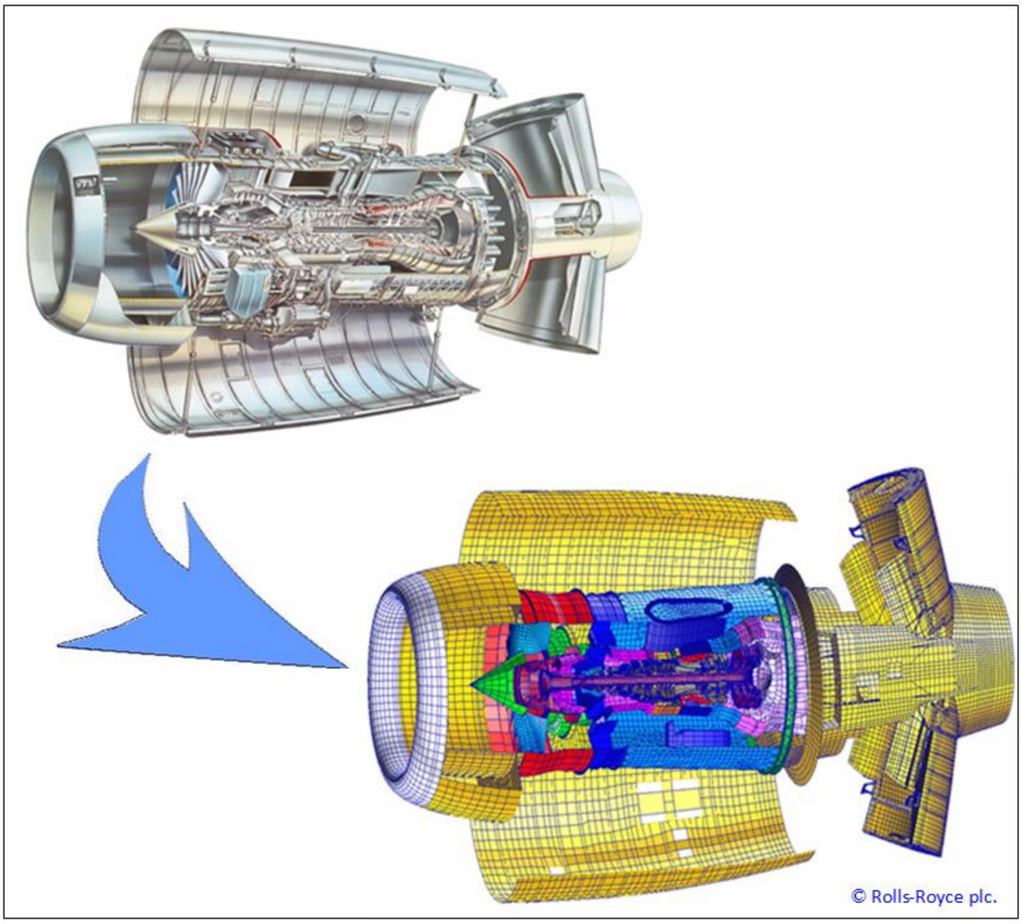

Figure 17: Illustration of a Whole Engine Mechanical Model (WEMM)

The WEMM static structure is normally modelled using the NASTRAN Finite Element software. The structure is generally represented by four noded shell (membrane) elements for the casing structures with simple beam elements representing the beam like structures such as flanges. Significant non-structural masses i.e. the generator, can be represented as point masses connected by either multi-point constraint elements or beam elements. The rotor and casing are connected together via an averaging multi-point constraint element (known in NASTRAN as an RBE3) that allows the centre node at the rotor bearing to be an average displacement of a set of nodes at the bearing housing flange; therefore allowing it to be the average centre of a ring of nodes. The connections between the rotor and casings that represent the bearings are normally linear springs with defined radial and axial stiffnesses. If squeeze film dampers are in the design, linear viscous damping elements can be incorporated into the spring stiffness elements (or in series, depending on the design being represented). The rotors are modelled as axisymmetric using separate software, and reduced into mass and stiffness matrices using Guyan centreline reduction. These matrices are connected into the NASTRAN WEMM at the bearings. Gyroscopic effects are superposed on the Guyan nodes at the centreline as velocity driven moments. Unbalances are applied to the rotor centreline nodes as rotating forces. Damping is applied as a damping parameter to the stator. A separately defined damping value is applied to the rotor.

A number of solutions are possible in NASTRAN with this type of model. The solution employed in the results presented in this thesis is a direct solution to a steady-state forced response (unbalance). Sensors of force are placed at the bearing spring elements, displacements are measured along the rotors, and accelerations are measured at the normal operational vibration monitoring locations on the casings.

4.4 Chapter Conclusions

This chapter discussed the current situation with the design of rotordynamic systems and balancing, with its current limitations and later than ideal influences on the design process. A Rotordynamics Design Process was proposed as a methodology to address/improve on these issues. The methods and tools proposed over the next chapters (5-0) are intended to be operated with this process in order to create an effective Robust Rotordynamic Design System.

5 The Unbalance Response Function (URF) Rotor Design Method

5.1 Chapter Introduction

It is clear from chapters 1-3 that an up to date set of design methods for rotordynamics and balancing is required to move the industry towards a much more cost-effective and informed solution.

Chapter 4 introduced the Robust Rotordynamics Design System and focussed on presenting the process part of that system. This chapter presents one of the analytical tools/methods that has been developed to facilitate the execution of that process ensuring timely determination of an optimal design solution. This is in accordance with thesis objective (iii) from section 1.5, which emphasises the need for fast solutions because the greatest value can be gained from a design solution at minimum cost if it is introduced early in the design process.

The design method described in this chapter was developed by the author from the results of a large number of Monte-Carlo analyses of rotor dynamic systems, and the methods were reduced down to a simple-to-use graph that can be used as a design method by following few rules.

Normally, with half a day's work the method gives the Engineer an understanding of how well the system in question will respond to low speed modular balancing and, if there are any challenges with the balancing, what are the options for solving the issue; these could lie in altering the balancing and build methods, or possibly altering the basic rotordynamics of the rotor through a design or manufacture change.

This chapter begins by introducing the basic concepts behind the method, introduces the method itself, then gives some examples of how it would be used on a real rotor design, using data from a real engine. This includes some validation cases performed by analysis on a Rolls-Royce WEMM.

5.2 Low Speed Balancing

Figure 18 shows static unbalances u_i distributed along a rotor at corresponding stations x_i where $i=1$ to j total unbalances. Axial distance along the rotor is denoted x. The rotor is simply supported at axial locations x_f and x_r, and being balanced by the addition of eccentric correction weights at the rotor support locations. In this thesis, complex numbers are used to represent the vector quantities of unbalance in a radial plane, where the real part signifies the horizontal plane, and the imaginary part represents the vertical plane as shown in the figure. Note that the convention is that the front of all rotors is drawn on the left, and this is the convention adopted throughout this thesis.

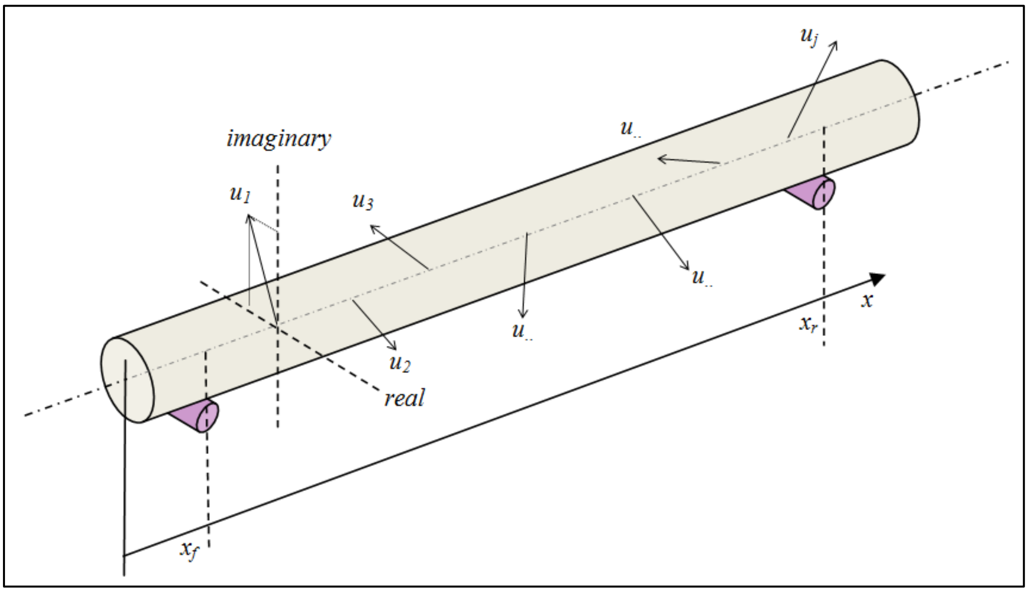

Figure 18: Rotor Unbalance Distribution

Column vector $\tilde{\mathbf{u}}_s$ represents the static unbalances as vector quantities at q stations along the length of the rotor represented as complex numbers (imaginary values representing the vertical plane and real values representing the horizontal). Column vector $\mathbf{x}$ contains their corresponding real valued axial locations, and therefore also has a length q. When a low speed balancing machine calculates the amount of correction to apply to the correction planes, it solves the following equations simultaneously for the complex forces at the locations x_f and x_r, so that the equivalent unbalance correction masses can be applied at these locations. These unbalance correction quantities are represented as single valued complex quantities $\tilde{f}$ and $\tilde{r}$. If we let $\mathbf{z}$ be a column vector of ones with a length q then,

$$\tilde{f} + \tilde{r} + \mathbf{z}^T \cdot \tilde{\mathbf{u}}_s = 0 \tag{5.1}$$

and

$$\tilde{f} \cdot x_f + \tilde{r} \cdot x_r + \mathbf{x}^T \cdot \tilde{\mathbf{u}}_s = 0 \tag{5.2}$$

It should be noted however that the low-speed balancing machine does not have any information about the individual elements of vector $\tilde{\mathbf{u}}_s$ or $\mathbf{x}$, only the total effects of the summed forces acting at the bearing locations.

5.3 The Principle of Linear-Superposition Applied to the Dynamic Response of Rotor Unbalance Distributions

Any distribution of unbalance along the rotor can be represented assuming static unbalances applied on a distribution of thin slices. This includes couple unbalances arising from misaligned thin discs that can be represented by equal and opposite static unbalances on adjacent rotor "slices".

If the real valued response amplitude is denoted 'a', and a vector $\tilde{\mathbf{k}}_u$ is defined comprising the complex response coefficients to each individual unbalance $\tilde{\mathbf{u}}_{s(i)}$ along the rotor, the following equation can be written to define 'a':

$$a = \left| \tilde{\mathbf{u}}_s^{\ T} \cdot \tilde{\mathbf{k}}_u \right| \tag{5.3}$$

The coefficients of $\tilde{\mathbf{k}}_u$ are generated from experiments on a dynamic rotating system or validated WEMM of a system, where unit static unbalances are individually applied to all the corresponding $\mathbf{x}_{(i)}$ locations along the rotor. The response is measured or calculated for a particular sensor (i.e. displacement / force) at a particular fixed location (i.e. centre of rotor/a bearing/a location on the supporting structure) at a constant speed. The values of $\tilde{\mathbf{k}}_u$ are dependent on speed, therefore a is only valid at the speed that a particular $\tilde{\mathbf{k}}_u$ is calculated.

In the case of aerospace gas turbine rotors, the speeds of most interest for rotordynamics are the critical speeds. At rotor speeds between the critical speeds, the vibration due to unbalance forcing is generally low. Therefore, if running at, near, or through critical speeds was not a requirement, then balancing would probably not be required at all on components that have been manufactured to aerospace tolerances. Consequently, the focus of any optimisation of rotordynamics or balancing is the critical speeds in the operating speed range. A margin is usually applied to the maximum speed to allow for transient speed excursions and inaccuracies in WEMM frequency predictions. A typical response curve is given in Figure 19 below.

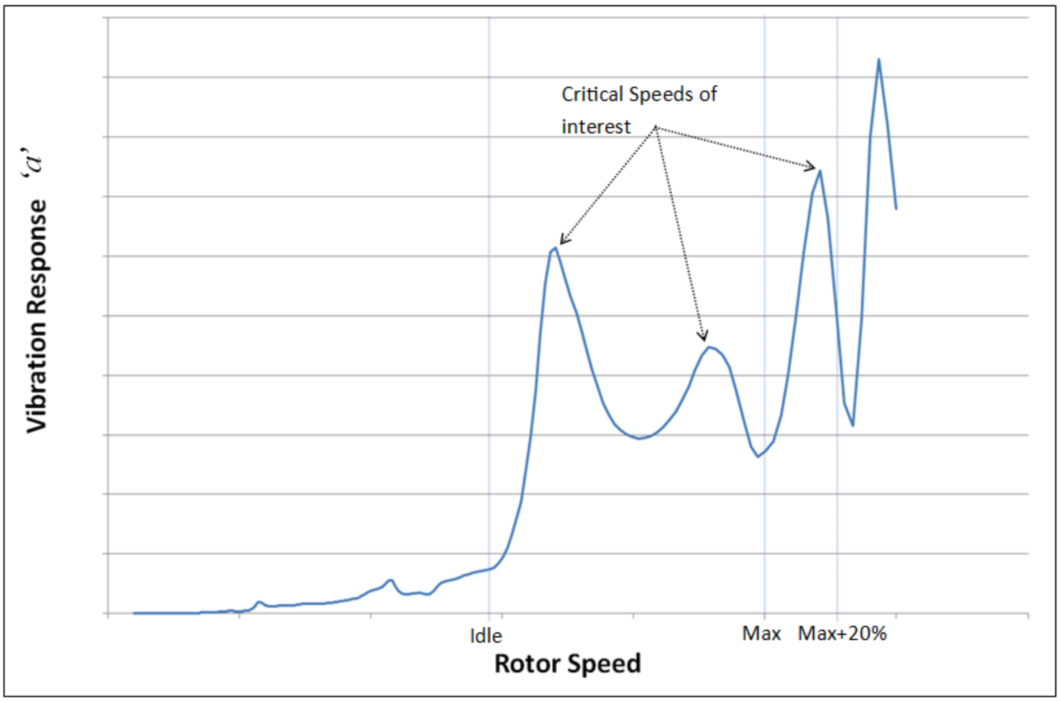

Figure 19: Typical aerospace gas turbine vibration response to unbalance with key critical speeds indicated

5.4 The Unbalance Response Function

The term Unbalance Response Function (URF) is used in this study to describe $\tilde{\mathbf{k}}_{u(i)}$ as a function of $\mathbf{x}_{(\mathrm{i})}$. An example plot of $\left|\tilde{\mathbf{k}}_{u(i)}\right|$ vs. $\mathbf{x}_{(\mathrm{i})}$ taken from a typical aero gas turbine WEMM of a HP rotor is shown in *Figure 20* below. The graph shows the operational deflection shape (ODS) of the rotor at this speed. The key point to note from the plot is that the URF can be seen to be non-linear with respect to x.

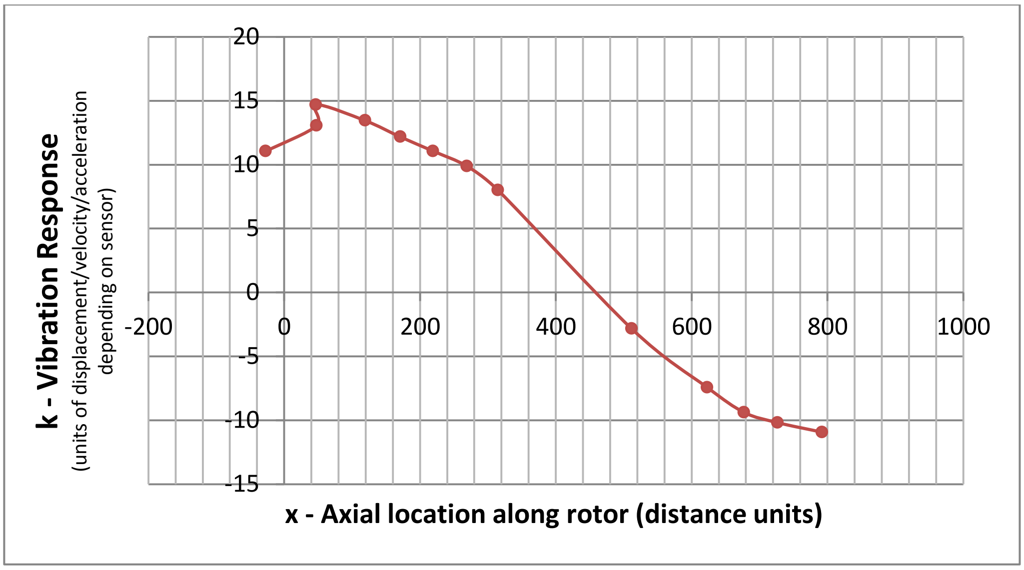

Figure 20: An Unbalance Response Function from a rotor on resonance displaying flexibility ($\mathbf{k}_n$ vs. $\mathbf{x}_n$)

At rotational speeds which are remote from the rotor resonances, a rotor can be said to be behaving in a pseudo-rigid state. In which case, $\tilde{\mathbf{k}}_{u(i)}$ are linear with respect to $\mathbf{x}_{(\mathrm{i})}$ axial locations, that is, eq. 5.4 is satisfied and $\left|\tilde{\mathbf{k}}_{u(i)}\right|$ vs. $\mathbf{x}_{(\mathrm{i})}$ would generate a straight line in a complex vector space; the subscript L is added to $\tilde{\mathbf{k}}$ to indicate linearity.

$$\tilde{\mathbf{k}}_L = \tilde{b} \cdot \mathbf{x} + \tilde{c} \tag{5.4}$$

As the rotor in the low-speed balancing machine is behaving rigidly, the balancing correction that is applied to the rotor is effectively determined by a URF with a linear relationship. It is demonstrated below in equations 5.5, 5.6 and 5.7 that, the balancing result will produce a theoretical result of zero vibration for any $\tilde{\mathbf{k}}_L$.

In equation 5.5 below, the two complex single plane unbalance corrections that were determined on a low-speed balancing machine (effectively from equations 5.1 and 5.2), have been separated from the $\tilde{\mathbf{u}}_s$ vector and are represented as single valued complex correction quantities $\tilde{f}$ and $\tilde{r}$ along with their corresponding complex unbalance responses, $\tilde{k}_f$ and $\tilde{k}_r$:

$$a = \left| \tilde{f} \cdot \tilde{k}_f + \tilde{r} \cdot \tilde{k}_r + \tilde{\mathbf{u}}_s^T \cdot \tilde{\mathbf{k}}_u \right|. \tag{5.5}$$

Assuming linearly related unbalance responses (all the $\tilde{k}$ values), $\tilde{\mathbf{k}}_L$ from eq. 5.4 can be substituted into eq. 5.5 to give:

$$a = \left| \tilde{f} \cdot \left(\tilde{b} \cdot x_f + \tilde{c} \right) + \tilde{r} \cdot \left(\tilde{b} \cdot x_r + \tilde{c} \right) + \tilde{\mathbf{u}}_s^T \cdot \left(\tilde{b} \cdot \mathbf{x} + \tilde{c} \right) \right| \tag{5.6}$$

where x_f and x_r correspond to the axial locations of unbalance corrections $\tilde{f}$ and $\tilde{r}$ respectively.

Rearranging eq. 5.6 and once again letting $\mathbf{z}$ be a column vector of ones the same length as $\tilde{\mathbf{u}}_s$ gives

$$a = \left| \tilde{b} \cdot \left(\tilde{f} \cdot x_f + \tilde{r} \cdot x_r + \mathbf{x}^T \cdot \tilde{\mathbf{u}}_s \right) + \tilde{c} \cdot (\tilde{f} + \tilde{r} + \mathbf{z}^T \cdot \tilde{\mathbf{u}}_s) \right|. \tag{5.7}$$

It can be seen that the two pairs of parentheses in equation 5.7 are identical to equations 5.2 and 5.1 respectively. Therefore, when equations 5.1 and 5.2 are satisfied (i.e. the rotor is rigidly balanced) both the parentheses in eq. 5.7 will be zero. This shows that the complex constants $\tilde{b}$ and $\tilde{c}$ will not influence the dynamic response amplitude (a) when the rotor is rigidly balanced, provided that the URF is linear. This means that the balancing of a rotor in its rigid state is valid at speeds when the rotor is sufficiently rigid, but incorrect when it is not. It also shows that, because $\tilde{b}$ and $\tilde{c}$ are functions of the support structure, the balancing is independent of the modes of the supporting structure response (when the rotor is rigid).

If the non-linear URF (with respect to x) of a rotor at high speed in an engine is denoted $\tilde{\mathbf{k}}_{hs}$ and the linear URF of the balancing machine mounted rotor at low-speed is denoted $\tilde{\mathbf{k}}_{bal}$, it is clear that they will not produce the same response (*a*) if individually substituted for $\tilde{\mathbf{k}}_{bal}$ in eq. 5.3 given the same unbalance distribution ($\tilde{\mathbf{u}}$). Therefore, in order to assess how successful a low-speed balancing process will be, it is necessary to understand the magnitude difference between $\tilde{\mathbf{k}}_{hs}$ and $\tilde{\mathbf{k}}_{bal}$ for any given unbalance distribution. However, because $\tilde{\mathbf{k}}_{hs}$ and $\tilde{\mathbf{k}}_{bal}$ are responses to different systems (i.e. engine structure versus balancing machine), it is not simply a case of calculating '*a*' from $\left|\tilde{\mathbf{u}}^T \cdot (\tilde{\mathbf{k}}_{hs} - \tilde{\mathbf{k}}_{bal})\right|$ as might be expected when considering eq. 5.3. Because $\tilde{\mathbf{k}}_{bal}$ is known to be a linear URF, we know from the discussion above that it can be represented by *any* linear URF ($\tilde{\mathbf{k}}_L$). The fact that the balancing machine has determined balance corrections $\tilde{f}$ and $\tilde{r}$ to counter-balance all the other unbalances along the rotor using a linear URF, means that it is the difference between a calculated linear URF ($\tilde{\mathbf{k}}_{bal}$) and $\tilde{\mathbf{k}}_{hs}$ where <u>the response coefficients are made equal at the unbalance correction planes</u>. To clarify this statement : if a linear URF is derived which has equal elements to $\tilde{\mathbf{k}}_{hs}$ at rotor locations x_f and x_r is determined and denoted $\tilde{\mathbf{k}}_L$, the relationships can be expressed as

$$\tilde{\mathbf{k}}_{L(f)} = \tilde{\mathbf{k}}_{hs(f)} \tag{5.8}$$

and

$$\tilde{\mathbf{k}}_{L(r)} = \tilde{\mathbf{k}}_{hs(r)}, \tag{5.9}$$

where the bracketed subscripts refer to the element of the URF which corresponds to the unbalance correction plane at x_f or x_r.

The full complex vector $\tilde{\mathbf{k}}_L$, which is the length of the total number of axial rotor stations represented (q), can be calculated from the following: Equation 5.10 below determines the slope of linear complex matrix from the balance correction plane responses in $\tilde{\mathbf{k}}_L$ with respect to $\mathbf{x}$

$$\tilde{b} = \frac{\partial \tilde{\mathbf{k}}_L}{\partial \mathbf{x}} = \frac{\tilde{\mathbf{k}}_{hs(r)} - \tilde{\mathbf{k}}_{hs(f)}}{\mathbf{x}_{(r)} - \mathbf{x}_{(f)}} . \tag{5.10}$$

Equation 5.11 then finds the single valued complex constant offset for $\tilde{\mathbf{k}}_L$

$$\tilde{c} = \tilde{\mathbf{k}}_{hs(f)} - \frac{\partial \tilde{\mathbf{k}}_L}{\partial \mathbf{x}} \cdot \mathbf{x}_{(f)} , \tag{5.11}$$

$\tilde{\mathbf{k}}_L$ can then be calculated from equation 5.4.

The amount of vibration resulting due to the differences in response functions (a_{error}), can be determined from a small adaptation to eq. 5.3 giving

$$a_{error} = \left| \tilde{\mathbf{u}}_s^T \cdot (\tilde{\mathbf{k}}_{hs} - \tilde{\mathbf{k}}_L) \right| . \tag{5.12}$$

This is one of the key findings of the URF methods; there has never been a predictive numerical way of defining how rigid a rotor needs to be in terms of its output response. This is discussed further in chapter 7.

During the simulations that were done on 5 different engine WEMMs as part of this study, it was observed that the complex responses of $\tilde{\mathbf{k}}_{hs}$ tended to lie close to one axial plane when on resonance. This is a key finding about the URF design methodology because it means that the URF can be plotted on a 2D graph which can be printed onto a piece of paper and lines can be drawn on it to visually weigh up the early design decisions being made. In order for a URF to be plotted in 2D and remain meaningful to the design process, the phase of the unbalance responses along the rotor relative to the applied unbalance must lie in or near a single plane (+/-20° is recommended, giving a ~ +/-7% magnitude error). In all of the rotors studied during the development of this method, a speed at or very near the key resonances could be found that satisfied this requirement. This observation is also independently confirmed by a comment from the Schenk Balancing Technology handbook (Schneider, Balancing Technology, 1991) section 2.4.3.5, where the Author states "In practice, rotor damping is so small that the mode deflection falls into one axial plane". If a particular rotor does happen to show responses outside of this angular phase limit, the graph would need to be generated in 3D in a capable computer program such as Matlab. The methods described below for the use of the URF graph would be very similar, but would not be possible to perform on a piece of paper. This 3D method is not described in detail in this thesis as it has been found to be unnecessary on the rotors considered to date.

The high-speed URF is based on an operating deflection shape as opposed to a natural mode shape. This is a very important feature of this process. The operating deflection shape is influenced by many factors in the engine other than the properties of the rotor being balanced. These include modes of the supporting structures, forces from other rotors interacting, and the dynamic properties of the bearings. In order to minimise a particular response, it is important that the operating deflection shapes are minimised.

In this chapter so far, the principles of the different URFs that are produced have been established with the significance of, and method for, determining the impact of the differences. Alongside this, the justification for being able to draw the modulus of the URF on a 2D graph when on resonance has been described. With these principles established, the next section goes on to describe the URF Rotor Design methodology.

5.5 The URF rotor design method

An example rotor design URF graph is shown in Figure 21. The graph is generated from a series of Steady State Forced Response (SSFR) analyses performed on the best available validated WEMM of the engine. The features of the graph are described below:

a) The '+' symbols are the magnitudes of the unit unbalance dynamic response vector $\tilde{\mathbf{k}}_{hs}$ that is: the amplitude of response at a single resonant speed at a constant response measurement parameter (e.g. force at one of the bearings), with each response plotted against the axial location $\mathbf{x}_{(i)}$ corresponding to where the unit unbalance was applied on the rotor.

b) The circle diameters proportionally represent the average unbalance distribution along the rotor that is likely to arise at the centre of gravity of each significant component or subassembly (i.e. disc assembly or shaft). The circles are representative of the magnitudes of the previously defined complex column vector $\tilde{\mathbf{u}}_s$. Note that the circles have no numerical scale on the graph. They are proportionally scaled relative to each other.

c) The vertical dotted lines show the boundaries of the two modules. To further emphasise this, the circles have been colour coded: blue circles are unbalances arising due to the HPC mass displacement, and the green the HPT unbalances.

d) A set of balancing planes has been labelled on the rotor using standard balancing notation : f_c and r_c for the front and rear locations on the compressor, and f_t and r_t for the front and rear locations on the turbine. The URF responses at these locations have been highlighted with arrows.

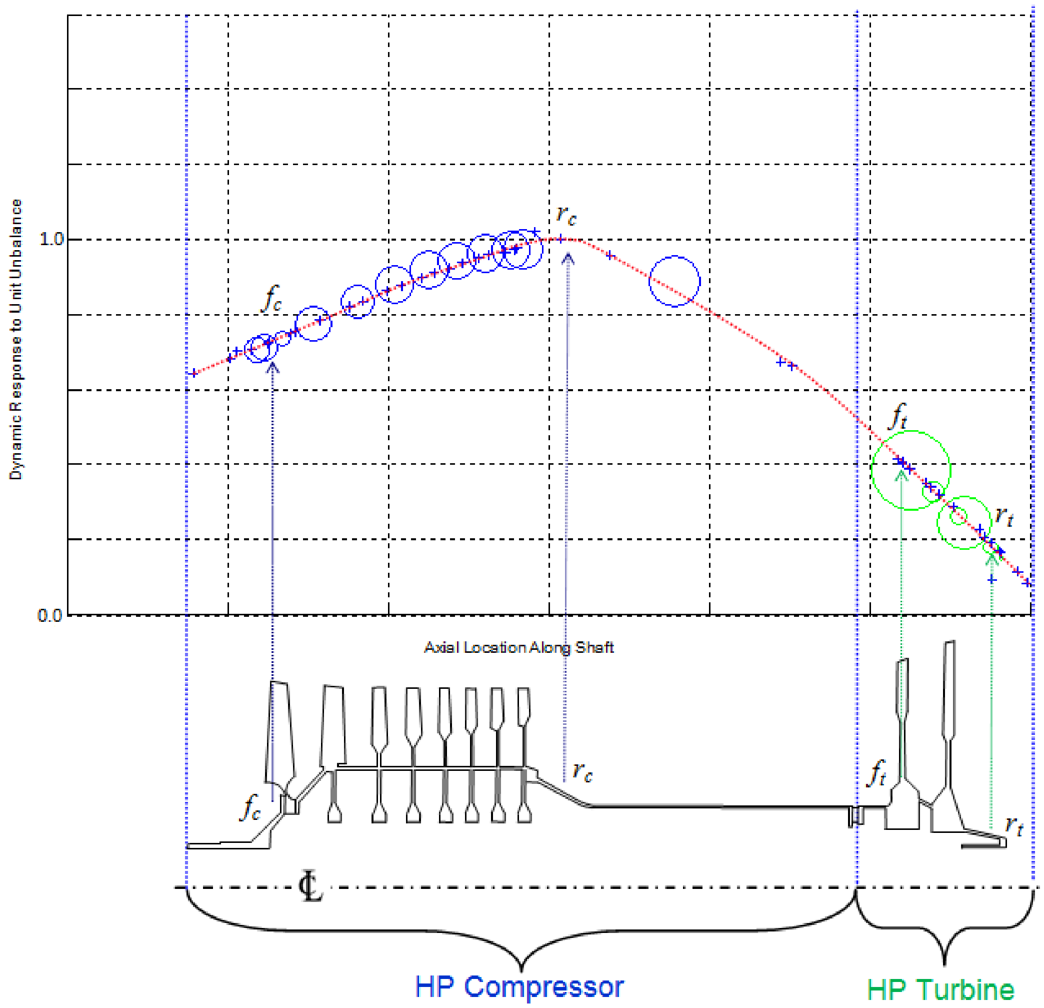

Figure 21: Description of an URF graph

There are a few points to note about the creation of the graph.

- Results are generated using the best available WEMM – with a dynamic representation of the supporting structure and other rotors.
- All results on one graph are for one output/sensor location.
- Results are at a selected resonant speed.
- The responses lie in one complex plane.

It is worth noting that this particular resonance has no zero crossings (that is, all responses are positive) because it is a rotor that is mounted on a relatively soft tuning spring at the front.

It is shown in section 0 that a linear URF ($\tilde{\mathbf{k}}_L$) can be determined and compared to the high speed URF ($\tilde{\mathbf{k}}_{hs}$) to calculate the vibration that would occur due to the difference between low-speed balancing and high speed flexible behaviour (a_{error}). The justification as to why the rotor deflections (and therefore the phases of the URF elements) will tend to lie approximately in one complex plane is also discussed. Because of these points, it is appropriate to represent a linear URF on a graph with the high speed URF, by constructing a straight line through the balancing corrections planes, as shown in Figure 22.

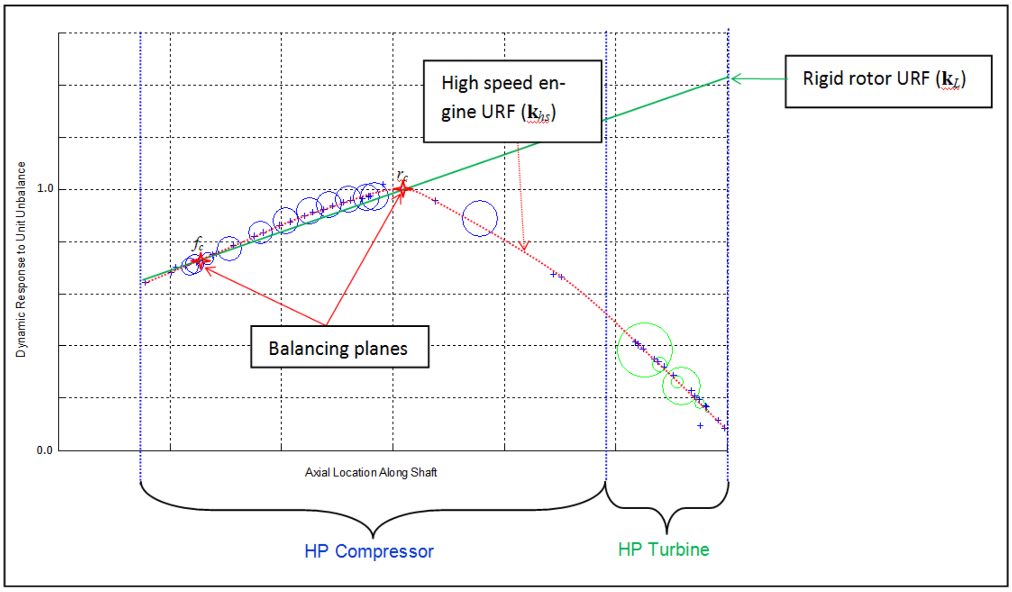

Figure 22: The URF graph showing k_L and k_{hs}

It can now be seen that all the terms that determine a_{error} from 5.12 are represented visually on the graph. This makes the graph into a very fast and powerful design tool for weighing up a multitude of options for rotor design, build and balancing; where the distance between the URF lines multiplied by the relative size of the circles can be considered as a "moment" and the general aim is to minimise the total moment using the practical options available.

This situation, where all the influencing factors can be visualised and their comparative importance understood with just the very rapid generation of one graph and the construction of some lines, should be contrasted to the current situation where the only official guidance was the conflicting guidance to “apply balance corrections near major masses” and “use mass simulators to represent major adjoining masses”.

As mentioned previously, all the coefficients in a dynamic URF have to be taken from only one sensor for the plot to be meaningful. The sensor measurement units can be force or displacement, but in the early design stages it is best to optimise for bearing forces. At this stage in the design the rotor and stator designs will not be finalised, a model of the casing structure may not be available and the vibration measurement locations on the casing will not be determined. However, any vibration response will have a primary load path through the bearings, so analysis of bearing loads gives the best possible representation of vibration response at this early design stage. Using the bearings means that there are multiple URF outputs to be considered (one for each bearing location), these should all be considered. Analysis of the URFs for the different bearing locations will tend to produce very similar conclusions (because they are a function of the same underlying mode shape) but may show emphasis on different parts of the rotor which can all be accommodated.

In the later design stages, the decision of what parameter to optimise is dependent on the requirements of the project. The most common retrospective use of URFs on existing designs is for pre-delivery engine vibration pass-off test rate improvement, in which case the response at the vibration sensor locations should be optimised. However if for example cabin noise was the main issue, then dynamic displacement and forces at the engine mounts should be considered.

In the development of this method, the initial aim was to develop an automated numerical optimisation process to minimise a_{error}. The variables that can be adjusted in a balancing and build process are very wide ranging. Modules can be balanced with or without mass simulators, with mass simulators with scaled properties, with long or short mandrels, with a combination of mandrels and simulators. Balance corrections can be applied at any number of balancing planes where the distribution between these planes can be determined through a wide variety of means (e.g. geometric measurements, knowledge of the manufacturing processes (see section 8.2), multiple simulators (see section 8.3), or more commonly, engineering judgement). The build alignment process, which involves the clocking of components relative to each other, also has a wide variety of options; two examples of which are covered in more detail in section 3.5. Rotor design variables are also important, such as where to put the inter modular joints, what is most appropriate tolerancing scheme, the required tolerance to achieve the required vibration levels, and the most appropriate joint type to achieve the required repeatability.

Capturing all these possible options of build, balancing, and rotor design options was extremely time consuming for one particular application and was eventually abandoned because it was clear that bespoke programming for every rotor of every new engine was going to be necessary. Therefore the process was not going to be fast or cheap enough to influence the rotor/structure design at the preliminary design stage which is the most cost-effective time. Therefore this graphing tool was developed to utilise the experiences of the user, but gave them much more information to make decisions and innovate solutions. This approach combined with a modelling process to test their decisions based on the graphs (see chapter 6) was determined to be the best solution.

5.6 Interpretation of URF Graphs

The optimisation of the engine Rotordynamics and Balancing is performed primarily at the resonances in the operating range. Secondarily it is performed at resonances in the sub idle or avoid-band ranges.

As described in section 0, the distance between the high speed URF and the linear URF lines multiplied by the relative size of the circles can be considered as a “moment” and the general aim is to minimise the total moment using the practical options available. Minimising the “moment” that is visualised effectively minimises the bending moments induced in the dynamically flexible regions of the rotor at the speed being analysed. There are two distinct areas to be considered when interpreting a URF graph, one is the looking at the region that is within the module being balanced, and the other is the region outside the module (the adjoining modules). They are considered separately because the practicalities of the modular requirements of an engine determine what can practically be done to minimise each.

Within the module, if the URF lines are close to each other, then a cost saving opportunity is identified because the assembly balance planes will adequately balance all the components or sub-assemblies that lie on the line. Conversely, if the URF lines are not close and the unbalance circles are significant, the unbalance at these points within the module needs to be controlled independently from the balancing with the assembly balancing features. A variety of methods are available to do this, such as component or sub assembly balancing, build alignment or tolerance control to minimise unbalance. Alternatively, the balancing planes could be moved in order to move the linear URF closer, and even modular break locations could be moved to allow a particular balancing plane location to be achieved that was originally in the other module.

Externally to the module being balanced, if the URF lines are close to each other and the unbalance circles are significant, this indicates the use of a full mass balancing simulator is appropriate to represent the adjoining module at this rotor speed. If the unbalance circles are very small, not using a mass simulator at all is likely to be the most appropriate and cost-effective solution. If the unbalance circles are significant and the URF lines are distant, then action must be taken to manage this error. One solution would be to use a modular straight build solution, possibly combined with component tolerance control. The use of a mass simulator with scaled properties could also be considered but the effects of this at other speeds should be carefully considered.

A case for special consideration on the URF graph is where components with a significant delta between their polar moment of inertia and their diametral moment of inertia cause localised couple unbalances on the rotor (reference eq. 3.2). In reality these components are the turbine discs and fan. The important factor to consider on the URF graph is whether the slope of the high speed URF line is the same where the unbalance couple arises (e.g. at the turbine) and the linear URF line through the balance correction planes. If it is not, then an error will arise.

The above descriptions can be summarised as a simple set of rules for interpretation of a URF graph that are summarised in table 1 below.

The Basic Rules of Use for a URF graph:

If…..	….. within module	….. in other modules
The unbalance responses lie on the straight line through 2 dynamic unbalance correction planes…..	No straight build or individual component balancing is required.	Full mass simulators can be used as per current balancing guidelines.
The unbalance response points do not lie on the straight line through 2 dynamic unbalance correction planes….	Other options to reduce the unbalance arising at these points should be considered i.e. component balancing, straight build, blade distributions etc.*	The use of mass simulators may or may not be appropriate, scaled mass simulators may be used (but are a compromise at other speeds).
Where the URF slopes (i.e. is not horizontal), the rotor response is sensitive to couple unbalances…	A method for correcting the couple unbalance must be used (i.e. two balance planes) and the slope between the correction planes and the couple unbalance source should be similar.	The slope between the correction planes and the couple unbalance source should be similar. If this is not the case than the scaled mass (and inertia) simulators can be considered.

Table 1. Basic rules for interpreting a URF graph

*Experienced balancing Engineers have innumerable methods for this. These were discussed in chapter 3.

These “rules” are demonstrated through their application to some example cases in the following sections.

5.7 Example 1: Compressor Balancing Evaluation

5.7.1 Scenario 1: Balancing planes at front and rear of an HPC module

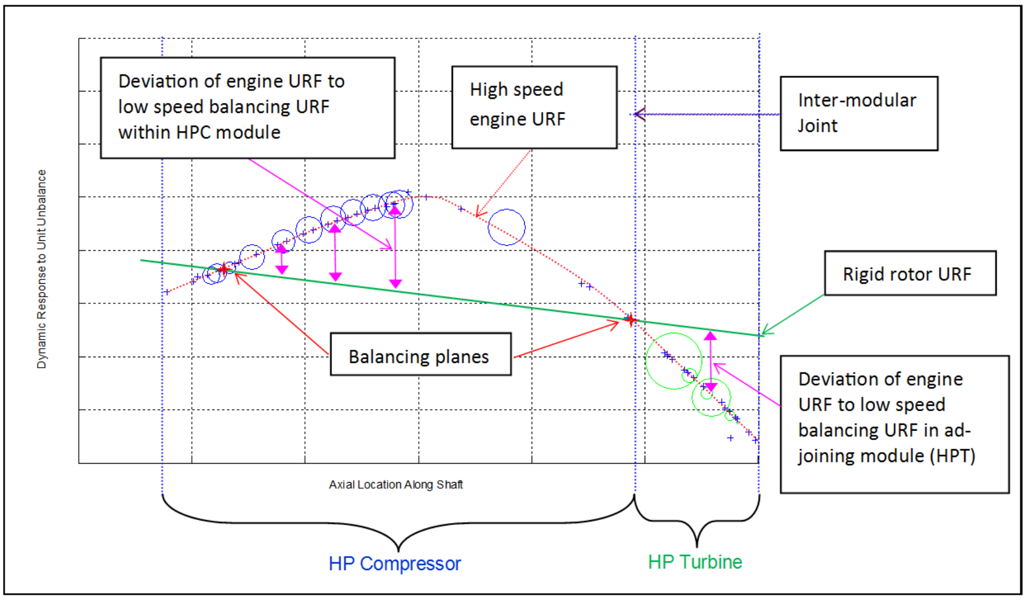

Figure 23: Example HP Compressor balancing approach: Scenario 1.

Figure 23 shows the URF for a real HP rotor with an HP Compressor (HPC) balancing procedure represented. The rigid rotor URF straight line passes through the front and rear balancing planes representing the relationship between the responses at the axial stations along the rotor on the balancing machine. The engine URF shows a deviation from the rigid URF within the HPC module therefore, if these balancing planes are used, options such as: component balancing, straight building the module, blade redistributions and three plane balancing should be considered in order to minimise the errors within the module (these would effectively make the impact of the balance errors (i.e. the circles) smaller).

In the module adjoining to the HPC (the HP Turbine) the URF shows that although balancing with a turbine mass simulator is appropriate because the turbine mass offset will cause a significant unbalance, it can be seen that the engine URF deviates from the rigid URF. This means that the use of a simulator with mass properties that represent the actual engine turbine would be inappropriate. This is covered in detail in section 5.9.

Furthermore, it can be seen that the slope of the engine URF through the HPT and the rigid URF are different. This will result in an error in the HPC unbalance correction to any unbalance couples generated by the simulator representing the HPT.

5.7.2 Scenario 2: Balancing planes at front and rear of compressor drum

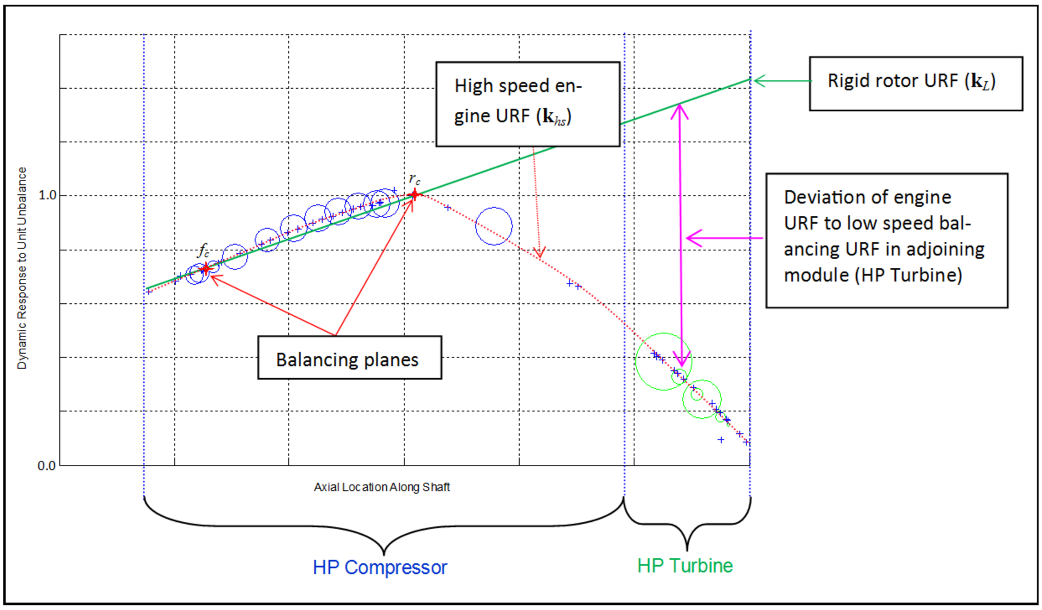

Figure 24: Example HP Compressor balancing approach: Scenario 2.

Figure 24 considers a different balancing procedure for the compressor, where it is balanced at the front and rear of the compressor disc stack changing the placement of the rigid URF line. It can be seen from the figure that the engine URF responses inside the HPC module lie much closer to the unbalance URF, therefore there is little or no requirement to minimise the unbalance in the individual disks (a significant cost saving compared to the current process where they are all balanced).

Conversely the rotor response at the centre of unbalance for the HPT is now much more distant from the rigid URF (approximately 75% lower, indicated by the magenta arrow on the graph). Therefore, at this speed, the unbalance from the turbine doesn't cause as much response as the linear relationship assumed between the rotor balancing planes on the balancing machine would assume. Therefore a scaled turbine mass balancing simulator may be required (see section 5.9), although this may present compromises at other speeds. Other options that would not compromise vibration at other speeds would include three plane modular balancing using multiple mass simulators (see section 8.3.1), or aligned build of the HPC module to minimise swash at HPT caused by the HPC inter-modular joint alignment.

5.8 Example 2: Using the URF to Make Balancing and Rotordynamic Design Decisions in Parallel

Figure 25 shows an URF graph for a real engine HP rotor system with a commonly used modular balancing approach. The rigid URF's for both the balancing of the HPC and HPT modules are represented through the current balancing planes for each. *Figure 26* gives one scenario that the Engineer is likely to explore because the URF analysis has led them to the conclusion that this would be a significant improvement. The design changes are listed below:

a) The modular break point has been moved to the engine URF point of maximum slope change, sometimes referred to as the modal "hinge" point .

b) The HPC rear balancing land has moved to the rear disc (adjacent to the new modular break)

c) The HPT front balancing land has moved to much further forward (made possible by (a))

d) The HPT rear balancing land has moved forward to be nearer the centre of mass of the turbine.

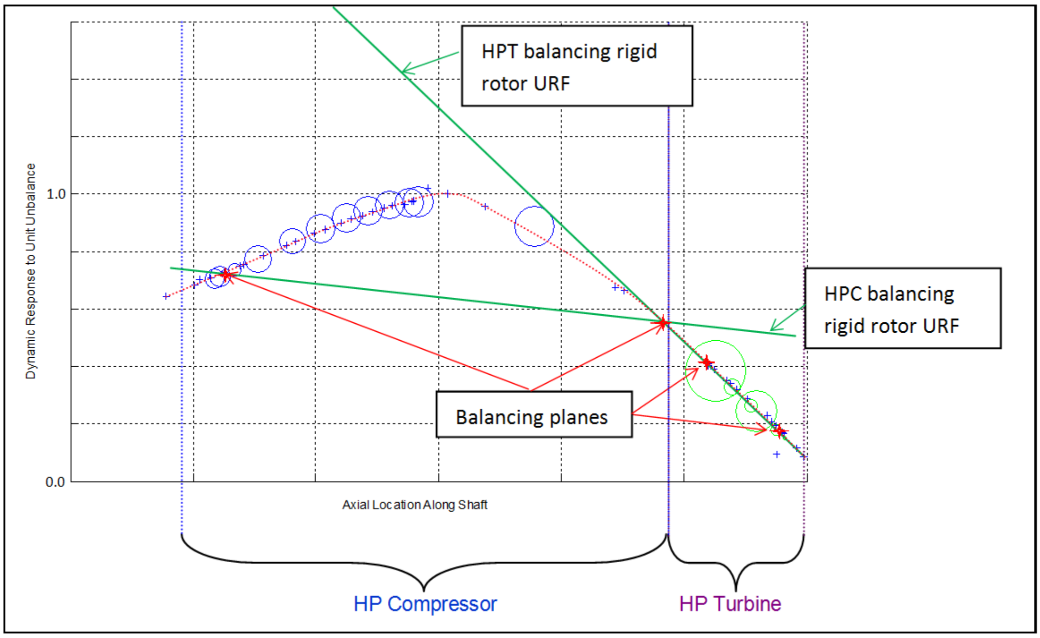

Figure 25: Example Engine Rotordynamic and Balancing Design

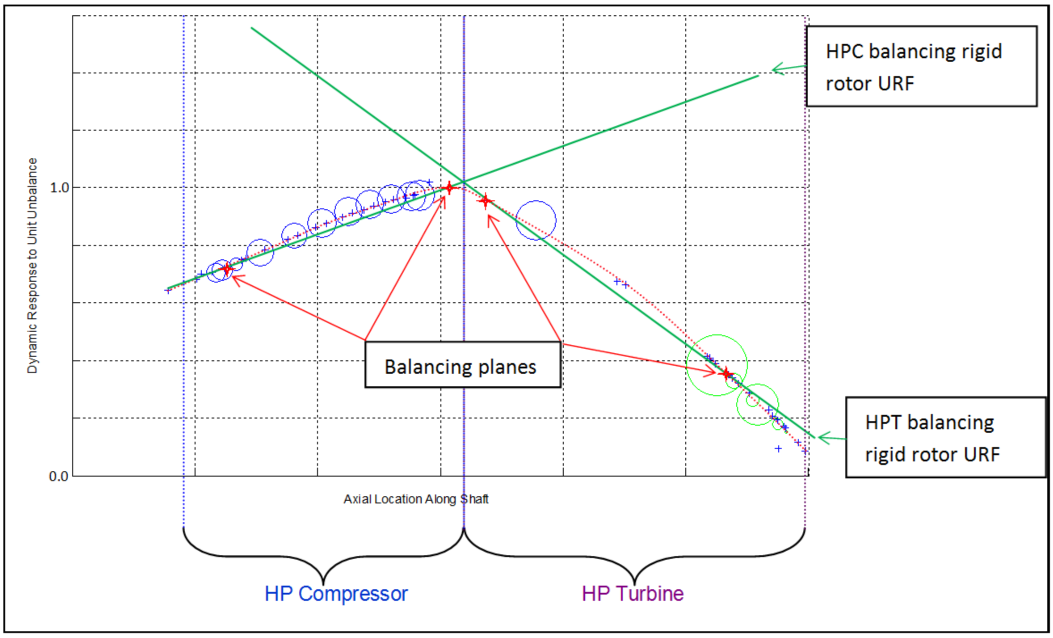

Figure 26: Proposal for reduced cost and vibration

The first thing to note about this design change is that within the individual modules, the engine URF and the associated module rigid URFs are almost aligned. This immediately means that all component balancing that is currently done (balancing individual discs and components, then weighing and patterning blade sets and swapping around blades and blade lock plates to balance the individual disc assemblies) can be deleted at a huge cost saving, because balancing can be adequately achieved at the assembly balancing planes (provided enough eccentric correction mass can be fitted/removed).

The main problem remaining with this arrangement is that if mass simulators were used in the balancing process, they would need to be scaled mass simulators, which means a compromise at other speeds/modes; this is discussed and illustrated further in section 5.10. One possible solution to this is to introduce an aligned build solution that focuses on minimising swash at the intermodular joint. This is achievable through a number of methods; straight build is commonly used in aerospace gas turbine assemblies to achieve the aim of the straightest rotor by measuring the variation in each component in the rotor and aligning the errors. If this process were re-targeted to achieve minimum swash at the module interface joint using the same methods, it would be likely to eliminate the need for balancing with simulators. One possibly cheaper solution would be to re-machine the joint face after assembly.

One side effect of moving the modular joint is to move a lot more material to the most responsive and highly strained position on the rotor. This will have two effects, one will be to lower the speed of the resonance due to moving mass to a more anti-nodal location (which is generally a positive move as forcing due to unbalance is a speed squared relationship, although care must be taken not encroach on dwell running speeds such as engine ground idle). The other will be to stiffen the area, increasing the resonance speed still further. This will mean that the URF graph should be regenerated to ensure that the optimisation is performed on the most valid state.

5.9 Example 3: Using the URF Graph to Estimate Scaled Balancing Mass Simulator Properties

The concept of balancing simulators is introduced in section 3.6.1. Traditionally, the mass and inertia properties of the simulator are determined based on the properties of the engine component that the simulator is representing on the balancing machine. However, if it is determined that at engine speeds the rotor's dynamic stiffness is having a significant effect on the balancing responses, a *scaled* mass simulator may be used to adjust the applied balance correction for the dynamic influence of that balancing simulator at an engine speed.

It should be noted however, that Scaled Mass Simulators should be used with caution. They improve the balancing for one mode/speed but are detrimental to the vibration response at all other speeds. Therefore, they are generally used as a last resort, after the engine design is fixed and cannot be altered.

The estimation of an optimum proportion for a scaled mass simulator can be made using the URF graph. This is helpful because it shows proportionally how far out the mass properties of the balancing simulator based on full engine component properties will be, but it also serves as a useful illustration of how the URF design method operates.

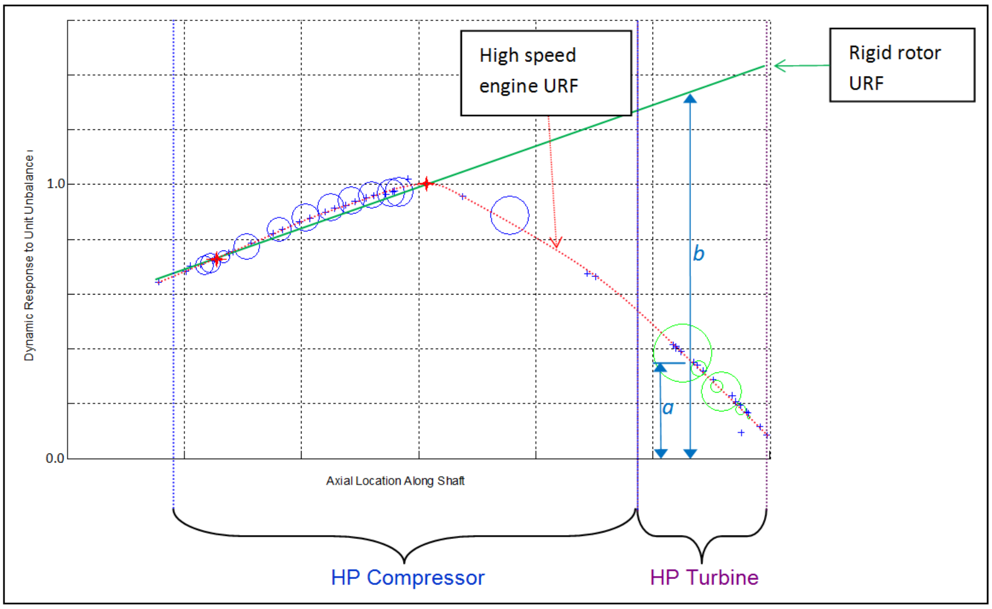

Figure 27: Prediction of mass simulator properties.

Figure 27 shows the URF graph for the balancing of the example HPC module (as shown previously in *Figure 24*), but adapted to show how scaled mass simulator properties can be estimated. It is possible to approximate the most appropriate mass properties by assuming that the centre of effort of the turbine unbalance occurs in approximately nearest the largest mass in the HP Turbine (the first disc stage). At this location it can be seen from the rigid URF that the low-speed balancing process would apply the equivalent of approximately 1.30 units of balance correction for a unit unbalance (labelled *b*), whereas the high speed URF shows that the engine would only generate 0.35 units for the same amount of unbalance at the same location (labelled *a*). Therefore, the unbalance correction process would tend to over-correct at this speed by a ratio of nearly 4 times (1.30/0.35≈3.8). One solution to this problem is to change the mass properties of the balancing mass simulator to reflect this situation. The optimum mass would be approximately 27% of the full turbine mass (0.35/1.3≈0.27). The effect of the simulator would be to cause the balancing machine to detect unbalance from the simulator in the proportion of the engine URF relationship between the HPT and the balancing lands, and therefore the corresponding corrections would be factored accordingly.

This is an approximate solution for the mass proportion of the simulator and the result should always be verified using the approach described in section 5.10.

5.10 Validation of URF Example 3: Scaled Mass Simulators

In order to provide an independent validation of the mass fraction for a scaled mass balancing simulator calculated from a URF, a series of Steady-State Forced Response (SSFR) analyses were performed on the validated WEMM.

The situation to be represented is given in *Figure 28*, where the joint alignment error (depicted here as swash) causes an offset of the HP Turbine centre of gravity. Because this unbalance is caused by a geometry error in the HPC, the unbalance correction should be applied to the HPC, ensuring that the error and associated correction remain together when the full engine is built. To facilitate this unbalance being captured during the HPC balancing, a balancing mass simulator representing the HPT is used during the balancing process. The bending moment graph in *Figure 28* shows the disadvantage of this approach where, if the rotor does not behave with sufficient rigidity throughout the speed range, the bending moment can drive a resonance that has bending of the rotor in its mode shape.

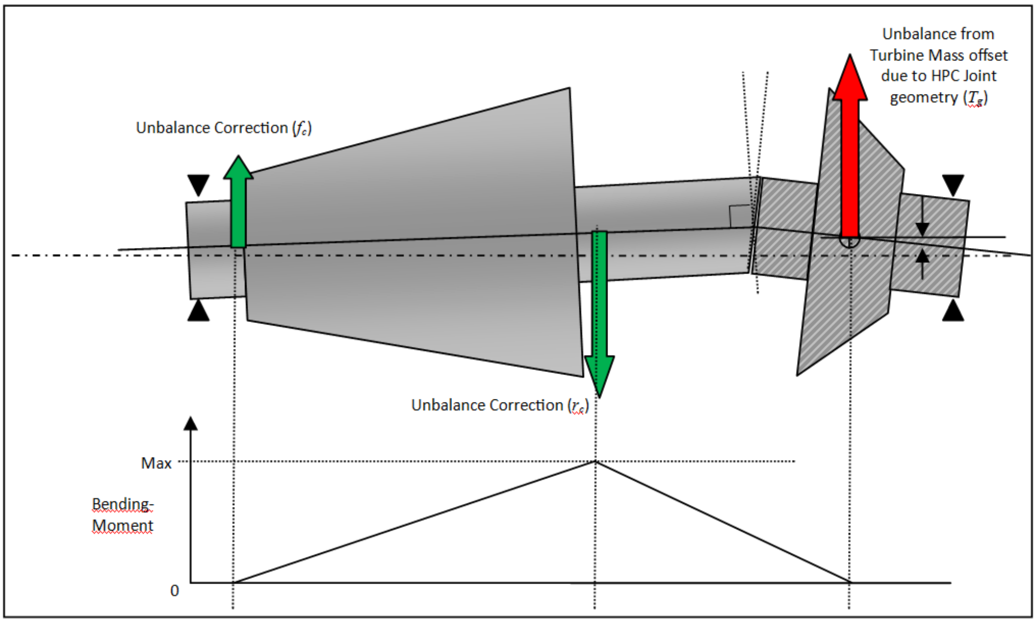

Figure 28: The HPC modular balancing process.

For each analysis setup a constant unit unbalance is applied at the adjoining module/balancing simulator centre of gravity (T_g). Then, using simple beam theory (i.e. simultaneously solving equations 5.1 and 5.2) the balancing correction that will be applied to the HPC correction planes (f_c and r_c) is calculated. Then the SSFR analysis is run with the set of applied unbalances responding throughout the engine operation speed range. For each subsequent SSFR analysis the applied unbalance corrections (f_c and r_c) are factored down proportionally through progressive steps, i.e. 90%, 80%, etc. but the applied unbalance at the HPT/simulator (T_g) remains constant. This method reflects the real situation where the properties of a balancing simulator are adjusted. The only thing that would change in the operating engine would be the applied corrections, the real HPT would still produce unbalance proportional to its full mass properties. The optimum solution is then found by inspecting the traces output from the analysis.

There are some simplifications being made for this analysis. Firstly the joint error influencing the HPT would produce some swash of the HPT itself, thereby forcing the HPT to generate an unbalance couple (see chapter 3, eq. 3.2). The engine URF graph in *Figure 27* clearly shows that the slope across the HPT is totally different (in fact opposite) to the slope of the URF line through the HPC balancing lands. Therefore the couple unbalance from the HPT centre (see) which is corrected on the rigid balancing process at the HPC balance lands, would not produce a cancelling response influence on 'a' (from eq. 5.3). This would normally cause residual vibration and the simulators inertia properties would need to be optimised in a similar fashion by applying a couple at T_g and analysing for various (F_c and R_c) factors. However, on this particular engine geometry, the inertia properties cause very little couple unbalance (i.e. $(I_p\text{-}I_d)\rightarrow 0$), so this serves as a useful simplified case for illustration on mass only.

The target is to minimise is the predicted vibration responses on the engine carcase at the locations of the vibration transducers, shown in *Figure 29* and Figure 30, targeting the response at the running speed that is most important (e.g. the main operation speed region). Because of the difficulty in accurately predicting vibration levels on the casings using a WEMM, the bearing loads are usually analysed as well as they are considered to be much more accurate and are plotted in Figure 31 and Figure 32.

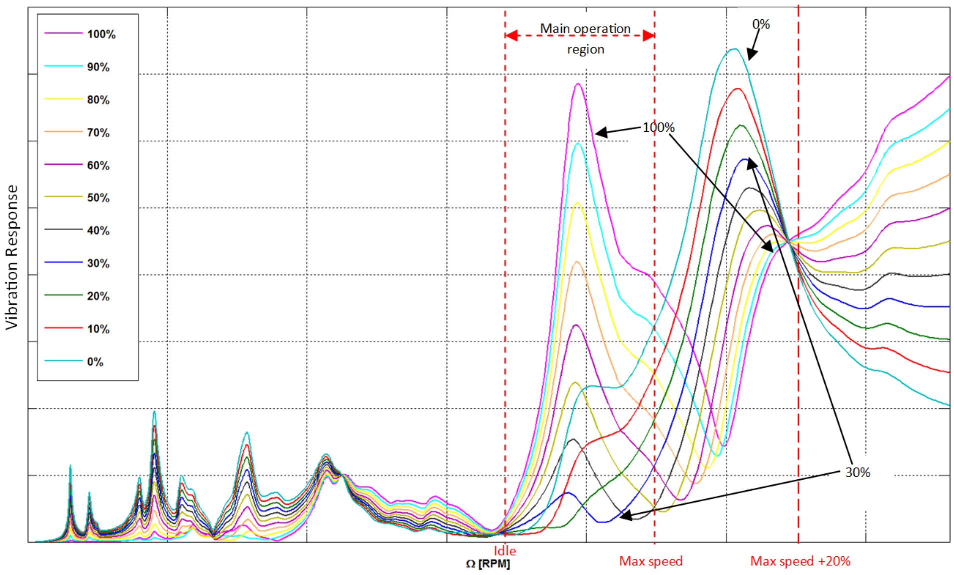

Figure 29: Relative front vibration transducer response to HPC balancing with scaled mass simulators of various reduced mass.

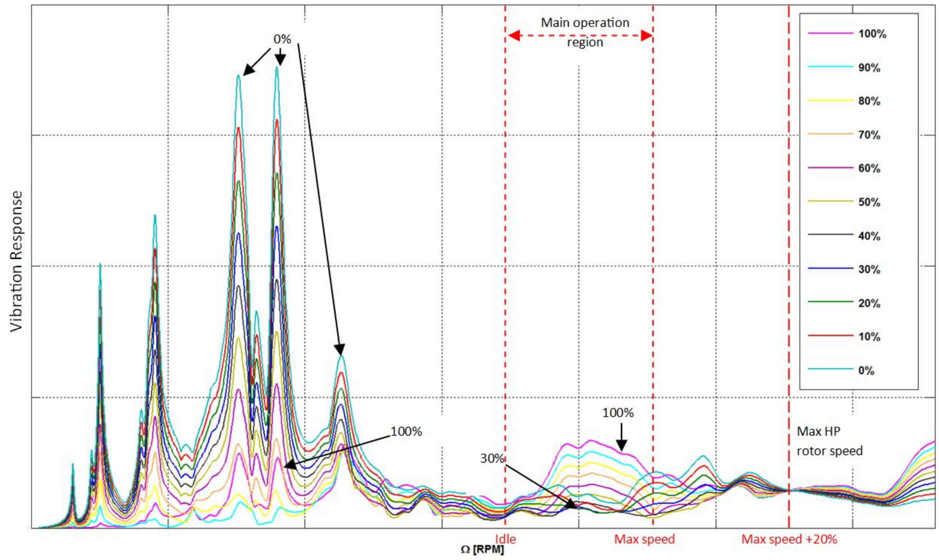

Figure 30: Relative rear vibration transducer response to HPC balancing with scaled mass simulators of various reduced mass.

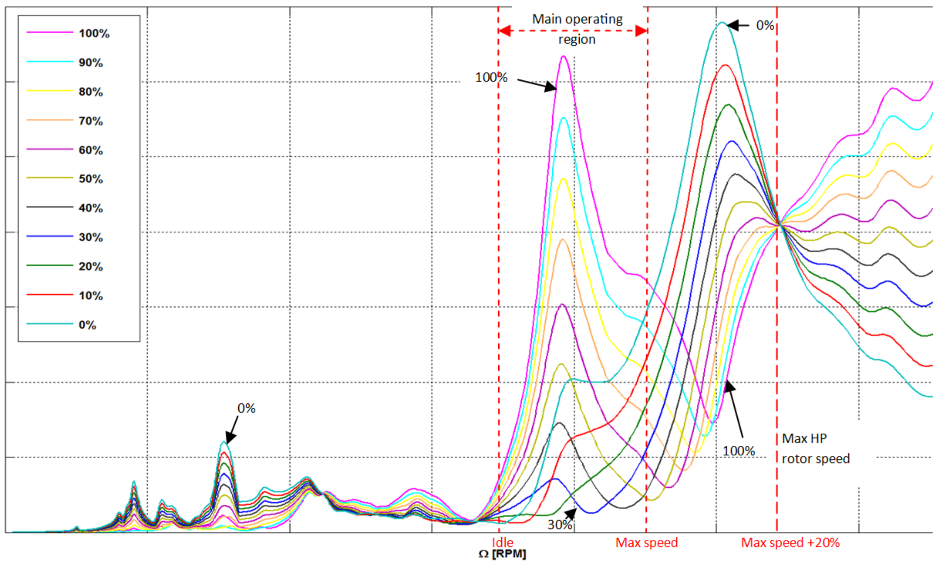

Figure 31: Relative force in front bearing due to HPC balancing with scaled mass simulators of various reduced mass.

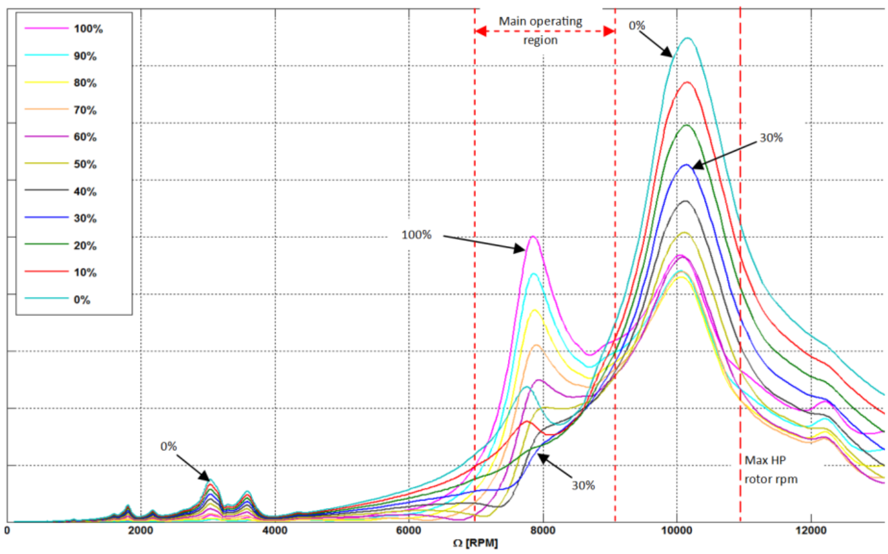

Figure 32: Relative force in rear bearing due to HPC balancing with scaled mass simulators of various reduced mass.

It is clear from the above figures that the optimum balancing simulator mass proportion in the main operation is ~30%, as predicted from the URF graph (~27%). From an engine design perspective there are 2 areas to highlight: firstly the sub-idle speed region on the rear vibration transducer looks very high with a <100% mass simulator, however the bearing loads in Figure 31 and Figure 32 show very small loads at these speeds which are below idle, so this must be a local casing resonance near the transducer and therefore is not of concern. Secondly, all of the graphs show that at the speed region between maximum and maximum+20% the scaled simulators would generally make the response significantly higher on the bearings. This is a significant concern and it highlights the need to assess the whole speed range if scaled mass simulators are used.

5.11 Chapter Conclusions

This chapter discussed the challenges of using low-speed modular balancing techniques on pseudo-rigid rotors. An "Unbalance Response Function" (URF) design tool, developed as part of this study, was introduced. This design tool takes the form of a graph, used together with a set of design rules, which can be used to make a large number of balancing related design decisions very quickly whilst taking into account the limitations of low speed balancing and the dynamics of the engine. Although this design tool can stand alone, to determine an optimum design it is intended that it is used in conjunction with the Rotordynamics Design Process (chapter 4) and the Monte-Carlo Software (chapter 6). One particular estimate that can be performed on the URF graph is the appropriate proportion of mass of a balancing simulator for a specific mode shape. As a verification exercise, this estimation was performed on a URF for two balancing operations with simulators and then the arising unbalances and balancing correction forces were applied to the WEMM to demonstrate the influence on vibration. The WEMM analysis was shown to agree with the URF estimation of the optimum mass for minimum vibration, offering some verification of the URF methodology and a demonstration of one aspect of its operation.

6 The Robust Rotordynamics Monte-Carlo Software

6.1 Introduction

Chapter 4 introduced the Robust Rotordynamics Design System and focussed on presenting the process part of that system. Chapter 5 introduced the Unbalance Response Function and its use as a preliminary analysis/design tool within that process. This chapter presents another of the analytical tools/methods that has been developed to facilitate the execution the Robust Rotordynamics Design process ensuring timely determination of an optimal design solution. This is in accordance with thesis objective (iii) from section 1.5, which emphasises the need for fast solutions because the greatest value can be gained from a design solution at minimum cost if it is introduced early in the design process.

At the heart of the Robust Rotordynamics Design System is a modelling method that can represent the key drivers for rotor dynamic design and model the balancing process to compare the effectiveness of each method for a statistically significant population of rotors. A simplified model called a “surrogate model” has been developed using a combination of unbalance response coefficients from the Whole Engine Mechanical Model and a geometric modelling technique that calculates the unbalance distribution along the rotor for a particular set of geometric errors and the associated applied unbalances from a low-speed modular balance process. This surrogate model has been packaged into a bespoke Monte-Carlo program with data analysis tools developed specifically for interrogation of rotor build and balance processes. This software is referred to as the “Monte-Carlo software” in this study. Section 4.2 shows where this analysis and software is embedded in the Robust Rotordynamics Design Process.

The aim of this chapter is to describe the methods used to create the surrogate model, the Monte-Carlo methods used, and the interrogation tools that were developed.

6.2 Description of the Surrogate Model

The surrogate model is fundamentally a combination of two modelling steps. Firstly, a geometric model is used to calculate unbalance distributions from geometric errors, and secondly the unbalance response coefficients are used to convert the unbalance distribution into a total vibration.

The geometric model takes the geometry of the rotor and associated component mass properties, that can have manufacturing tolerance effects imposed (i.e. on rotor joints) to determine the static rotor deflections that will occur. To generate the model, the rotor is divided into significant masses that have an axial length short enough to be approximated as rigid. Mostly this means that each disc stage is approximated as a rigid component, with shafts needing to be divided into sections to adequately represent their bending. The diagram in *Figure 33* a) shows an example component where the face tolerances (eccentricity and swash (“e_n” and “θ_n”)) are defined for each component relative to the reference frame of the mass properties. *Figure 33* b) shows a stick model representation of the component, and c) shows how the components are assembled together in a theoretical rotor and the offsets of each component are interdependent on each other.

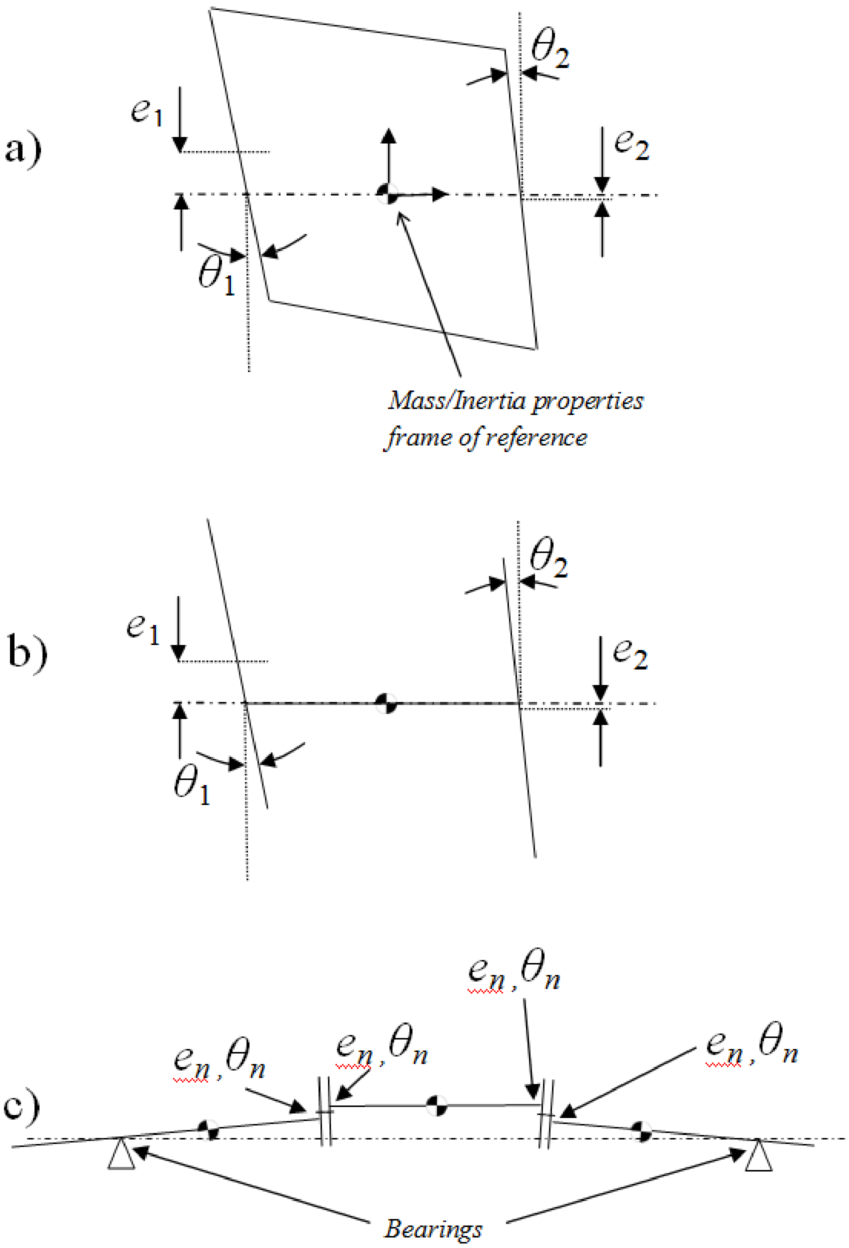

Figure 33: a) How rotor component joint face tolerances are defined, b) A representation of the component in (a) as a stick diagram, c) Simple rotor with three components on bearings.

In reality, for manufacturing purposes, the tolerances of faces are usually defined relative to each other because the inertial frame of reference is not an easily measurable quantity; however this definition relative to the inertial properties is useful because tolerance errors could also simulate the repeatability of the assembly of a single joint. Another method that was explored was introducing only one swash and eccentric error per joint instead of an eccentric and swash error per joint face, thereby halving the number of variables in the model. However, this method was abandoned when the early studies on rotors revealed a very important and counter-intuitive result that the two mating joint face tolerances could have very different sensitivities to vibration. This finding is explored further in section 6.3.1.

Figure 34 shows the detail of discretisation of a real engine rotor into geometry elements. The size of the elements is driven by two factors: firstly, every joint with a tolerance that controls the position of a significant mass in the real engine should be represented by a two faced joint with independently defined tolerances, and secondly, in the dynamic mode(s) of interest the rotor should behave approximately rigidly between joint faces. Some judgement is needed for the second factor, the flexible mode shape of interest for the rotor pictured in *Figure 34* is indicated by the URF graph pictured in *Figure 22* where it can be seen that the most major flexibility in this particular rotor in this mode is at the transition between the cone and straight shaft section at the rear of the HPC. The straight part of the shaft is not totally rigid in this mode, so it has been split into three parts as indicated in *Figure 34* b). Also of note in the diagram is the representation of the turbine blades. There are two reasons that they have been singled out for representation, firstly they are very heavy and at very high radius, and secondly because they have very large clearances in their blade roots due to clearances required for the thermal conditions in the turbine. Therefore it is useful to be able to assess the impact of these tolerances as the blades move around. It should be noted that as long as the discretisation of the rotor is sufficient to represent the general shape(s) of the key mode(s) and the major masses, the model will be adequate for the task. This is because the results from the model are compared relatively rather than absolutely.

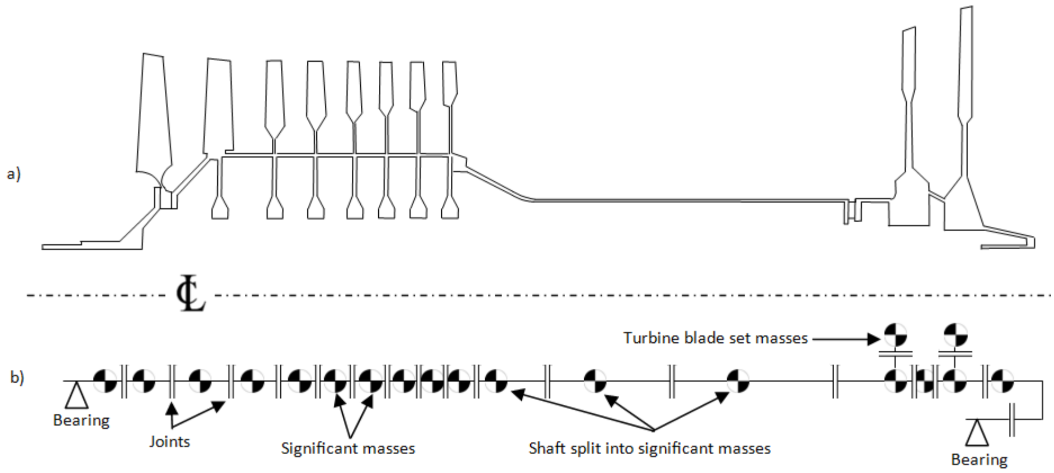

Figure 34: Example of typical rotor (a) discretised into rigid "stick" sections (b) for calculation of rotor static deflections.

In order to calculate vibration responses, the WEMM must be used to generate responses to unbalance at each major mass and at each potential balance plane for a defined set of sensor locations (i.e. vibration transducer on the casings or bearing loads). Section 5.3 describes the generation and use of these coefficients and defines equation 5.3 which is restated here for convenience[1]:

$$a = \left| \tilde{\mathbf{u}}_s^{\,T} \cdot \tilde{\mathbf{k}}_u \right| \tag{5.3}$$

where the real response amplitude is denoted 'a', and $\tilde{\mathbf{u}}_s$ is a complex column vector containing the static unbalance distribution for the rotor at all axial stations along the rotor defined in column vector $\mathbf{X}$. The coefficients of $\tilde{\mathbf{k}}_u$ are generated from a WEMM, where unit static

[1] This equation assumes that any distribution of unbalance along the rotor can be represented assuming static unbalances applied on a distribution of thin slices, as described in section 5.3. (This includes couple unbalances arising from misaligned thin discs that can be represented by equal and opposite static unbalances on adjacent rotor "slices").

unbalances are individually applied to all the corresponding stations along the rotor and the response is measured or calculated for a particular sensor (i.e. displacement / velocity / acceleration / force) at a particular location (i.e. centre of rotor/a bearing/a location on the supporting structure) at a constant speed. Note: the values of $\tilde{\mathbf{k}}_u$ change at different speeds, therefore a is only valid at the speed that a particular $\tilde{\mathbf{k}}_u$ is calculated.

A key element of the Monte-Carlo part of the Robust Rotordynamics process, is to make sure that optimisations made for one resonant mode using the URF assessment method are not significantly detrimental for resonances at other speeds. Therefore a vector $\tilde{\mathbf{k}}_u$ is generated for each speed of operation at a resolution appropriate to capture the resonant peaks of the system with reasonable accuracy. A resolution of 2Hz rotor speed increments was found to be sufficient for the models used by the author. This resolution would need to be reduced if low damped structures or low frequency modes are being considered. The matrix $\tilde{\mathbf{R}}_u$ is a concatenation of $\tilde{\mathbf{k}}_u$ vectors for every speed increment analysed, therefore each column represents a $\tilde{\mathbf{k}}_u$ vector at each speed increment and each row represents the axial station along the rotor with the axial location of these stations defined in the vector $\mathbf{x}$.

The unbalance distribution along the rotor is represented by the complex static unbalances in the vector $\tilde{\mathbf{u}}_s$. Initially the unbalances are calculated by simple geometric stacking of the rotor components at their joint interfaces, based on the swash and eccentricity at each joint face. Once the rotor stack up is geometrically assembled, the static unbalance distribution is calculated from the distance to the centreline (the centreline is determined by a straight line between the bearings) multiplied by the associated mass of that component, as defined in equation 3.1. Equation 3.1 is adapted into a complex form in eq. 6.1 to construct the complex unbalance column vector $\tilde{\mathbf{u}}_s$ from the column vector of real valued component masses $\mathbf{m}$ and the complex column vector of component eccentricities defined in $\tilde{\mathbf{e}}$.

$$\tilde{\mathbf{u}}_s = \mathbf{m} \times \tilde{\mathbf{e}}^T \tag{6.1}$$

As defined in eq. 3.2 (in chapter 3), the couple unbalances are generated from each component due to their inclination to the axis of rotation and their inertia properties. For eq. 5.3 to remain valid, all of the unbalance couples must be converted into static unbalances and included in $\tilde{\mathbf{u}}_s$. This can be done by calculating equal and opposite static unbalances on adjacent rotor components and adding them to the appropriate elements of $\tilde{\mathbf{u}}_s$, which is necessary if the WEMM finite element (FE) software being used cannot represent a unbalance couple at a single rotor node (which is the case with some software available). However, most rotordynamic FE software is capable of this, so an equivalent to vector $\tilde{\mathbf{k}}_u$, called $\tilde{\mathbf{k}}_c$ is generated representing the complex response to unit couple unbalances along the rotor so eq. 5.3 is updated to explicitly include the couple unbalances:

$$a = \left|\tilde{\mathbf{u}}_s^T \cdot \tilde{\mathbf{k}}_u\right| + \left|\tilde{\mathbf{u}}_c{}^T \cdot \tilde{\mathbf{k}}_c\right| \tag{6.2}$$

where $\tilde{\mathbf{u}}_c$ is a column vector containing complex unbalance couples at each component mass along the rotor, and a is the real dynamic response magnitude at the sensor where $\tilde{\mathbf{k}}_u$ and $\tilde{\mathbf{k}}_c$ were measured. If $\tilde{\phi}$ is a complex valued vector containing the angle of incidence of each component at the appropriate angular phase, and $\mathbf{I}_p$ and $\mathbf{I}_d$ are real valued column vectors containing the polar and diametral inertias of each component, then, in a complex valued development of eq. 3.2, $\tilde{\mathbf{u}}_c$ can be defined as

$$\tilde{\mathbf{u}}_c = \tilde{\phi} \times \left(\mathbf{I}_p - \mathbf{I}_d\right)^T . \tag{6.3}$$

The stacked rotor components (or modules) and associated measurements are shown in *Figure 35* simplified to a single plane. The measurements are indicated as complex because the actual measurements are taken as vectors in a complex plane. The subscripts indicate the component/module and therefore the corresponding element of the vector indicated.

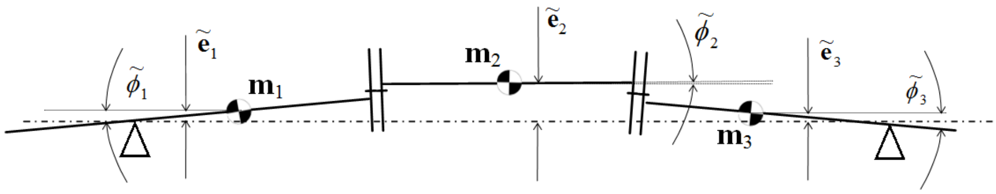

Figure 35: Alignment measurements from the assembled rotor model

From the above defined $\tilde{\mathbf{u}}_s$, $\tilde{\mathbf{u}}_c$, $\tilde{\mathbf{k}}_u$ and $\tilde{\mathbf{k}}_c$ it is possible to populate and calculate the dynamic response from eq. 6.2 for a single speed. If the $\tilde{\mathbf{k}}_u$ vectors for a range of speeds were horizontally concatenated into a matrix $\tilde{\mathbf{R}}_u$ as previously described and $\tilde{\mathbf{k}}_c$ vectors were similarly concatenated into matrix $\tilde{\mathbf{R}}_c$, then eq. 6.2 becomes

$$\mathbf{a} = \left|\tilde{\mathbf{R}}_u{}^T \cdot \tilde{\mathbf{u}}\right| + \left|\tilde{\mathbf{R}}_c{}^T \cdot \tilde{\mathbf{c}}\right|, \tag{6.4}$$

where $\mathbf{a}$ is a real valued column vector, each value being the dynamic response to $\tilde{\mathbf{u}}_s$ and $\tilde{\mathbf{u}}_c$ at the speed increments that were used to define $\tilde{\mathbf{R}}_u$ and $\tilde{\mathbf{R}}_c$. It is effectively a pseudo steady-state forced response analysis, with the forcing defined by the full unbalance distribution of the rotor.

6.2.1 Modelling the balancing process

Since the process of balancing is normally through the introduction or removal of radially offset weights at a limited number of axial stations along the rotor, the effects of the balancing process are modelled through the introduction of static unbalances on the rotor. If the rotor is assembled and mounted on the balancing machine in the same configuration and using the same bearing locations as it is in the engine, then the balancing correction calculations can be carried out solving eq. 5.1 and eq. 6.5 which assume rotor rigidity. Note that eq.6.5 is adapted from eq. 5.2 to explicitly include defined point couples, these were not necessary in the examples in chapter 4 because the couple unbalances had been included as equal and opposite offset static unbalances in the static unbalance distribution $\tilde{\mathbf{u}}_s$. 5.1 is repeated here for convenience,

$$\tilde{f} + \tilde{r} + \mathbf{z}^T \cdot \tilde{\mathbf{u}}_s = 0 \tag{5.1}$$

$$\tilde{f} \cdot x_f + \tilde{r} \cdot x_r + \mathbf{x}^T \cdot \tilde{\mathbf{u}}_s + \tilde{\mathbf{u}}_c = 0 \tag{6.5}$$

The complex single valued variables $\tilde{f}$ and $\tilde{r}$ are the balancing correction vectors applied at the front and rear of the rotor/module/component being balanced. Note that the front of rotors and rotor components are conventionally drawn on the left, and this convention is adopted in this study. Rearranging eq. 5.1 and eq. 6.5, the complex variables $\tilde{f}$ and $\tilde{r}$ can be found from

$$\tilde{r} = -(\mathbf{x} - x_f)^T \cdot \tilde{\mathbf{u}}_s + \tilde{\mathbf{u}}_c \tag{6.6}$$

$$\tilde{f} = -\tilde{\mathbf{u}}_s - \tilde{r} \ . \tag{6.7}$$

If $\tilde{\mathbf{u}}_{corr}$ is a column vector of zeros the same length as $\tilde{\mathbf{u}}_s$ (and therefore $\tilde{\mathbf{x}}$), then $\tilde{f}$ and $\tilde{r}$ are incorporated into $\tilde{\mathbf{u}}_{corr}$ at the element position where x_f and x_r axial coordinate values are found in the vector $\tilde{\mathbf{x}}$. Then a new unbalance distribution vector that includes the applied balancing corrections is defined as $\tilde{\mathbf{u}}_b$ and is calculated from

$$\tilde{\mathbf{u}}_b = \tilde{\mathbf{u}}_s + \tilde{\mathbf{u}}_{corr} \tag{6.8}$$

And the dynamic response of the system to the rotor that has been through the balancing process can be calculated by substituting $\tilde{\mathbf{u}}_b$ for $\tilde{\mathbf{u}}_s$ in eq. 6.4 giving

$$\mathbf{a} = \left|\tilde{\mathbf{R}}_u^{\,T} \cdot \tilde{\mathbf{u}}_b\right| + \left|\tilde{\mathbf{R}}_c^{\,T} \cdot \tilde{\mathbf{u}}_c\right| . \tag{6.9}$$

If balancing tooling is going to be used, such as mass simulators or mandrels, then a rotor model specifically to represent the build for the balancing process has to be used to calculate the unbalances applied to the component(s). The rotor shown in *Figure 35* has three rigid components or sub-assemblies, but to illustrate the modelling of modular balancing it is going to be treated as if component 1 was a module to be balanced with a mass simulator representing the presence of modules 2 and 3, therefore the properties of modules 2 and 3 have been combined into one set of properties with a subscript ‘t’ (for tooling), as shown in *Figure 36*. It is important to note the tooling has no geometric errors, it is only being offset from the centre of rotation by the geometric errors in component 1. This perfection in balancing tooling is not generated through manufacturing accuracy, but by performing a standard indexing process during balancing that mathematically eliminates errors generated by the geometry of the tool, but retains the unbalance caused by the presence of the mass properties. It is also important to note that the balancing corrections $\tilde{f}$ and $\tilde{r}$ are indicated on the component being balanced only, because they are applied to correct for errors in component 1, therefore they must remain with component 1.

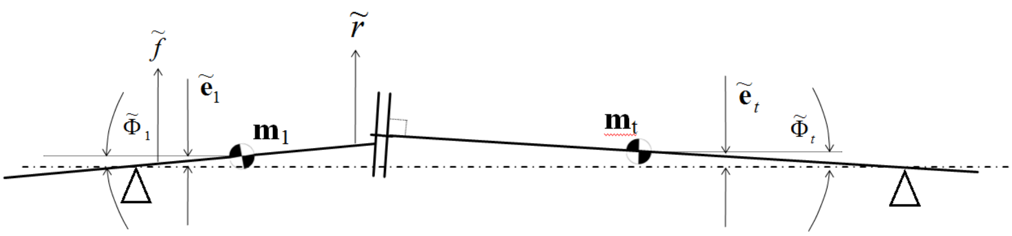

Figure 36: Surrogate model with balancing tooling

It should be noted that if the balancing is performed with simulators as defined above, the only output from the balancing process calculation that is retained for use in the dynamic response calculation is the balancing corrections. When the dynamic response is calculated, the unbalance distributions $\tilde{\mathbf{u}}_s$ and $\tilde{\mathbf{u}}_c$ must be calculated for the rotor as it is assembled into the engine for the calculation of the dynamic response. The calculated unbalance correction vectors, defined in vector $\tilde{\mathbf{u}}_{corr}$ above, must be added to these final state distributions, and the phasing must be taken into account if alignment operations have been carried out on the components or modules as described below. A $\tilde{\mathbf{u}}_{corr}$ vector specific to each component will be generated where a balancing operation is modelled and correction calculated and applied.

6.2.2 Rotor Build Alignment

Rotor build alignment is where the rotor components or sub-assemblies are clocked relative to each other to achieve some centreline alignment goal (see section 3.5 for more detail). When alignment operations are carried out during rotor builds, the parameters that need to be rotated to model effects of a rotation are the geometric errors at the joints and the calculated unbalance. In the surrogate model, the joint face errors of swash and eccentricity for the entire rotor are defined in complex coordinates and captured in column vectors $\tilde{\mathbf{j}}_s$ and $\tilde{\mathbf{j}}_e$. If $\tilde{\mathbf{j}}_{s,1}$ and $\tilde{\mathbf{j}}_{e,1}$ are a subset of the geometric errors of the rotor that represent the component tolerances in module 1, and similarly $\tilde{\mathbf{u}}_{corr,1}$ is the balancing correction vectors that were generated from the balancing operations on module 1. Then rotation of that module relative to the rest of the rotor by angle ψ (defined in radians) is achieved through the following three equations:

$$\tilde{\mathbf{j}}_{s,1} = e^{i\psi} \times \tilde{\mathbf{j}}_{s,1}\,, \tag{6.10}$$

$$\tilde{\mathbf{j}}_{e,1} = e^{i\psi} \times \tilde{\mathbf{j}}_{e,1}\,, \tag{6.11}$$

$$\tilde{\mathbf{j}}_{1} = e^{i\psi} \times \tilde{\mathbf{u}}_{corr,1}\,. \tag{6.12}$$

With these new vectors, the new rotor offset geometry can be determined, the $\tilde{\mathbf{u}}_s$ and $\tilde{\mathbf{u}}_c$ vectors can be created for the entire build rotor and the $\tilde{\mathbf{u}}_{corr,1}$ vector can be vertically concatenated with the other module balancing vectors to make the full rotor vector $\tilde{\mathbf{u}}_{corr}$ with all the balancing corrections for all the modules in the rotor. Then $\tilde{\mathbf{u}}_b$ can be calculated from eq. 6.8 and the dynamic response can be calculated from eq. 6.9. The actual value of ψ depends on the alignment scheme being adopted for that particular component/module and rotor. This is discussed further in the section 6.3.1 and the general issues and motivations behind build alignment are discussed in section 3.5.

6.2.3 Rotors with more than two bearings

The method described in the sections above relies on the construction of a rotor with geometric errors at the joints being theoretically assembled and then, by simple geometric calculations, the eccentricities and slopes of the centreline are determined. If a rotor were constrained by indeterminate bearing supports, i.e. three well-spaced bearings, this would not work because an assumption would have to be made as to whether the rotor would be stiffer than the bearing supports or vice versa, which would change the static deflections of the rotor. The problem is even more complex than the static stiffness, because throughout the speed range the relative dynamic stiffness of the rotor and structure will change.

In many FE rotordynamic analysis codes, it is possible to enforce a bend into a rotor and analyse the results. The bend can be imposed by defining a joint tolerance error (i.e. swash or eccentricity). With all of the bearing constraints modelled, the FE code will correctly determine the static deflection in the rotor and casing, and it will also correctly determine the dynamic deflections of both throughout the speed range. With some small adaptations, this analysis can be used to create a surrogate model that can be used with indeterminately mounted rotors. The following describes the approach.

Equation 6.2 is adapted to the following form:

$$a = \left|\tilde{\mathbf{j}}_s^T \cdot \tilde{\mathbf{k}}_s\right| + \left|\tilde{\mathbf{j}}_e^T \cdot \tilde{\mathbf{k}}_e\right| + \left|\tilde{\mathbf{u}}_{corr}^T \cdot \tilde{\mathbf{k}}_u\right| \tag{6.12}$$

Where $\tilde{\mathbf{k}}_s$ and $\tilde{\mathbf{k}}_e$ are complex column vectors, the same length as $\tilde{\mathbf{j}}_s$ and $\tilde{\mathbf{j}}_e$, now comprising the dynamic responses to unit joint errors of swash and eccentricity respectively. Note that because $\tilde{\mathbf{u}}_{corr}$ is a vector of mostly zero values, time could be saved by only generating unit unbalance response coefficients at the balancing lands positions to populate the $\tilde{\mathbf{k}}_u$ vector.

6.3 Description of the Monte-Carlo Analysis Software

The Monte-Carlo software was programed in Matlab. The main graphical user interface of the software is pictured for context in *Figure 37*. The zoomed part of the image on the right of the figure shows the three modes of operation ("Run Types") that were developed during trials of the analysis cycle, these modes are:

1. Main Effects
2. Monte Carlo
3. Input Set

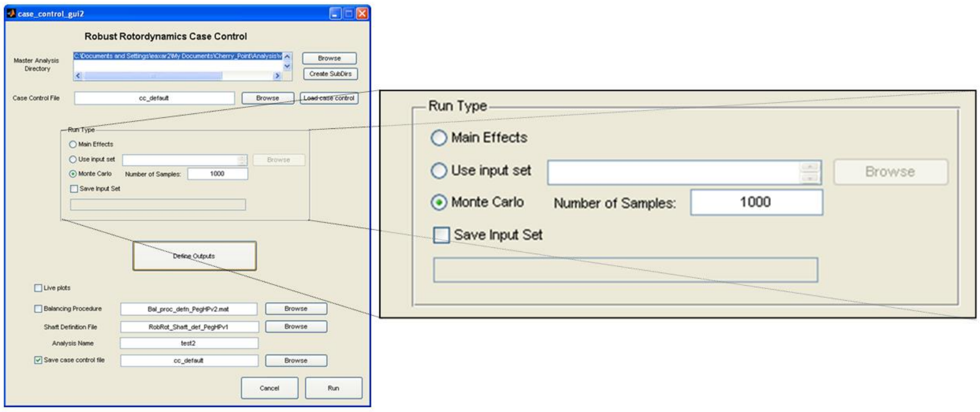

Figure 37: Monte-Carlo Software Main Graphical Interface

Each of these analysis modes is described in turn in more detail below.

6.3.1 Main effects analysis

The main effects analysis is where the dynamic response is calculated with each of the rotor joint tolerances set at their maximum value in turn. This analysis can be performed with or without balancing or alignment processes in place. It is informative at first to perform the analysis without any balancing operations so that the underlying sensitivity to joint tolerances is revealed. Subsequent analysis with balancing and build alignment schemes modelled reveals how well they are managing the most sensitive joints and which joints remain or become the key tolerances that are driving the peak dynamic responses. Balancing and build methods, and manufacturing tolerancing can all be explored with this knowledge.

Figure 38 shows the output from a main effects analysis performed on a WEMM containing the rotor pictured in *Figure 34*. This version of the rotor model had 17 joints in total, each joint has two faces, and each face has a swash and eccentricity tolerance as previously defined. On the graph, the joint faces (JF) are labelled sequentially from front to back of the rotor (JF1 to 34). Therefore joint face 1 is the adjoining face to joint face 2, as 3 is to 4, 5 is to 6, and so on. Note that the turbine blade locating joints shown in *Figure 34* were not included in this particular analysis. All results were taken at one resonant speed. The responses to maximum tolerance of eccentricity and swash at each joint are shown side by side with the eccentricities in blue (to the left) and the swashes in red.

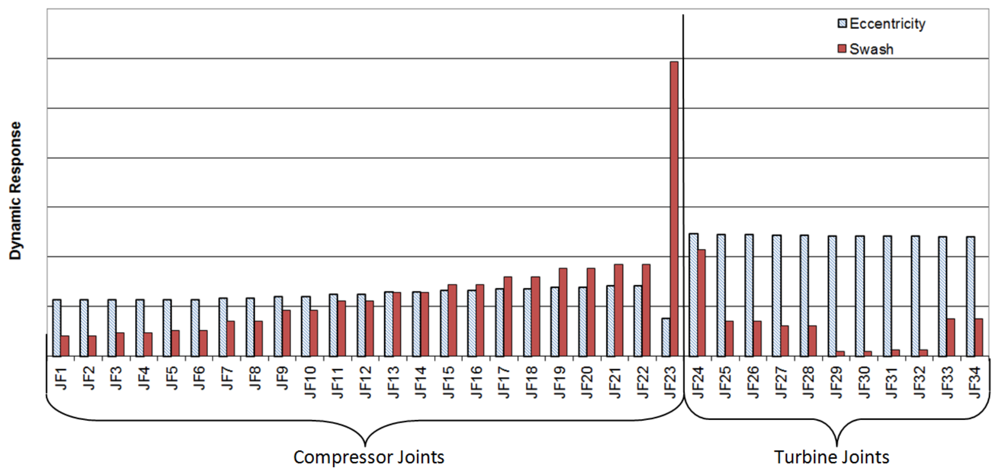

Figure 38: Main Effects Analysis Output Example

It can be seen that on the majority of joint faces, the sensitivity to tolerances on each mating pair of joint faces is the same for the same tolerance error; however on JF 23 and JF24 which are a mating pair, there is a significant difference in response sensitivity to both swash and eccentricity between the two sides. This joint can be seen at the rear of the compressor rear shaft where the compressor joins the turbine. This is the modular break point for this rotor, and the reason that the response is so different, is that this is the joint used to locate the modules when balanced.

This means that the unbalance effects of the tolerances of the left hand face are corrected for on the balance planes of the compressor, and the effects of the right hand face are corrected for on the turbine. Also, the left hand face offsets the mass simulator that represents the turbine during the balancing and the right hand face offsets the compressor, therefore they are balanced under entirely different unbalance distributions.

The most evident result from this output is that JF23 is very sensitive to swash, and insensitive to eccentricity. This has impacts on the tolerance of the compressor rear shaft, and the overall rotor build alignment scheme employed. Therefore the compressor shaft should be defined and manufactured so that the priority is on ensuring a minimal swash error between the end faces, and the straight build should focus on stacking up the rotor to minimise the resultant swash at this face when built. In the turbine it is clear to see that, excepting JF24, all the joints are more sensitive to eccentricity than swash, therefore the focus of a tolerance or build alignment scheme should be to minimise eccentricity in the turbine module.

This analysis can also be performed to aid design decisions. It is very clear that any joint swash errors occurring at JF23 will be very detrimental to the engine. Therefore a joint type that performs particularly well on minimising swash may be chosen above one that performs better on eccentricity. The curvic coupling is often assumed to be the most repeatable joint to use at modular interfaces. However, it is more difficult to machine a curvic coupling to a minimum swash than a simple face bolted flange joint with a spigot. In theory, a simple flange could even be machined square after rotor module assembly. A simple flange is also much easier to clean and maintain than a multi-toothed joint, and less prone to damage on assembly. Another option to explore may be to move the modular joint to another location, so that the sensitivities are reduced. The final decisions will be based on more influences than just the joint performance with respect to vibration, but this information makes the quantified vibration performance part of the design decision process, which is a new and valuable result of this method.

6.3.2 The Monte-Carlo Analysis

The Monte-Carlo analysis can be performed either with or without balancing and build alignment operations being performed. Monte-Carlo without balancing is recommended in step 3 of the Robust Rotordynamics Design Process outlined in section 4.2. The most important output at this step is the unbalance distribution along the rotor for input into the URF analysis (section 5), because it defines the size of the circles representing the arising unbalance on the graph. It also calculates the dynamic response from the rotor without aligned build and balancing, giving a vital reference point from which to test each process. Once the URF analysis is complete, the rotor balancing strategies determined can be tested and refined.

In order to perform an analysis using the Monte-Carlo software the user provides a number of inputs. Firstly, the geometry of the rotor such that the “stick” model (i.e. *Figure 34*) can be generated, which means axial joint locations, component axial centre of gravity, and bearing locations. Secondly, the unbalance response coefficients from the WEMM must be created to populate the $\tilde{\mathbf{k}}_u$ and $\tilde{\mathbf{k}}_c$ vectors for every speed increment of interest. Thirdly, the joint tolerances must be defined. Finally the balance and build alignment process must be defined.

The Monte-Carlo analysis randomly varies the joint error inputs, randomising the complex variables of the $\tilde{\mathbf{j}}_s$ and $\tilde{\mathbf{j}}_e$ vectors between executions of the surrogate model. The random function employed was a continuous uniform distribution. The more instinctive choice for a random distribution is the normal distribution, however when manufacturing with fine tolerances, the existence of a normal distribution is unusual. This is because, when achieving a dimension to a small tolerance, the manufacturer will tend to cut it oversized and then take very fine cuts until the dimension is within tolerance. This results in a tolerance distribution that is skewed to the maximum tolerance. Unfortunately no distribution data for joint swashes and eccentricity could be found or generated that could inform the most appropriate to use. Therefore, it has been assumed that a uniform flat distribution is achieved between the tolerance bands. This is an area where further investigation could improve the fidelity of these analysis outcomes.

The number of samples in the Monte-Carlo is selected by the user. The user needs to be sure that the number of samples is large enough to be representative of the entire population. The method adopted here for ensuring that a sufficient number of samples were used was to increase the population of samples progressively in increments 100. When the last two analyses produce similar results, the penultimate increment sample size is defined as the optimum size for the analysis. The author found that 200 samples was the usual required sample size on the models trialled, and the simulation would run in about 2 minutes on a standard laptop PC.

For each Monte-Carlo sample (or loop of the surrogate model), the software outputs the initial unbalance distribution, the final unbalance distribution (after balancing and alignment operations) and the unbalance distribution at each step of the balancing and alignment process. Alongside the unbalance distribution, the randomly generated joint errors for each sample output, the rotor centreline offsets, and the dynamic response at all defined sensors. Obviously, to receive all of this data for every sample in a 200+ Monte-Carlo is only useful if it can be easily interpreted. The following examples are given to demonstrate how this has been done, and the tools that have been developed in order to assist this process.

The primary output from the analysis is the dynamic response levels. The aim of any balancing and alignment process is to produce the smallest vibration response possible. The program produces a summary of the output from each sensor as the maximum and mean dynamic response at each speed point for which the vectors $\tilde{\mathbf{k}}_u$ and $\tilde{\mathbf{k}}_c$ exist. An example output from the sensor that detects deflection at the centre of the rotor is shown in *Figure 39*.

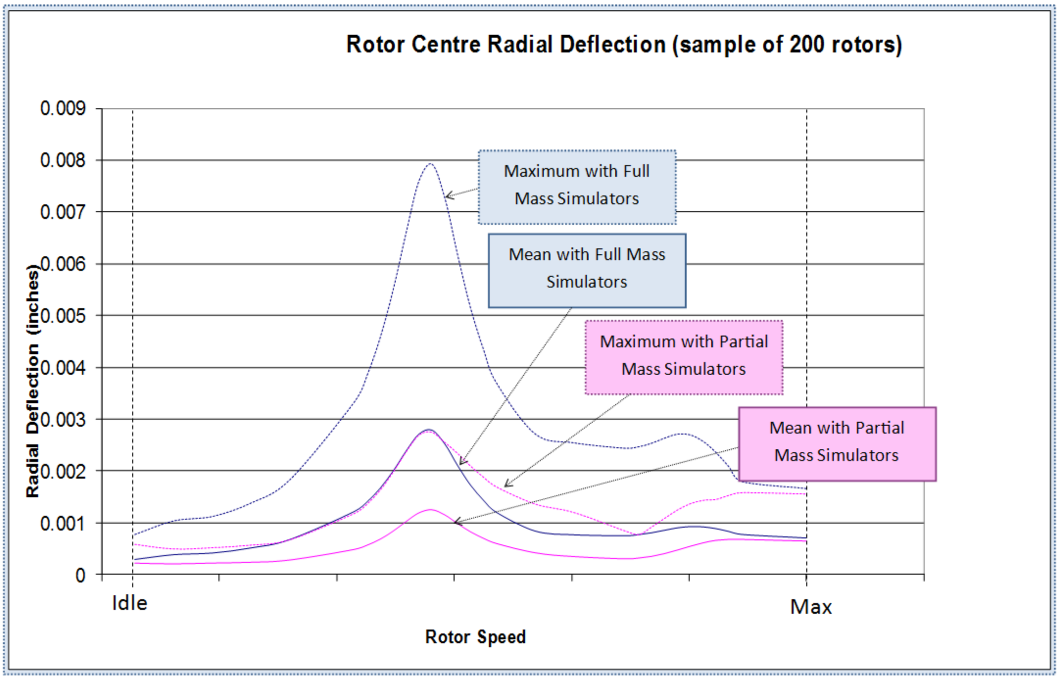

Figure 39: Dynamic response levels from two competing balance/build processes

The two balancing/build processes analysed in *Figure 39* were identical, apart from the mass properties of the Balancing Simulators that were used. The blue lines represent the full mass simulator results, and the magenta lines represent the scaled mass simulators from a 200 sample analysis. The method that determined the mass of the scaled simulators for this rotor is detailed in section 5.9. It is clear from the response plot that there is one major mode of interest in the operating speed range. The first aim of the analysis is to check that the process of making balancing decisions with the URF at particular resonances has not detrimentally affected the vibration at other speeds. In this case it can be seen that the scaled mass simulators are certainly effective at the resonance, and are generally beneficial over the whole speed range. The much more remarkable point to note from these results is the reduction in scatter. The mean response level has approximately halved, however the maximum vibration level is now reduced by 65%. This is a much greater benefit than that appreciated from observation of the mean, and demonstrates a particular improvement in robustness of the process. The vibration limit on pre-delivery pass off tests is often close to the average level achievable on an engine, therefore controlling scatter is extremely critical. This benefit alone justifies the effort that goes into the Surrogate Model/Monte-Carlo approach, without which the scatter would not have been known.

When this kind of analysis has been performed and all the data is available, it is possible to run a linear regression analysis to determine the key drivers. This is an important step, because the main effects analysis does not include interaction results. However the results can be often counter-intuitive and it is very important that the Engineer is able to gain insight into why the design or process should be changed. Therefore a plotting method to interrogate the balancing process results was created to be able to visualise the individual samples in the Monte-Carlo, and within that sample, look at the effects of the individual steps in the balancing process, *Figure 40* shows an example of the plot.

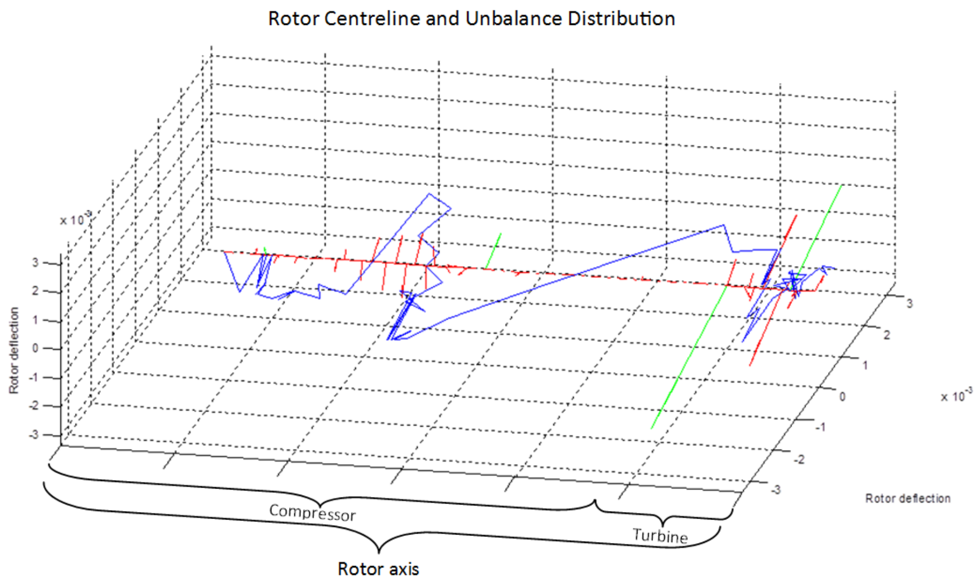

Figure 40: Visualisation of the Surrogate model output

The plot shown is created using Matlab. When viewed live in Matlab, the user benefits from the ability to be able rotate the viewing angle and gain the correct perspective visualisation. The blue line is the rotor centre line, offset due to rotor joint errors. The undeflected centreline is shown as a red dash-dot line. The red and green vectors are the unbalance distribution along the rotor, with the red vectors representing the rotor unbalance due to the rotor offsets, and the four green vectors representing the balancing corrections applied (two balance planes on each module in this case). It should be noted that for this graph, the unbalance couples have been split into two equal and opposite static corrections and added to the static unbalance distribution, therefore both static and couple distribution is represented in red vectors of the static distribution. An alternative option that has been shown to be useful in the display is to multiply the unbalance vectors by their unbalance response coefficients ($\tilde{\mathbf{k}}_u$) for a particular mode, thereby allowing their influence on dynamic response to be directly compared visually for each mode (since eq. 5.3 is applicable).

The individual balancing process steps can be visualised using the same graphing method for each sample rotor in the analysis; an example is pictured in *Figure 41*.

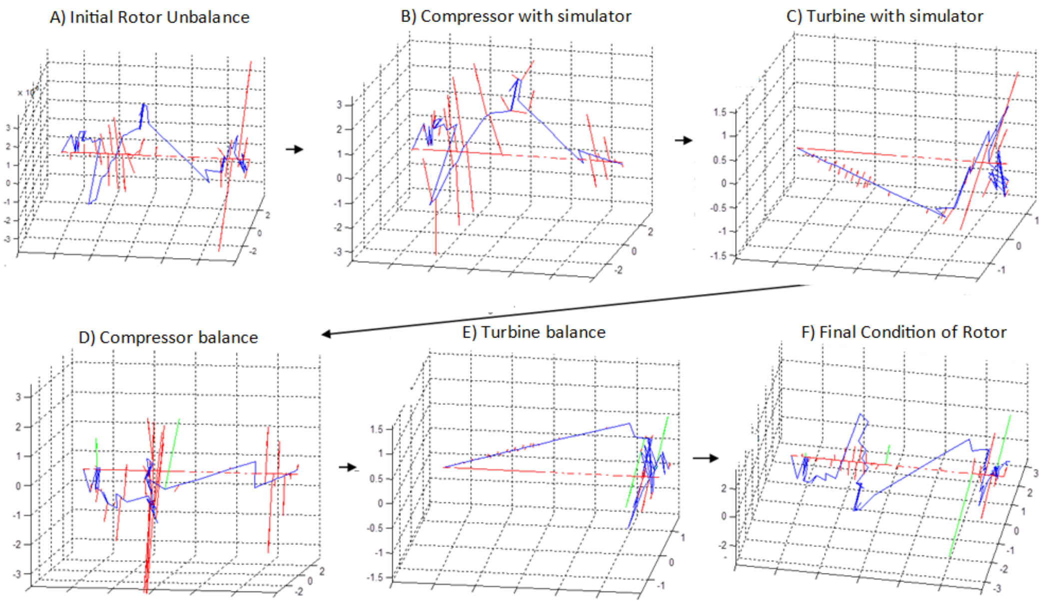

Figure 41: Visualisation of each step in the balancing/alignment process

With reference to *Figure 40* for the key and more detailed labelling, the balancing/alignment steps shown in *Figure 41* are described below:

A. The rotor centreline displacement and unbalance distribution when it is first (theoretically) built in a randomly aligned configuration.

B. The compressor is assembled onto the balancing machine with the turbine mass simulator. It can be observed that, unlike the turbine in A, the turbine has no geometric errors of its own (it appears straight) and its mass is simply offset by geometry errors in the compressor. This is just an unbalance measurement operation (no balancing or alignment is done at this stage).

C. Is the exact inverse of step B, where the turbine is assembled onto the balancing machine with the compressor mass simulator. It can be observed that the compressor has no geometric errors of its own and its mass is simply offset by geometry errors in the turbine. Like step B this is also just an unbalance measurement operation.

D. Based on the offset data calculated in step B, the compressor is rotated to put the highest point of swash of the compressor face of the intermodular joint at the zero datum angle (in reality the joint is stamped with an ‘h’ at this angle). Then the compressor balancing is performed and balancing corrections are added (using a full mass simulator in this case).

E. Based on the offset data calculated in step C, the turbine is rotated to put the highest point of swash of the turbine face of the intermodular joint 180° opposite the zero datum angle (in reality the joint is stamped with an ‘h’ at this angle). Then the compressor balancing is performed and balancing corrections are added (using a full mass simulator in this case).

F. In reality at this point, the ‘h’ marks are opposed by 180° and the rotor is built. The software achieves the same effect by putting what would be the ‘h’ marks at the datum angle and 180° opposite as described above. Diagram F shows the finished state of the rotor and can be seen on a larger scale in *Figure 40*.

By using this level of interrogation, the user not only sees the final state of the rotor and where the most significant driving unbalance or vibration is coming from, but is able to see how the balancing/build process is influencing that unbalance. This is key information when the process is being optimised, as it becomes very clear which steps could be improved and which are adding no significant value. It is worth noting that there have been instances found where the assembly balancing process being used, particularly with mass simulators, has actually been found to be detrimental to the vibration of the engine.

6.3.3 The Input Set Analysis

The “Input Set” analysis is identical to the Monte-Carlo analysis, except that it does not generate random input data. Instead it requests an input set from the user. This input set is normally a file saved from a previous Monte-Carlo analysis. This option was introduced because it was found to be informative to be able to compare the performance of a particular balancing method on identical unbalance distributions. For example, taking the highest responding (i.e. worst performing) unbalance distribution from a particular balancing method Monte-Carlo analysis, and comparing it to the performance of another balancing method on the identical rotor would provide key insights to the reasons for the poor performance on that rotor.

6.4 Chapter Conclusions

This chapter described a method of calculating rotor unbalance distributions and their associated vibration responses by generation of a simplified representation of the rotor with its geometric errors combined with vibration coefficients from the WEMM. This is a very fast calculation technique that makes Monte-Carlo analyses of large populations of rotors with their balancing methods entirely feasible. Several analysis types and data visualisation/evaluation tools are described that were developed as part of this study to support the Robust Rotordynamics Design System.

Although this software can stand alone, to determine an optimum design it is intended that it is used in conjunction with the Rotordynamics Design Process (chapter 4) and the URF design tool methods (chapter 5).

7 Rotordynamic Design Acceptance Criteria

7.1 Introduction to Rotordynamic Acceptance Criteria

The Robust Rotordynamics Design System has been described in chapters 4-6. The purpose of the system is to create a rotordynamic design for an engine that is optimised for vibration performance and for minimum cost. This raises the question of how the Engineer would know when enough refinement has been done to deliver an engine with satisfactory vibration performance. For this there must be a calculable measure and threshold for a modelled rotordynamic system that will deliver acceptable and repeatable vibration. This chapter examines methods that are currently used and explores a proposed new set of criteria. These criteria form an integral part of the Robust Rotordynamic Design System in accordance with thesis objective (ii) from section 1.5.

In the aerospace industry, the principle criterion applied to determine whether the preliminary design of an engine is likely to achieve acceptable vibration levels is to limit the relative proportion of strain energy in the rotor of any particular critical speed (i.e. mode shape). This is referred to as the Strain Energy Criterion in this thesis. There also are other more subjective measures used alongside the strain energy criterion. There are a number of short-comings with these criteria which are described in this chapter.

Other known methods are discussed and a new proposal is described which is effectively a further extension of the URF method (see section 5).

7.2 The Current Criteria

The percentage Strain Energy Criterion (%SE), the general principles of which are believed to be widely used across the aerospace gas turbine industry is where, for each resonance of an engine through the speed range, the percentage of the total system strain energy in the rotor being assessed is calculated. The principle behind the strain energy criterion is that, for any mode, the greater the amount of strain energy in the rotor, the more sensitive it is likely to be to imbalance. The reasons for this are twofold; firstly, the more bend in the rotor, the more sensitive it is to unbalance and secondly, strain in the rotor cannot be easily damped. In practice, the approach works well in the design process of an aerospace gas turbine, because the static structure also provides the vast majority of the damping; therefore the greater the proportion of the strain energy that is in the structure the more damping it will be able to provide to the resonance. Furthermore, this approach de-risks the engine design as it moves through its development as damping can be added to the static structure at a later stage in the design process, traditionally through the use of squeeze film dampers.

A generic strain energy assessment scheme is given below, as an example of how such a measure is commonly used:

% Strain Energy **Action**

0% to XX% The mode is acceptable at any speed in the operating range.

YY% to ZZ%The mode is acceptable provided that an effective squeeze film damper can be designed to restrict the response of the mode under normal running conditions.

>ZZ% This mode is unacceptable and a redesign is warranted.

Alongside these criteria, an unbalance forced response analysis is usually performed on the WEMM. There are not usually fixed limits for these results, but the considerations are:

(a) Considering rotor to casing relative displacement, or bearing forces, is this engine's unbalance response greater or less than that of another?

(b) What are the vibration response performance requirements for this engine with respect to a reference engine?

Other criteria in use across the industry tend to focus on the damping of the systems predicted or measured response. Many of these criteria are based on those outlined and published in the American Petroleum Institute (API) specification 616, 4th edition (American Petroleum Institute, 1998).

The API use criteria based on what they term as the "Amplification Factor" (AF) that is equivalent to the commonly used 'Q' factor which is a measure of damping, from (Friswell, Penny, Garvey, & Lees, 2010, p. 26) it is defined as

$$Q = \frac{1}{2\zeta} = \frac{1}{2\frac{c}{c_c}} \qquad (7.1)$$

where, c and c_c are defined as *damping* and *critical damping* respectively and therefore ζ is termed as the critical damping ratio. The same reference also states that "it can be shown that for a lightly damped system, an equivalent definition for Q is $Q=\omega_{pk}/\omega_{b\omega}$", where ω_{pk} is the frequency of the peak of the resonance, and ω_{bw} is the *half-power bandwidth* which is the frequency width of the peak at $1/2^{½}$ (i.e. 0.707) of the height of the peak. Therefore it can be stated that, for systems with low damping:

$$Q = \frac{\omega_{pk}}{\omega_{bw}} = \frac{1}{2\zeta} \tag{7.2}$$

The API specification then goes on to define a criteria based on AF, which can broadly be summarised as:

a) If the AF is less than 2.5, the response is considered critically damped and this mode is allowable at any speed.

b) If the AF is 2.5–3.55, a speed separation margin of 15% above the maximum continuous speed and 5% below the minimum operating speed is required.

If the AF is greater than 3.55, greater speed separation margins are required. Equations are given in the API specification to derive these required margins.

7.3 The limitations of the strain energy criterion

The Strain Energy based rotordynamic acceptance criterion is widely used in the aerospace industry, but must not be used in isolation; some recognition of the forcing function and mode shape sensitivity to a particular forcing function (unbalance distribution) must be taken into account to avoid missed cost and weight saving design opportunities and high rates of vibration pass-off tests.

The strain energy criterion attempts to mitigate the risk of excessive responses from unbalance sources that can be separated into two categories:

(1) Built-in unbalance and normal degradation.

(2) Unbalance due to component failure.

Built-in unbalance is the *residual* unbalance that is in the rotor when the engine is first built. This comprises a combination of unbalance sources: from the repeatability of the rotor joints during the engine assembly, blades adopting slightly different positions in their root slots, the internal bending moments that occur due to the low-speed balancing process, and the resolution and accuracy of the balancing process and machine and compromises therein. Normal degradation occurs due to a variety of factors, including blade wear over time, abradable linings wearing down, debris build-up, small movements in rotor joints, etc. Both built-in unbalance and normal degradation are relatively low levels of unbalance, normally expected to be within 10 times the original final unbalance tolerance of the rotor when new and balanced.

Unbalance due to component failure is normally due to “core blades” being released from the rotor(s) (“core blades” are defined as blades other than the fan blades). This normally results in a very high unbalance force. Fan blade-off is considered a special case and not discussed here because mechanical fuses are often employed which totally alter the rotordynamics.

For category (1) unbalance where modes have a medium amount of strain energy in the rotor, vibration is normally successfully managed with the introduction of squeeze film dampers. For category (2), squeeze film dampers are not usually able to cope with the forces produced and effectively lock-out. Some increased damping in the static structure is believed to be achieved during these higher force events because the structure is driven harder and bolted joints will start to move generating extra damping.

This single %SE criterion is currently catering for all of these unbalance situations above, for any engine rotor (LP, IP, or HP), for any rotor mode shape, for any size/type of engine, and for any performance requirement. It is argued below that this is too broad an application of these criteria and improved generic criteria are needed in order to open up the design space and gain competitive advantage.

The limitations of the current criterion are highlighted below using very simple examples of contrived rotors.

Discussion

Figure 42 shows two machines with equal total mass, equal left and right support stiffnesses, and equal span. Shaft mass is assumed negligible. Rotor A has a 20Kg disc mass in the middle, and Rotor B has a 10Kg disc mass at each end. A mode shape predicted from a critical speeds analysis on both systems is pictured as a red deflected centreline. Obviously if the shaft stiffnesses were identical then the modes would occur at different speeds, but either could appear in the running range of a machine. It is clear that the strain energy distribution could be identical for this mode shape in the two systems. For discussion, assume that the strain energy distribution is 40% in the rotor, 60% in the stator.

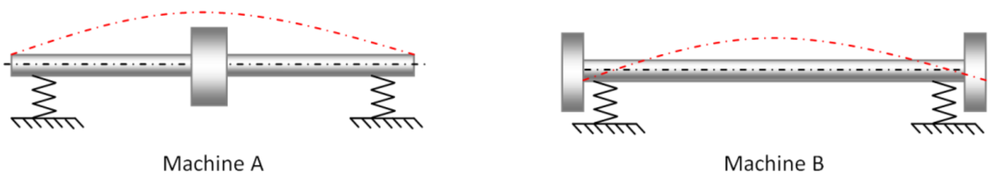

Figure 42: Two separate machines with identical total mass, isometric bearing stiffness, and span.

It is very clear from the mode shapes of the machines that an unbalance applied to the centre of the rotor (the anti-node) will cause a significantly higher deflection response than one applied at the ends of the rotor (the nodes). On Machine A, the majority of the mass lies at the anti-node of the mode shape, therefore the build of the disc mass at the centre of the rotor means that the alignment of that mass needs to be very tightly controlled and balanced. Comparing this to Machine B, where the mass lies near to the nodes of the mode shape, the disc masses can be more loosely controlled on build and balance. Therefore, for category (1) unbalance (built-in unbalance and normal degradation), the balancing and build needs of the system are entirely different for the two machines, but they score an identical %SE.

As explained previously, category (2) unbalance usually occurs due to core blade release. As the blades are always at the discs, the requirements for locations where the machines need to tolerate the resulting unbalance is the same as those described above for category (1).

Therefore, once again, the two machines have very different requirements.

The operational performance requirements of these machines should also be considered. Again, for the sake of discussion, assume that the critical performance of these machines is determined by minimising blade tip and air-seal orbit sizes that are located at the disc masses. It should be noted that these clearances are determined by a “worst deflection” event in an engine’s life, because the worst deflection causes the abradable lining to cut the blade/seal tips on contact, permanently widening the operating clearance. With this consideration in mind, it is clear by inspection that the rotor orbit of machine A is much more critical to control than the rotor orbit of machine B, but the %SE score is the same; however, with current criterion, the vibration of the two machines would be managed identically.

Reading the current %SE criteria, both machines would require squeeze film dampers, which add cost, weight and complexity to the machines whilst also reducing gas turbine performance; this is because the squeeze film damper radial clearance will normally bottom out at some point during normal operation either under gravity or aircraft manoeuvres (depending on their design). Vane tip/seal clearances are determined on the maximum deflection because this is when the maximum material is abraded from the blade tips or seals. Therefore there is a significant performance incentive to avoid the use of a squeeze film damper. What is clear from the examples above is that Machine A needs much more care on build and design, and has a much greater need for squeeze film dampers, whereas Machine B will be much more robust and may not need squeeze film dampers.

Likening the above Machines to real rotors, there are similarities between the architecture of Machine B and an LP rotor, where the large masses tend to concentrated near the bearings and a long flexible shaft connects them. The LP shaft does not wear or carry blades, so has very stable unbalance. Machine A can be likened to an HP rotor, because the discs, blades and seals tend to be slung along more of the length of the rotor between the bearings.

Therefore it is clear that using the same %SE criterion for two rotors of the same engine is not appropriate.

Simple inspection of a small engine when compared to a large civil engine leads to a further consideration of how appropriate a single scale strain energy criterion can be for all aerospace gas turbine engines. Examples are pictured for comparison in *Figure 43* where it can be seen that on a small engine the static supporting structure is a very large proportion of the total mass of the engine. On a large engine, the rotors massively dominate the supporting structure. Therefore the percentage of strain energy in the static structure of the small engine is likely to have a much greater effect on the behaviour of the rotor than a large engine.

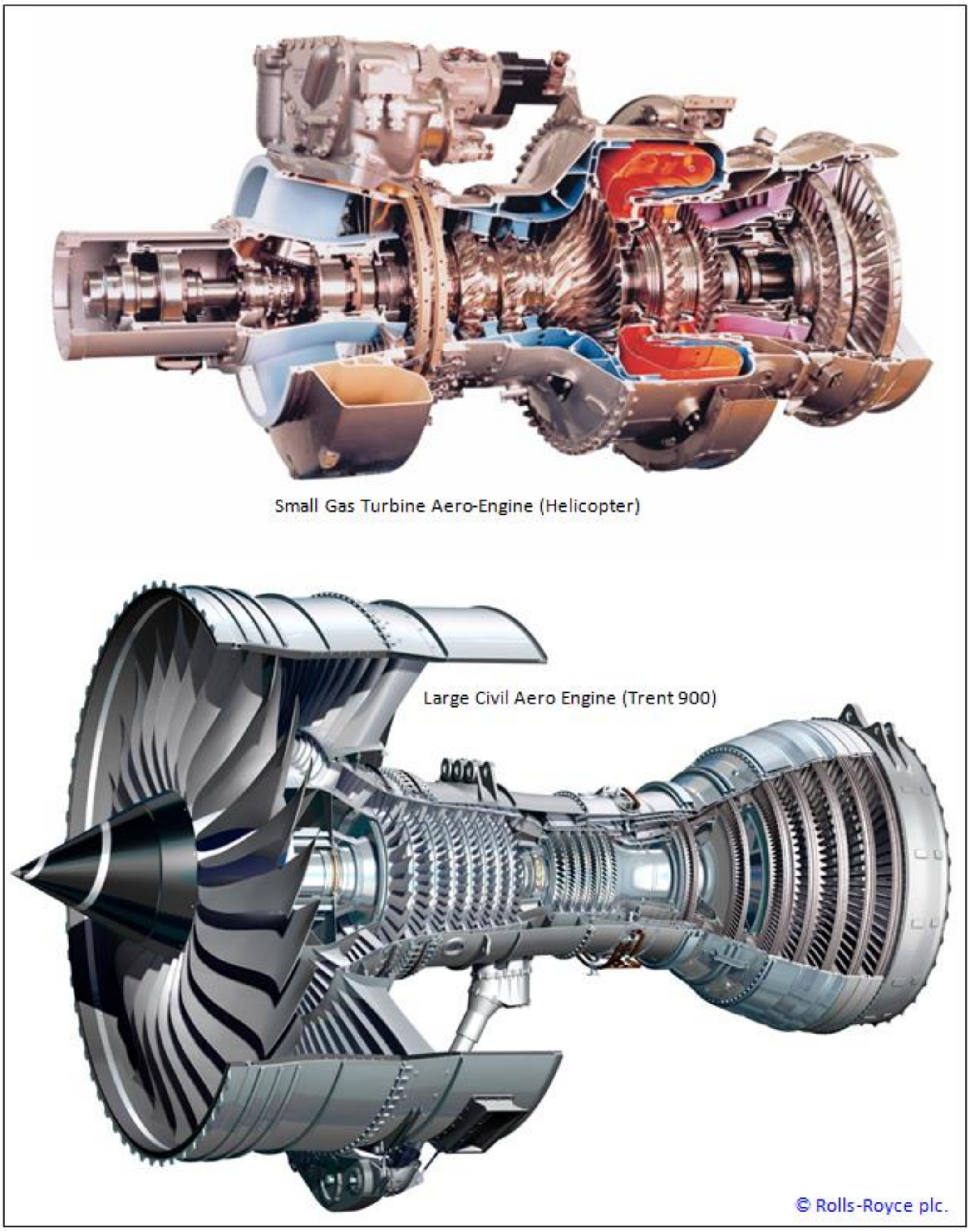

Figure 43: A large civil engine architecture compared with a small engine (not to same scale)

The above arguments make clear that a set of criteria should account for the sensitivity of the rotor with respect to the functions of the rotor, the sensitivity to the likely unbalance distribution, and the likelihood of being able to control the resonance(s) through low-speed balancing and damping.

7.3.1 The limitations of the API (Amplification Factor) criterion

The API specifications are obviously produced as guidelines for the Petroleum industry, which relies entirely upon ground based rotating machinery. Because of this, weight is not a key driver for the design of the machines and therefore the bearing supporting structures are extremely stiff. This is so normal for this industry that several of the main rotor dynamics analysis packages in use cannot actually model the dynamics of the supporting structure. In this situation it is clear why the strain energy criterion is not employed, because by default all of the strain energy is in the rotor.

Therefore the industry developments are highly focussed on the modelling and prediction of journal bearings, because the stiffness of the bearings is a key parameter that determines the frequency of the modes, but the damping in the bearings is the key method for controlling the response to residual unbalance. Note that sometimes squeeze film dampers are used in series with the journal bearings to increase the damping capacity.

In aero gas turbines, damping is extremely difficult to predict and model with any accuracy. Many of the squeeze film designs are difficult to predict in either stiffness or damping because they are complex to model and they operate in an environment with many unknown variables. Also the variability temperature environment that they operate within is extremely challenging. The support structure (the casings) are even more challenging, because the damping is largely generated in bolted joints which is an amplitude dependent damping which, at the time of writing, has not yet been successfully predicted with good accuracy. Therefore the damping likely to be achieved by the whole engine is not considered to be an easily predictable quantity with today’s FE modelling methods.

The consequence of this is that having damping as the key criterion for aero gas turbines is not considered reliable as a predictive design tool with current modelling methods.

7.4 Proposal for a Rotor Dynamic Acceptance Process and Criteria

It is clear from the above that the current %SE criteria are not relevant across a wide gas turbine multi-spool product range. New criteria would need to answer the following fundamental questions:

i. Will the system produce an acceptable response to normal operation and normal degradation?
ii. Will the system produce an acceptable response to a core blade release and subsequent unbalance?
iii. Will the rotor be balanceable using low-speed modular techniques?

In order to address questions (i) and (ii) a new measure of system responsiveness to unbalance is proposed and termed α. In order to address question (iii) a new measure of the linearity of the unbalance response function is proposed and termed β. The process of assessment and these new measures are described in the following sections.

7.4.1 **The Rotordynamics** Assessment Process

For this analysis the WEMM is used with damping values standardised to provide a datum level for back to back comparison of responses across different engines of different sizes, thereby removing one variable of complexity whilst maintaining a realistic damping distribution. In all analyses, all rotors in the engine shall be represented with a defined percentage of damping in each rotor, and rotation speeds and directions correctly represented relative to each other. The casing shall have a defined level structural damping applied. Initially no squeeze film damper representation should be included.

7.4.2 Construct a Campbell Diagram

Initially a Campbell diagram should be constructed as shown in *Figure 44* below:

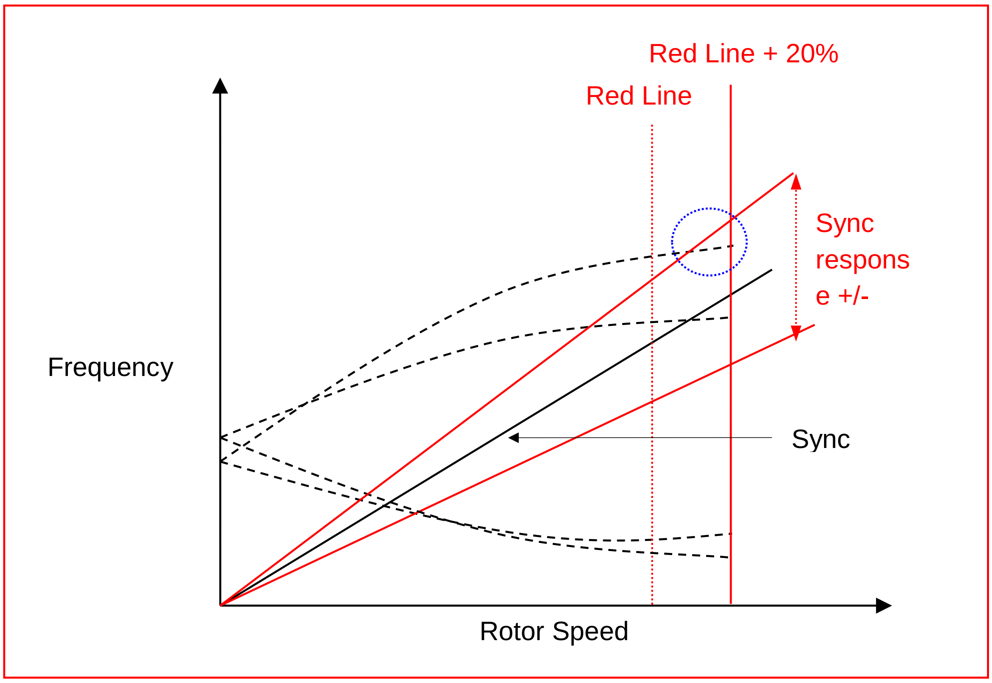

Figure 44: Example Campbell Diagram

The main purpose of the Campbell diagram here is to identify potential problem modes that will not automatically be caught by the steady-state forced response (SSFR) analysis later. As shown in the diagram, the envelope of interest around the synchronous (sync.) response line is ±20% on frequency and up to red-line speed +20%. The dotted blue circle identifies one such mode which will have to be checked to understand its sensitivities; the strain energy distribution and mode shape will need to be studied and any sensitive areas that could potentially reduce its frequency during the design process to cause it to cross with the synchronous response line need to be communicated to the designer. Modes that cross, or are likely to cross, the synchronous response line below the “red-line” speed +20% will be assessed against the acceptance criteria. The value of 20% is derived from empirical experience.

7.4.3 Steady-state Forced Response (Unbalance Response) Analysis

A series of forced response analyses are carried out in exactly the same way as those performed to generate data for an Unbalance Response Function as detailed in chapter 5. It is assumed that, in practice, the same data generated would be used to generate the URF and perform this acceptance testing process. The process for generating the data is briefly described here for convenience.

An unbalance response throughout the operating speed range is generated using the WEMM by placing a unit unbalance at each bearing and one at each major mass or span that may experience bending. The results for each run are stored. Figure 45 gives an example of the mass locations:

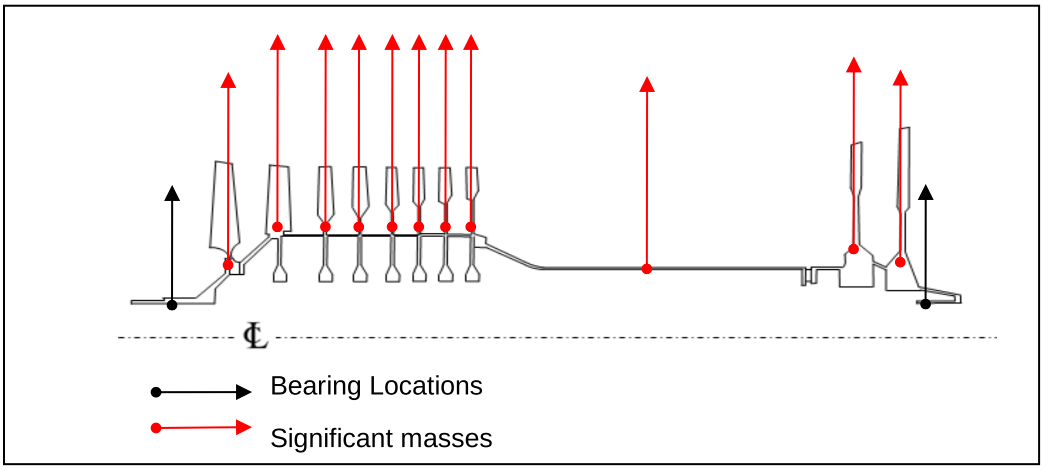

Figure 45: Example of locations of unit unbalance for SSFR runs.

In the case shown, 13 separate runs would be carried out, with a unit unbalance at each marked location. Complex radial force responses should be recorded from the bearings (spring elements).

A plot from each bearing should be produced with the radial force response magnitude plotted up to 150% of the normal operating speed. If a peak appears in any of the plotted lines it is recorded as a “speed of interest" denoted ω_n.

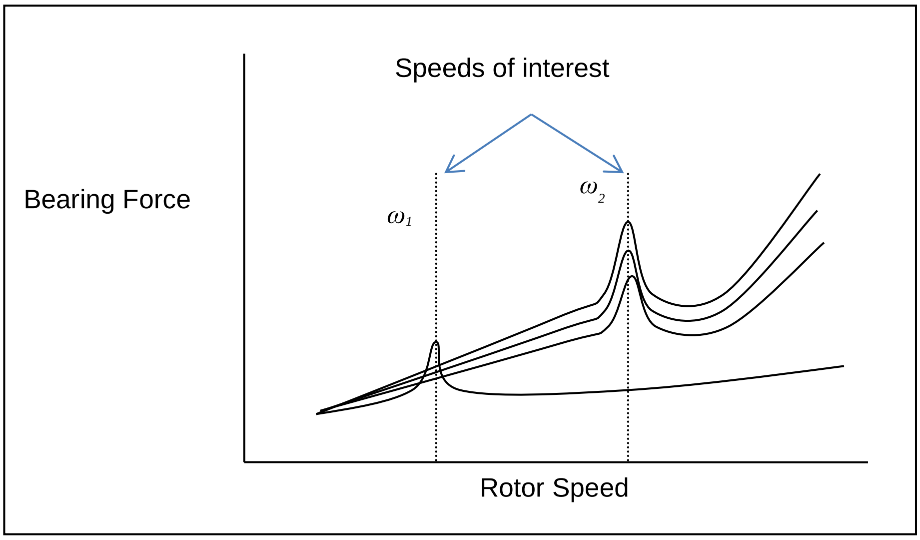

Figure 46: Identifying speeds of interest

From the SSFR data, at each of these 'n' speeds of interest, the complex column vector $\tilde{\mathbf{k}}_{n,b}$ is generated for each bearing 'b' comprising a complex response value for each station $\mathbf{x}_i$ along the rotor.

7.4.4 System Sensitivity Calculations:

The system sensitivity values (α and β) described below are calculated at each speed of interest.

7.4.5 The system sensitivity to arising unbalance and inter-modular joint repeatability errors (α)

In order to determine sensitivity to arising unbalance the likely magnitude of arising unbalance along the rotor must be determined. This is captured in the vector of static distributed unbalances, $\mathbf{u}_p$. Vector $\mathbf{u}_p$ is the same length as $\mathbf{x}$, consisting of real values representing the magnitude of mean unbalance arising at each major mass location due to assembly build (inter-modular joint errors), component manufacture, loose fits (blade slots, locking plates, etc.). The most appropriate method for this currently available is the Monte-Carlo method described in section 6.3.

The system sensitivity ‘α’ is developed below. The relationships between rotor eccentricity ‘e’, rotor mass ‘M’, and unbalance ‘u’ are well known. The ISO guidance (section 5.2 of (ISO1940-1, 2003)) states[2] “In general, for rotors of the same type, the permissible residual unbalance [U_{per}] is proportional to rotor mass [M]: $U_{per} \propto M$. If the value of the permissible residual unbalance is related to the rotor mass, the result is the permissible residual specific unbalance e_{per}, as given by the following equation:

$$e_{per} = \frac{U_{per}}{M} \text{”.} \tag{7.3}$$

The ISO guidance also goes on to state that, in general, the unbalance value e_{per} varies inversely with the service speed of the rotor and defines the equation:

$$e_{per} \cdot \omega = C \tag{7.4}$$

where C is a constant value, and ω is the rotational speed of the rotor (in rad/s).

If $\mathbf{m}$ is a real valued column vector where each element is the mass of the rotor at the axial stations defined in $\mathbf{x}$, and $|\mathbf{m}|=M$, then each of the elements of the real-valued column vector $\mathbf{e}_p$ can be defined as

[2] The square brackets indicate that the nomenclature has been substituted for consistency with this document.

$$\mathbf{e}_{p(i)} = \frac{\mathbf{u}_{p(i)}}{\mathbf{m}_{(i)}} \tag{7.5}$$

where i=1 to q.

The total static eccentricity of the rotor (at each major mass station) defined as

$$e_t = \sum_{i=1}^{q} \mathbf{e}_{p(i)} \tag{7.6}$$

where q is the number of elements in e_t.

The sum of the total force F_t from the sum of the complex forces at each bearing b, where no dynamic amplification is present, can be calculated from

$$F_t = \left| \sum_1^v \tilde{F}_b \right| = M e_t \omega^2 \,. \tag{7.7}$$

A total bearing load unit unbalance response column vector $\mathbf{k}_t$ can be created for a particular speed from the previously defined $\tilde{\mathbf{k}}_{n,b}$ for each bearing:

$$\mathbf{k}_t = \sum_{b=1}^{v} \sum_{i=1}^{q} \left| \tilde{\mathbf{k}}_{n,b(i)} \right| \tag{7.8}$$

Similarly to eq. 5.3, the total bearing dynamic response due to the average unbalance arising in the rotor population can now be calculated from:

$$a_b = \mathbf{u}_p{}^T \mathbf{k}_t \,. \tag{7.9}$$

This is clearly a pessimistic assumption, as all the unbalances will arise at the same time and in the same phase, but this is not of concern because this measure is being used to compare the sensitivity of different engine designs, not to predict their actual behaviour in service.

The aim of a new criterion is to develop a method by which all aero gas turbine rotors, regardless of mass or speed, can be compared. The relationship stated in the ISO guidance in eq. 7.4 effectively states that the acceptable rotor eccentricity for an engine type is inversely proportional to the rotor speed. Therefore, as the rotor speed is known, a measure of eccentricity of the rotor in the dynamic state would enable the constant value to be calculated and therefore used as a comparison between rotors. To facilitate this, the following definition of eccentricity in a dynamic system has been developed and termed "dynamic eccentricity" (e_{dyn}):

$$e_{dyn} = \frac{a_b}{M\omega^2} \tag{7.10}$$

Combining equations 7.10 and 7.4, the definition of system sensitivity to arising unbalance and inter-modular joint repeatability errors (α) can be represented by a single velocity value for each speed of interest as

$$\alpha(\omega) = \omega \cdot \left(e_{dyn}\right). \tag{7.11}$$

This sensitivity value not only incorporates the dynamic sensitivity of the rotor, but also weights that sensitivity to the likely arising unbalance in the rotor, and makes it possible to compare values between different sizes of aero gas turbine engines.

7.4.6 The system sensitivity to inherent unbalance (β)

As described previously, the value β is intended to be a universal measure of how easy it will be to achieve a satisfactory balance condition using low-speed modular balancing techniques.

For illustrative purposes, the influence of rotor bending sensitivities on the unbalance response function (URF) graph, is described below (N.B. the URF graph is formally introduced in chapter 5). At a particular speed of interest if a rotor has a high dynamic stiffness the URF will appear linear. This is shown in *Figure 47* where the response force measured at bearing b, at rotor speed ω, to unit unbalances placed along the rotor are plotted. The function described by these responses with respect to axial location is the URF. The black markers are where the unbalances were applied directly at the bearing locations; the red markers are where unbalances were applied at significant mass components and sub-assemblies of the rotor to define the vector $\tilde{\mathbf{k}}_{u,b}$.

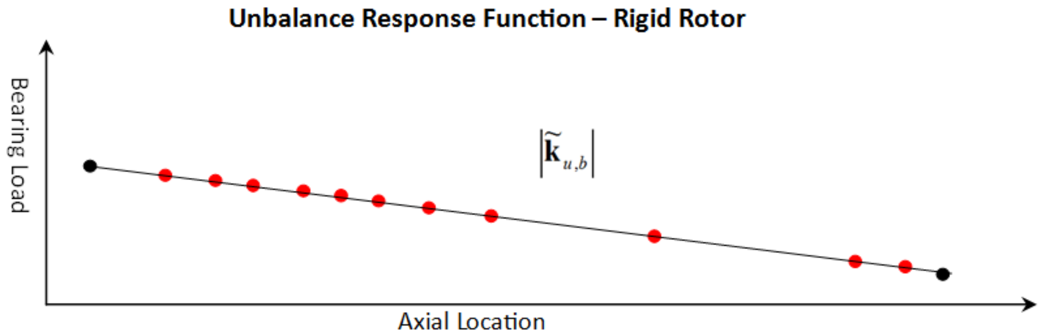

Figure 47: Force responses measured at bearing b, at constant speed ω, to unit unbalances placed along the rotor where the dynamic stiffness of the rotor is high (pseudo rigid).

Figure 48 shows a typical URF for a rotor which has significant dynamic flexibility.

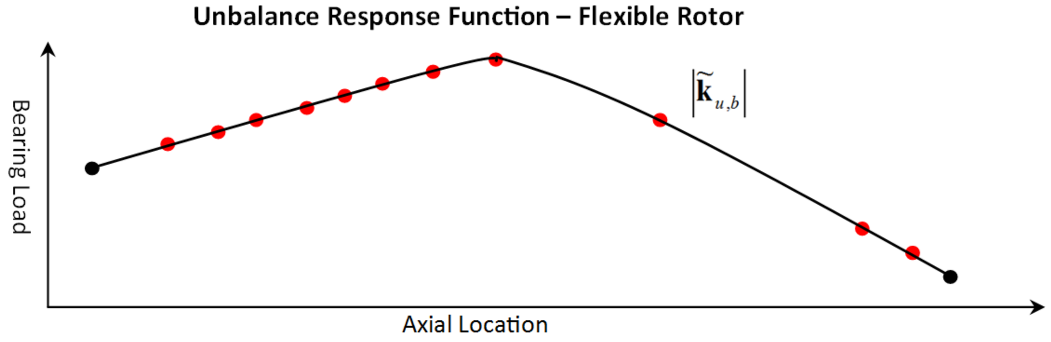

Figure 48: Force responses measured at bearing b*, at constant rotor speed* ω*, to unit unbalances placed along the rotor where significant dynamic flexibility is present.*

In a very similar manner to the percentage strain energy methods, for a particular mode shape it is useful to be able to determine the proportion of flexibility that is in the rotor, and the proportion that is in the casing. If a force is applied at a bearing, and the bearing deflects, it is the static structure that has flexed and incurred all of the strain required to achieve the displacement. Static structure strain is termed ε_{s}. If a force is applied on the rotor, away from a bearing and a deflection is measured, the strain that caused this displacement is a combination of the static structure strain and strain in the rotor. This combined strain of the static structure and the rotor is denoted ε_{s+r}. Therefore, to determine the proportion of strain in the rotor only (ε_r) the following equation applies:

$$\varepsilon_r = \varepsilon_{s+r} - \varepsilon_s \,. \tag{7.12}$$

The following description details the method for isolating the response caused by strain in the rotor:

In order to do this a straight line vector of coordinates between the bearing responses must be constructed, this complex vector is denoted $\tilde{\mathbf{c}}_b$ and is pictured in *Figure 49*. Vector $\tilde{\mathbf{c}}_b$ is the same length as $\mathbf{x}$ and represents a calculated response assuming the unbalance forces were transferred to the bearings via a rigid rotor. It should be noted that this is not the same as modelling the response with the existing rotor replaced with a rigid rotor because the dynamic behaviour of the original rotor is still represented in the modal response; it is just the strain in the rotor induced directly due to the unbalance force that has been theoretically removed.

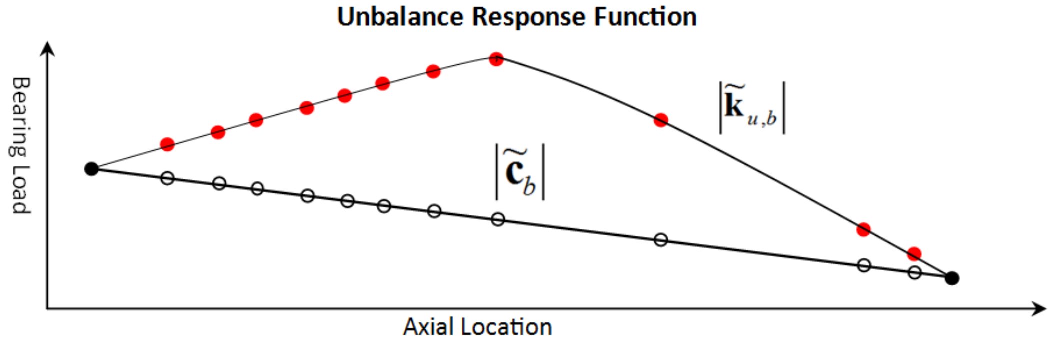

Figure 49: Force responses measured at bearing b, constant speed, to unit unbalances placed along the rotor. Black unfilled markers are the calculated response assuming the unbalance forces were transferred to the bearings via a rigid rotor.

The response due to unbalance induced rotor bending moments only can then be calculated by taking vector $\tilde{\mathbf{c}}_b$ from vector $\tilde{\mathbf{k}}_{u,b}$; this is denoted $\tilde{\mathbf{g}}_b$ which is shown graphically in Figure 50.

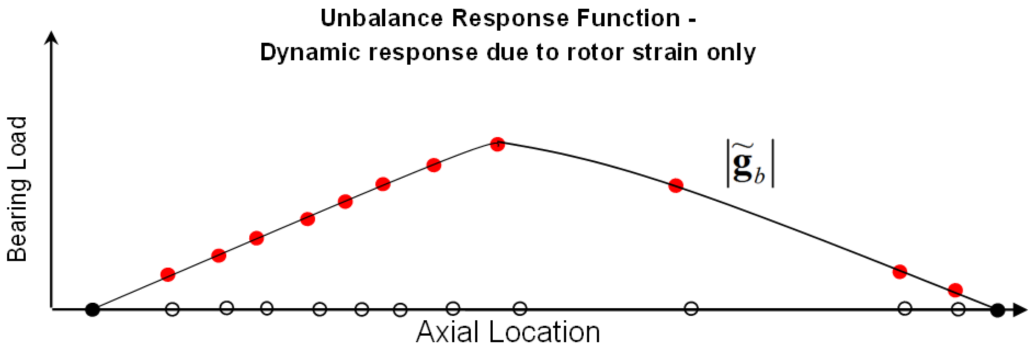

Figure 50: Force responses to unbalance induced bending moments in the rotor measured at bearing b, at constant speed.

The methods for calculating $\tilde{\mathbf{c}}_b$ and $\tilde{\mathbf{g}}_b$ and using them to calculate the rotor sensitivity to arising unbalance induced bending moments are given more formally below.

The figures above (*Figure 48-Figure 50*) show a simple rotor on two bearings which simplifies calculations considerably because it is a statically determinate system. For a rotor with more than two bearings the system becomes statically indeterminate. This means that relative stiffnesses between the rotor, support structure, and bearings need to be taken into account. Because the main aim of this thesis is to communicate a concept, the equations below (7.13 & 7.14) assume a two bearing rotor. Rotors with more than two bearings are discussed separately in section 7.5.

One $\tilde{\mathbf{c}}_b$ and one $\tilde{\mathbf{g}}_b$ vector is calculated for each speed of interest and each bearing. $\tilde{\mathbf{s}}_b$ is a complex vector, the same length as $\mathbf{x}_b$, that represents radial forced response measured at bearing *b*, to unit unbalances applied at each bearing in turn (from 1 to q) at speed ω.. $\tilde{\mathbf{s}}_{b(i)}$ is the element of $\tilde{\mathbf{s}}_b$ that corresponds to an unbalance applied at bearing number i. The axial location of bearing i is denoted $\mathbf{x}b_{(i)}$. If a two-bearing rotor is assumed and the bearings are denoted bearing 1 to the left and bearing 2 to the right, $\tilde{\mathbf{c}}_b$ and $\tilde{\mathbf{g}}_b$ vectors for b=1 and b=2 must be calculated for this speed of interest,

$$\frac{\partial \tilde{\mathbf{s}}_b}{\partial \mathbf{x}_b} = \frac{\tilde{\mathbf{s}}_{b(2)} - \tilde{\mathbf{s}}_{b(1)}}{\mathbf{x}_{b(2)} - \mathbf{x}_{b(1)}} \tag{7.13}$$

$$\tilde{\mathbf{c}}_b = \mathbf{x}\frac{\partial \tilde{\mathbf{s}}_b}{\partial \mathbf{x}_b} + \tilde{\mathbf{s}}_{b(1)} - \mathbf{x}_{b(1)}\frac{\partial \tilde{\mathbf{s}}_b}{\partial \mathbf{x}_b} \tag{7.14}$$

$$\tilde{\mathbf{g}}_b = \tilde{\mathbf{k}}_b - \tilde{\mathbf{c}}_b \ . \tag{7.15}$$

$\tilde{\mathbf{g}}_b$ is a complex vector that represents the dynamic response due to the strain in the rotor only.

$\mathbf{h}$ is a real column vector that represents the initial (inherent) unbalance before assembly balance of each significant mass, e.g. a bladed disc. There are a number of ways that this can be calculated in detail: standard calculations for manufacturing errors, stochastic methods (Monte-Carlo Model (section 6) or covariance matrix method (section 8.2)) or simple assumptions. Initially, the simple assumptions will be used for experimental purposes. Therefore initially, $\mathbf{h}$ will be calculated from:

$$\mathbf{h} = 40e\mathbf{m} \tag{7.16}$$

this represents 40× the ISO unbalance tolerance.

System sensitivity to bending (β) is then calculated:

$$\beta(\omega) = \frac{\sum_{i=1}^{n} |\, \mathbf{h}_i \left(\tilde{\mathbf{g}}_{1(i)} + \ldots + \tilde{\mathbf{g}}_{q(i)} \right) |}{M\omega}\,. \tag{7.17}$$

The units of β are velocity. This is intended to indicate how non-linear the URF is weighted by the likely arising unbalance. This arising unbalance has to be corrected on a low-speed balancing machine, which by definition has a linear URF. Therefore the vibration levels will be driven by residual unbalance after the balancing process, which is indicated by β.

7.4.7 Using α and β sensitivity measures to influence design

The variable α represents the sensitivity of the engine to arising unbalance and inter-modular joint repeatability errors. If α is large the response can be controlled using squeeze film dampers (SFD), support springs or structural mass/stiffness changes. Inspection of the bearing responses indicates which location to include the SFD.

If β is large it is possible to trade rotor design and balancing strategy decisions in order to minimise rotor bending moments on the dynamically flexible parts of the rotor. As described in detail in chapter 5, the Unbalance Response Function (URF) graphs (defined as part of the Robust Rotordynamics Design system) can be used as a tool that is very useful in this process. With this method a number of decisions can be quickly informed including: positioning balancing lands, modular break points, mass simulator requirements, build alignment methods, etc. However, if β is to be reduced by reducing the amount of unbalance at certain locations i.e. pre-balancing a bladed disc assembly, and/or ensuring the joints locating that disc have a very accurate location tolerance, then the initial unbalance vector $\mathbf{h}$ (eq. 7.16) must be produced using stochastic modelling – such as a Monte-Carlo Model (section 6) or covariance matrix method (section 8.2)). It should be noted that β is actually a measure of rotor bending sensitivity as if the entire rotor was balanced with balancing planes at the bearings, whereas the optimised solution should be measured as if the individual modules were balanced at their balancing lands. However, in order to provide a feasible very early design stage comparison (where balance lands and modular break points of the design will not have been defined) a general measure of sensitivity is required and the bearings provide a convenient universal comparison point.

7.5 Chapter Conclusions and Further Work

The method of calculating rotordynamic sensitivities described differs from previous methods, such as percentage strain energy or the use of steady-state forced response to compare to previous similar engines because:

1. It considers the size of the potential unbalance source as well as the response.
2. The sensitivity values are comparative between different engine sizes and speeds.

3. It recognises that vibration is driven by very different sources of unbalance that drive the vibration response in different ways.

4. Both the sensitivity of the design to inherent and arising unbalance sources are assessed as a system response. Therefore these relative sensitivities can be compared directly to each other.

5. It eliminates issues about forward and backward classification of modes which causes a lot of confusion / inconsistency with the current criteria.

This new criteria is proposed in support of objectives (ii) and (iii) [detailed in section 1.5]. The aim of new criteria will very fast determine whether a design is likely to be feasible and cost effective, without over constraining the design space available. This is achieved because it takes account of the specifics of a particular engine weight/speed or rotor type (i.e. LP or HP) and its performance duty.

Before these methods are implemented two pieces of further work will be required:

1. The α and β sensitivity measures must be tested on various existing engines for which WEMM models have been validated and normal measured vibration levels are well established in order to provide benchmark values. These values will constitute the acceptance criteria. It will be appropriate that different engine applications will require different α and β values as criteria because different businesses require different vibration levels.
2. In many cases, rotors will have more than two bearings. The normal low-speed modular balancing treatment of these rotors is to treat the part of the rotor between each bearing span as a separately balanced module. Therefore the criteria should look at the rotor in these module spans between two bearings. Clearly this does not consider the cross-talk between these modules which will exist, but it will still be a representative guide to how difficult the rotor will be to balance in the early engine design stages. This approach will

need to be validated.

8 Using Other Data to Inform the Low-Speed Balancing Process

8.1 Chapter Introduction

As described in detail in chapters 1 and 2, low-speed balancing is a cost-effective incumbent constraint on gas turbine turbomachinery, and low-speed balancing technology relating to pseudo-rigid rotors has not advanced significantly in recent years. Improving the outcome of low-speed balancing means that either the vibration level of a system can be reduced, or other expensive and time consuming processes (e.g. build alignment) can be removed. The big advantage of improving the balancing outcome by influencing the balance process is that it can be done without changing the rotor design, therefore it is useful on both new designs and existing products.

In this chapter two methods of improving the outcome of low-speed balancing operations are introduced. The first being the Unbalance Co-variance Matrix in section 8.2, and the second being the use of a Dual Mass Balancing Simulator in section 8.3.

8.2 The Unbalance Co-variance Matrix

In rotor balancing, one seeks to minimise some overall measure of total residual unbalance response of the machine during operation. To do this optimally requires that insight into the state of unbalance be available in some form. It is noted at this stage that if balance correction can be made at only a very limited number of planes on a rotor (usually only two), the scope for exploiting detailed information about the state of unbalance of a given rotor is limited. Currently, the main reason why most rotors utilise only two or three unbalance correction planes is that it is not possible to obtain information which would make it useful to deploy unbalance correction at a greater number of planes. In most cases, it is quite conceivable that more planes could be used if the appropriate information could be obtained.

With current modelling methods, it is feasible to obtain more data about the unbalance distribution in a rotor than is currently available. This knowledge can be obtained in a number of ways, for example by modelling of the manufacturing and assembly process. The methods presented in this chapter consider techniques to obtain and exploit this knowledge for maximum benefit (i.e. minimise vibration).

This section is concerned with rotors that are balanced in either a balancing machine or in a stator which may be different in properties from the stator in which the rotor is finally required to run. Such differences might arise if the rotor is required to be interchangeable or if the dynamic properties of a stator might change with respect to time. If a rotor is balanced in the stator which will host it for its entire running life, and if the dynamic properties of that stator will not change, then the “mode shapes of significant residual unbalance” (which will be defined later) are invariant and it is not necessary to correct any components of unbalance distribution which are orthogonal to these mode shapes. In this case, provided that the balancing tests can be done over the complete range of intended operating speeds for the machine, the methods presented here have no relevance. For all other rotor balancing requirements, they have value and it will be seen that the level of value depends on the strength of the information present in the co-variance matrix.

The section is developed from a paper co-authored with Prof. S D Gravey and Dr. S Jiffri (Jiffri, Garvey, & Rix, 2009). It initially begins by outlining a Finite Element Analysis of a particular rotor. It then explains how the states of unbalance existing in a batch of rotors may be used to estimate the covariance matrix of unbalance. The eigenvalues and eigenvectors of the co-variance matrix are discussed next, after which the direct use of the co-variance matrix as an estimator of relative likelihood is explained. The next section comprises a detailed explanation of the use of the co-variance matrix to enrich balancing test data such that the vector of unbalance which is most likely to exist – given the limited information from the balancing measurements – is found. An explanation of the cost function and balancing so as to minimise this is given next. All of the theory presented in the above sections is subsequently illustrated through two separate examples, one of which is based upon a simple disc and the other being a more detailed simulation more specific to rotor balancing.

Finally, this section examines whether correcting this particular state of unbalance is the best approach to achieve the final objective of minimising the vibration of the rotor in its respective high speed machine.

8.2.1 Covariance Matrix Nomenclature

This section was published as a self-contained paper. Therefore the extensive notation for just this section is listed here.

Symbol	Description
ω	rotation speed (rad/s)
$\mathbf{A}$	a matrix defining cost
$\tilde{C}$	the transpose of a matrix relating unbalance components to measurable outputs
$\mathbf{C_R}$	real part of $\tilde{C}$
$\mathbf{C_I}$	imaginary part of $\tilde{C}$
$\mathbf{C_X}$	the $\tilde{C}$ matrix rearranged into the expanded, real form
Cov	co-variance matrix of unbalance
DoF	degrees of freedom
d	the Mahalanobis Distance
$\mathbf{D}$	system damping matrix
$\mathbf{f}$	vector of generalised forces

$\mathbf{g}$	intermediate vector used to compute u_k
$\mathbf{h}$	intermediate vector used to compute u_k
J(u)	cost function evaluated at a given state of unbalance
$\mathbf{K}$	system stiffness matrix
$\mathbf{\Lambda}$	eigenvalue matrix of co-variance matrix
$\mathbf{\Lambda}_{new}$	above eigenvalue matrix with small value added to all entries
$\mathbf{M}$	system mass matrix
$\mathbf{p}$	vector containing corrective unbalances
$\mathbf{Q}$	eigenvector matrix of co-variance matrix
SVD	singular value decomposition
$\mathbf{S}$	selection matrix that restricts corrective unbalances to the designated balance planes
$\mathbf{S}_{C1}$	singular value matrix obtained from singular value decomposition of $\mathbf{C}_X$
$\mathbf{S}_{C2}$	modified version of $\mathbf{S}_{C1}$
$\mathbf{S}_L$	input selection matrix
$\mathbf{S}_R$	transpose of output selection matrix
$\mathbf{T}$	matrix containing basis vectors used to compute u_u
u	scalar representation of a known component of unbalance
u_c	scalar representation of a corrective unbalance applied to balance u
u_x	unbalance component on a thin disc in the x-direction
u_y	unbalance component on a thin disc in the y-direction
$\mathbf{u}$	vector of unbalance
$\mathbf{u}_c$	corrective unbalance vector, giving nodal and directional positions
u_k	known component of initial unbalance
u_u	unknown component of initial unbalance
$\mathbf{U}_{C1}$	left matrix obtained from singular value decomposition of $\mathbf{C}_\mathbf{X}$
$\mathbf{U}_{C2}$	modified version of $\mathbf{U}_{C1}$

v	scalar representation of an unknown component of unbalance
v_c	scalar representation of a corrective unbalance applied to balance v
$\mathbf{V}$	eigenvector matrix of co-variance matrix
$\mathbf{V}_{C1}$	transpose of right matrix obtained from singular value decomposition of $\mathbf{C}_{\mathbf{X}}$
$\mathbf{V}_{C2}$	modified version of $\mathbf{V}_{C1}$
$\mathbf{W}$	weighting matrix for the outputs
$\mathbf{x}$	generalised displacements
$\tilde{\mathbf{y}}$	outputs
$\mathbf{y}_R$	real part of $\mathbf{y}$
$\mathbf{y}_I$	imaginary part of $\mathbf{y}$
$\mathbf{y}_X$	outputs rearranged into the expanded, real form

8.2.2 Modelling

This work employs Finite Element Analysis (FEA) to model rotor systems. For the examples presented, the rotor will be considered to comprise a shaft and some discs at various locations along the shaft. In fact, the methods are applicable to rotors of any form. In reality a rotor has an infinite number of Degrees of Freedom (DoFs) – as it is a continuous system. The application of FEA requires that the system be discretised so that a finite number of DoFs will be employed and therefore only a finite number of modes of vibration will exist. It is well known that provided the discretisation is sufficiently fine, the model will capture all relevant behaviour of the actual system.

Timoshenko beam elements are used to model the rotor shaft in the examples given here. Each node has a total of four DoFs – two translations and two rotations. It is considered that the rotor axis of rotation is horizontal and that this defines the global x-axis positive to the rear (right), that the y-axis is vertical with positive y being upwards and that the z-axis is a transverse axis such that O_{xyz} is a right-hand-screw axis set.

Loads applied to the nodes of the rotor could be either forces (corresponding to translations) or moments (corresponding to rotations). It will be considered that the shaft discretisation is sufficiently fine that the distribution of unbalance on the rotor can be represented by transverse forces only. Figure 51 shows a particular rotor configuration, which will be used throughout this paper. This shall be referred to as the “Example Rotor”. Tables 1 and 2 provide various details of this rotor.

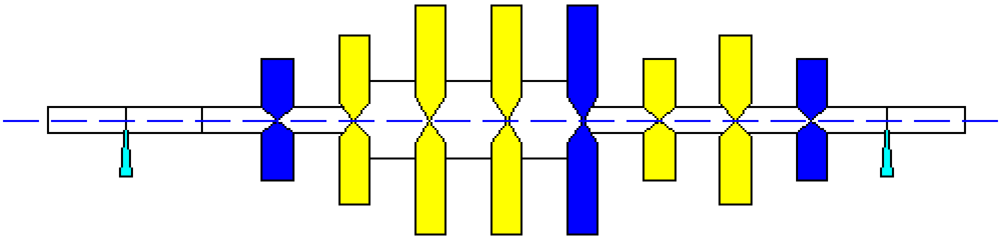

Figure 51: Example Rotor

Example Rotor Configuration	
Number of elements	12
Number of nodes	13
Number of DOFs	52
Number of discs	8
Number of bearings	2 bearings at nodes 2 and 12
Diameter of shaft	elements 1:4 and 9:12 = 35 mm
	elements 5:8 = 100 mm

Diameter of discs	discs 1,6,8 = 160 mm
	discs 2,7 = 225 mm
	Discs 3,4,5 = 300 mm
Thickness of discs	40 mm

Table 1: Description of the Example Rotor model

Material Properties	
Young's Modulus (E)	211 GPa
Poisson's Ratio (v)	0.3
Shear Modulus (G)	E/2(1+v)
Density	7810Kg/m3

Table 2: Material Properties used in the example rotor model

The synchronous vibration response caused by a given state of unbalance is calculated from the equations of motion for a system in natural second-order form:

$$\mathbf{f} = \mathbf{S}_L \omega^2 \mathbf{u}$$

$$\mathbf{M}\ddot{\mathbf{x}} + \mathbf{D}\dot{\mathbf{x}} + \mathbf{K}\mathbf{x} = \mathbf{f} \tag{8.1}$$

$$\mathbf{y} = \mathbf{S}_R^{\mathbf{T}} \mathbf{x}$$

where $\mathbf{u}$ is the vector of unbalance on the rotor (two entries per node); $\mathbf{S}_L$ is a selection matrix that converts $\mathbf{u}$ into the generalised force vector $\mathbf{f}$; $\mathbf{M}$, $\mathbf{D}$ and $\mathbf{K}$ are the system mass, damping and stiffness matrices respectively; $\mathbf{x}$ is the vector of generalised displacements and $\mathbf{S}_R^T$ is another selection matrix that converts $\mathbf{x}$ into the output vector. The output vector will contain all vibration resultants of relevance and these may include absolute rotor displacements, absolute stator displacements, displacements of rotor relative to stator (very important for control of clearances), rotor and stator stresses, bending moments, bearing reactions and so forth. Matrices **K, D, M,** $\mathbf{S}_L$, $\mathbf{S}_R$ are all real.

When the usual complex substitutions for $\mathbf{x}$ are made to convert this into the frequency domain, the result is:

$$\tilde{\mathbf{y}} = \mathbf{S}_R^T(\mathbf{K} + i\Omega\mathbf{D} - \mathbf{M}\Omega^2)^{-1}\mathbf{S}_L\omega^2\mathbf{u} \tag{8.2}$$

where $\tilde{\mathbf{y}}$ is now a complex valued function of ω only.

8.2.3 States of Unbalance and the Co-Variance Matrix

The method advocated here rests on the assumption that a population of rotors manufactured by the same processes and under the same conditions will have unbalance vectors characterised by some co-variance matrix. This scatter of unbalance can be simulated given knowledge of the independent geometry and symmetry errors likely to be caused by the different component processes. A large sample of r different representative rotor unbalance vectors can be assembled from this knowledge and it is straightforward then to extract a good estimate for the underlying co-variance matrix. Co-variance is a measure of the inter-dependence of two random variables. If two variables are completely independent of each other, then the co-variance between them is zero. Denoting the co-variance matrix as $\mathbf{Cov}$, the general entry, (i,j) can be found as:

$$\mathbf{Cov}(i,j) = E\left[(\mathbf{u}(i) - \boldsymbol{\mu}(i))(\mathbf{u}(j) - \boldsymbol{\mu}(j))\right] \approx \frac{1}{r-1}\sum_{p=1}^{r}\left(\mathbf{u}_p(i) - \mathbf{m}(i)\right)\left(\mathbf{u}_p(j) - \mathbf{m}(j)\right)$$

- (8.3)

Where $\boldsymbol{\mu}$ denotes the population mean of the unbalance vectors, and

$$\mathbf{m}(i) := \frac{1}{r}\sum_{p=1}^{r}\left(\mathbf{u}_p(i)\right) \tag{8.4}$$

In the above equations, vector $\mathbf{u}_p$ describes the state of unbalance of the p^{th} rotor of the sample. Two important observations can be made about the co-variance matrix. Firstly, its leading diagonal can be recognised as the variances of the nodal unbalances. Secondly, the matrix is symmetric.

Once the co-variance matrix has been computed, information about the significant patterns of unbalance in the batch can be extracted from it. The eigenvalues are variances of the multiplication coefficients used on the eigenvectors that combine linearly to form a given state of net unbalance. The eigenvectors form a new basis that can be used to describe any individual state of unbalance, and indicate the patterns of unbalance that exist in the batch. In this new basis, the random variables are the multiplication coefficients and these are independent of each other (i.e. the co-variance between them is zero).

The eigenvalues and eigenvectors should be considered together, so as to judge whether a given unbalance pattern has substantial presence in the batch (i.e. an eigenvector that is associated with a larger eigenvalue has a higher presence within the batch as compared to one that is associated with a small eigenvalue). Therefore it is the larger eigenvalues and associated eigenvectors that are of concern.

8.2.4 The Co-Variance Matrix as an Estimator of Relative Likelihood of Particular Unbalance States

The co-variance matrix can also be used more directly to assess the relative likelihood of a given state of unbalance. The Mahalanobis Distance d [(Mahalanobis, 1936), (Kumar, 2005)] of a given unbalance vector $\mathbf{u}$ is given by:

$$d^2 = \mathbf{u}^{\mathbf{T}}\left[\mathbf{Cov}\right]^{-1}\mathbf{u} \tag{8.5}$$

The meaning of this distance is best illustrated with a simple, 2-dimensional case, where:

$$\mathbf{u} =: \begin{Bmatrix} u_1 \\ u_2 \end{Bmatrix} \tag{8.6}$$

In this case, d is a measure of the distance in standard deviations of the equal conditional probability density contour of u_1 and u_2 from the centre of the joint distribution. Thus, it is a measure of the relative likelihood of any vector $\mathbf{u}$, where large values of d correspond to a large number of standard deviations, and thus low probability densities, while small values of d correspond to a small number of standard deviations, and thus high probability densities. The standard deviation units are with reference to the Standard Normal Distribution - as u_1 and u_2 have been normalized with respect to their respective standard deviations – and therefore d is dimensionless. The general case of the Mahalanobis distance extends this concept to an n–dimensional space.

It is found that if the individual random variables within $\mathbf{u}$ follow a Normal Distribution, then the values of distance d follow a Chi-square Distribution with a number of degrees of freedom (in the statistical sense) equal to the dimension of ($\mathbf{u}$-1).

8.2.5 Enriching Readings from a Balancing Test Using the Covariance Matrix

Equation 8.2 may be used – in theory - for the purpose of finding the unbalance that would cause an observed response, provided that $\mathbf{y}$ contains at least as many entries as $\mathbf{u}$. However, a problem is encountered at this stage. The natural modes of a flexible rotor make a significant contribution to response only at rotational speeds somewhere in the range of the critical speed corresponding to these modes. Unfortunately the rotor cannot be spun at high speeds, and therefore the measured responses do not contain information about components of unbalance that excite the higher frequency modes. This means that a comprehensive balancing operation of the rotor cannot be performed based only on the readings of a balancing machine.

Equation 8.2 may be expressed in the compact form

$$\tilde{\mathbf{y}} = \tilde{\mathbf{C}}^{\mathbf{T}}\mathbf{u}\,. \tag{8.7}$$

In the case of the example rotor introduced in section 8.2.2, $\tilde{\mathbf{C}}^{\mathbf{T}}$ will have 26 columns. The number of rows is equal to the number of outputs. In the above equation, $\tilde{y}$ and $\tilde{\mathbf{C}}^{\mathbf{T}}$ are complex (this is evident from eq. 8.2) whereas $\mathbf{u}$ is real. Equation 8.7 may be readily transformed into fully real form as follows:

$$\tilde{\mathbf{y}} =: \mathbf{y}_{\mathbf{R}} + i\mathbf{y}_{\mathbf{I}} \text{ and } \tilde{\mathbf{C}}^{\mathbf{T}} =: \tilde{\mathbf{C}}_{\mathbf{R}}^{\mathbf{T}} + i\tilde{\mathbf{C}}_{\mathbf{I}}^{\mathbf{T}} \tag{8.8}$$

$$\mathbf{y}_{\mathbf{X}} = \begin{Bmatrix} \mathbf{y}_{\mathbf{R}} \\ \mathbf{y}_{\mathbf{I}} \end{Bmatrix} = \begin{Bmatrix} \mathbf{C}_{\mathbf{R}}^{\mathbf{T}} \\ \mathbf{C}_{\mathbf{I}}^{\mathbf{T}} \end{Bmatrix}\mathbf{u} = \mathbf{C}_{\mathbf{X}}^{\mathbf{T}}\mathbf{u} \tag{8.9}$$

Generally, the rank of $\mathbf{C}_{\mathbf{X}}^{\mathbf{T}}$ will be substantially lower than the number of rows in this matrix. The linear dependence of certain rows in this matrix is a reflection of the linear dependence of certain rows in $\mathbf{y}_{\mathbf{X}}$, arising from its lack of information about higher modes of excitation within the rotor. By performing singular value decomposition (SVD) on $\mathbf{C}_{\mathbf{X}}$, it may be written as:

$$\mathbf{C}_{\mathbf{X}} = \mathbf{U}_{\mathbf{C1}}\mathbf{S}_{\mathbf{C1}}\mathbf{V}_{\mathbf{C1}}^{\mathbf{T}} \tag{8.10}$$

where $\mathbf{U}_{\mathbf{C1}}$ and $\mathbf{V}_{\mathbf{C1}}$ are orthogonal matrices and $\mathbf{S}_{\mathbf{C1}}$ is diagonal and positive definite. It is the zero or near zero singular values (i.e. entries in $\mathbf{S}_{\mathbf{C1}}$) that cause of $\mathbf{C}_{\mathbf{X}}^{\mathbf{T}}$ to be low-rank. Thus, such singular values are eliminated from $\mathbf{S}_{\mathbf{C1}}$, along with the corresponding columns of $\mathbf{U}_{\mathbf{C1}}$ and rows of $\mathbf{V}_{\mathbf{C1}}^{\mathbf{T}}$. The threshold for elimination of near-zero singular values may be set based on the resolution of most measurement instruments. It may be asserted that all singular values that are less than a thousandth of the largest one are effectively zero.

The truncated SVD matrices will be called $\mathbf{U_{C2}}$, $\mathbf{S_{C2}}$ and $\mathbf{V_{C2}^T}$ respectively. This action makes $\mathbf{S_C}$ a diagonal, square and invertible matrix. Note that there will not be a noticeable change to the values in $\mathbf{C_X}$ when it is reconstructed with the truncated, smaller SVD matrices using the following equation:

$$\mathbf{C_X} = \mathbf{U}_{\mathbf{C}2}\mathbf{S}_{\mathbf{C}2}\mathbf{V}_{\mathbf{C}2}^{\mathbf{T}} \tag{8.11}$$

Now the full vector of unbalance – which as yet is unknown – may be divided into a known (detectable) and unknown (undetectable) component:

$$\mathbf{u} = \mathbf{u}_k + \mathbf{u}_u \tag{8.12}$$

The known component is that which can be obtained directly from the measured outputs. This can always be expressed as a product between $\mathbf{U_{C2}}$ and some vector $\mathbf{g}$.

$$\mathbf{u}_k = \mathbf{U_{C2}g} \tag{8.13}$$

Substitute equations 8.11, 8.12 and 8.13 into eq. 8.9 to get

$$\mathbf{y}_x = \mathbf{V_{C2}S_{C2}U_{C2}^T}\left(\mathbf{U_{C2}g} + \mathbf{u}_u\right). \tag{8.14}$$

As vector $\mathbf{u}_u$ is orthogonal to $\mathbf{C_X}$,

$$\mathbf{C_X^T u}_u = \mathbf{0} \tag{8.15}$$

This, together with the orthogonal nature of $\mathbf{U_{C2}}$ allows simplification of eq. 8.14 to give

$$\mathbf{y_X} = \mathbf{V_{C2}S_{C2}g} \tag{8.16}$$

and pre-multiply eq.8.16 by $\mathbf{U_{C2}S_{C2}^{-1}V_{C2}^T}$ to get

$$\mathbf{u}_k = \mathbf{U_{C2}g} = \mathbf{U_{C2}S_{C2}^{-1}V_{C2}^T y_X}. \tag{8.17}$$

Thus, an expression is obtained relating $\mathbf{u}_k$ and the measured outputs. The above approach to finding $\mathbf{u_k}$ ensures that this vector takes the best possible numerically conditioned value; i.e. its Euclidean norm is a minimum. Other vectors $\mathbf{u}_k$ can also satisfy eq. 8.9.

A suitable expression for $\mathbf{u}_u$ may now be found. Let:

$$\mathbf{u}_u = \mathbf{Th} \tag{8.18}$$

where $\mathbf{h}$ is a vector unknown as yet and $\mathbf{T}$ is a matrix forming an orthogonal basis for all possible vectors $\mathbf{u_u}$ satisfying eq. 8.15, that fills the null space of $\mathbf{U_{C2}^T}$. A good choice of $\mathbf{T}$ is the set of columns of $\mathbf{U_{C1}}$ that are absent from $\mathbf{U_{C2}}$.

Now, eq. 8.12 becomes:

$$\mathbf{u} = \mathbf{u}_k + \mathbf{Th}\,. \tag{8.19}$$

Since $\mathbf{u}_k$ is determined from eq. 8.17, the only unknown variable in the above expression is the vector $\mathbf{h}$. Therefore the objective now is to find a suitable value for this. The most likely unknown component of unbalance of a particular rotor can be estimated using the covariance matrix of the batch by minimising the Mahalanobis distance, defined by:

$$d^2 = (\mathbf{u}_k + \mathbf{Th})^{\mathbf{T}} [\mathbf{Cov}]^{-\mathbf{1}} (\mathbf{u}_k + \mathbf{Th}) \tag{8.20}$$

Differentiating the expression with respect to $\mathbf{h}$, then equating to zero results in the following expression for the best vector $\mathbf{h}$:

$$\mathbf{h} = -\left(\mathbf{T^T}[\mathbf{Cov}]^{-1}\mathbf{T}\right)^{-1}\left(\mathbf{T^T}[\mathbf{Cov}]^{-1}\mathbf{u_k}\right) \tag{8.21}$$

Multiply this by $\mathbf{T}$ to get

$$\mathbf{u}_u = -\mathbf{T}\left(\mathbf{T^T}[\mathbf{Cov}]^{-1}\mathbf{T}\right)^{-1}\left(\mathbf{T^T}[\mathbf{Cov}]^{-1}\mathbf{u}_k\right) \tag{8.22}$$

Thus, the most likely value for the undetectable component of unbalance has been computed. When this is summed up with $\mathbf{u_k}$, the most likely state of complete unbalance is obtained.

Since most of the eigenvalues of $\mathbf{Cov}$ are near-zero, the matrix itself is almost singular. This problem can be overcome by adding a very small number to all the eigenvalues, and using the modified eigenvalue matrix and original eigenvector matrix (which is orthogonal) to express $\mathbf{Cov}^{-1}$. Viz.,

$$\mathbf{Cov} = \mathbf{Q}\Lambda_{\mathbf{new}}\mathbf{Q^T}$$

$$\mathbf{Cov}^{-1} = \mathbf{Q}\Lambda^{-1}{}_{\mathbf{new}}\mathbf{Q}^{\mathbf{T}} \tag{8.23}$$

where $\mathbf{Q}$ is the original matrix of eigenvectors and $\mathbf{\Lambda}_{\mathbf{new}}$ is the reconstructed non-singular matrix of eigenvalues. The number that is added should obviously be a proportion of the largest original eigenvalue, and a sensitivity study should be conducted to ensure that this value is neither too small (causing the eigenvalue matrix to remain almost singular) nor too large (causing the non-zero eigenvalues to increase by a significant amount such that the calculated values of $\mathbf{u}_{\mathrm{u}}$ begin to change).

The vector $\mathbf{u}_{\mathrm{u}}$ that is obtained by this procedure takes the *most likely* value. Therefore if balancing is performed on all rotors in the batch taking into account the respective most likely vector $\mathbf{u}_{\mathbf{u}}$ of each rotor, there is no guarantee that the residual vibration will have reduced in all cases. However, in most cases it would be less than that obtained if balancing had been performed assuming $\mathbf{u}_{u}$ to be zero.

It is worth mentioning that the requirement to determine the complete state of unbalance would not exist if it is possible to rotate the rotor at very high speeds in the balancing tests. In this case, the influence coefficient method may be used to balance the rotor at the required speeds.

8.2.6 The Cost Function – A Measure of Residual Vibration

In the general case, the cost function is a weighted sum of squares of the outputs at selected locations within the rotor. In the present work, it is defined as the weighted sum of squares of translations at all nodes of the rotor, in both planes. Therefore it is sought to minimise cost via the balancing procedure.

The cost function may generally be expressed as follows:

$$cost = \mathbf{y}_{\mathrm{X}}^{\mathrm{T}}\mathbf{W}^{2}\mathbf{y}_{\mathbf{X}} \tag{8.24}$$

where $\mathbf{W}$ is a diagonal matrix that weights the entries in $\mathbf{y}_{\mathbf{X}}$. Substituting for $\mathbf{y}_{\mathbf{X}}$ from eq. 8.9 gives:

$$cost = \mathbf{u}^{\mathrm{T}}\mathbf{C}_{\mathrm{X}}\mathbf{W}^{2}\mathbf{C}_{\mathrm{X}}^{\mathrm{T}}\mathbf{u} \tag{8.25}$$

where a separate version of the $\mathbf{C}_{\mathbf{X}}^{\mathbf{T}}$ matrix is used such that the weighted sum of squares of all nodal translations is computed. For simplicity, the above may be expressed as:

$$cost = \mathbf{u}^{\mathrm{T}}\mathbf{A}\mathbf{u}. \tag{8.26}$$

When a corrective unbalance is applied to the existing unbalance, this becomes

$$cost = (\mathbf{u}+\mathbf{u}_{\boldsymbol{c}})^{\mathrm{T}}\mathbf{A}(\mathbf{u}+\mathbf{u}_{\boldsymbol{c}}). \tag{8.27}$$

Note that the corrective unbalances can only be applied at the designated balancing planes. Therefore a constraint should be applied to $\mathbf{u}_{\mathbf{c}}$ such that the corrections are located at these nodes. Viz.,

$$\mathbf{u}_{\mathrm{c}}=\mathbf{S}\mathbf{p} \tag{8.28}$$

where the length of $\mathbf{p}$ is equal to the number of balance planes and $\mathbf{S}$ is a selection matrix that chooses the correct locations for the corrective unbalances. Now the cost expression becomes

$$cost = (\mathbf{u}+\mathbf{S}\mathbf{p})^{\mathrm{T}}\mathbf{A}(\mathbf{u}+\mathbf{S}\mathbf{p}) \tag{8.29}$$

This expression is differentiated with respect to p and equated to zero to find its value which gives rise to minimum cost; the following expression is then obtained:

$$\mathbf{p} = -\left(\mathbf{S}^{\mathbf{T}}\mathbf{A}\mathbf{S}\right)^{-1}\left(\mathbf{S}^{\mathbf{T}}\mathbf{A}\mathbf{u}\right) \tag{8.30}$$

Multiply by S to get:

$$\mathbf{u}_{\mathbf{c}} = -\mathbf{S}\left(\mathbf{S}^{\mathbf{T}}\mathbf{A}\mathbf{S}\right)^{-1}\left(\mathbf{S}^{\mathbf{T}}\mathbf{A}\mathbf{u}\right) \tag{8.31}$$

8.2.7 Example of a disc.

Consider the simple example of a single thin disc, where a coordinate system can be established with one of the axes aligned with, say, a keyway in the disc, as shown in the diagram below:

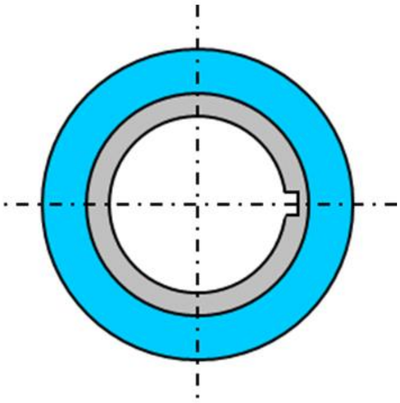

Figure 52: Thin disc with a keyway

Suppose that all discs in the batch were clamped at a certain fixed orientation during the manufacturing phase. It is very likely, therefore, that a component of unbalance could be caused along this direction either due to the embedding of foreign particles or due to the removal of material from the disc.

$$\mathbf{u}_p = \begin{Bmatrix} u_x \\ u_y \end{Bmatrix} \tag{8.32}$$

In this context, an unbalance "pattern" is any given instance $\{u_x, u_y\}$ which is defined in vector $\mathbf{u}_p$ in equation (8.23). The covariance matrix for a batch of these discs will be (2×2), and may be expressed as follows

$$\mathbf{Cov} = \begin{bmatrix} \sigma_x^2 & \sigma_{xy}^2 \\ \sigma_{xy}^2 & \sigma_y^2 \end{bmatrix} \tag{8.33}$$

where the diagonal terms are the x and y variances respectively, and the off-diagonal terms are the covariance between the unbalance in these two directions and indicate the coupling between them. Suppose that the co-variance matrix for a certain batch of these discs is found to be:

$$\mathbf{Cov} = \begin{bmatrix} 0.0577 & 0.0768 \\ 0.0768 & 0.1024 \end{bmatrix} \tag{8.34}$$

This matrix will have eigenvalues and eigenvectors given by $\mathbf{L}_{disc}$ and $\mathbf{V}_{disc}$

respectively, where

$$\mathbf{L}_{disc} = \begin{bmatrix} 1 & 0 \\ 0 & 0.0001 \end{bmatrix}, \quad \mathbf{V}_{disc} = \begin{bmatrix} 0.6 & 0.8 \\ 0.8 & -0.6 \end{bmatrix} \tag{8.35}$$

By inspection of the eigenvalues, it can be seen that it is more likely that any unbalance will lie in the direction $\begin{Bmatrix} 0.6 \\ 0.8 \end{Bmatrix}$, than in the orthogonal direction $\begin{Bmatrix} 0.8 \\ -0.6 \end{Bmatrix}$. In fact, this likelihood may be estimated as being $\sqrt{\frac{1}{0.0001}} = 100$ times higher.

Suppose it is known that the unbalance in the x-direction is exactly u_x = 24 gr.mm, but nothing is known about the unbalance in the y-direction, u_y**.** The most likely value for this may be estimated, using the covariance matrix of the batch given above. From eq. 8.5,

$$d^2 = \{24 \quad u_y\} \begin{bmatrix} 0.0577 & 0.0768 \\ 0.0768 & 0.1024 \end{bmatrix}^{-1} \begin{Bmatrix} 24 \\ u_y \end{Bmatrix} \tag{8.36}$$

The value of u_y which results in a minimum of d gives the most likely case of u**.** This value is found to be 31.944 g.mm.

8.2.8 Simulated example of a rotor

Here, we consider a batch of rotors produced by the same manufacturing processes, under the same conditions. The shafts of these rotors are hollow. Suppose that the centreline of the shaft bore is not a straight line between the geometric centres of the outer cylinder but that it follows a curve composed predominantly of the four components illustrated in *Figure 54.*

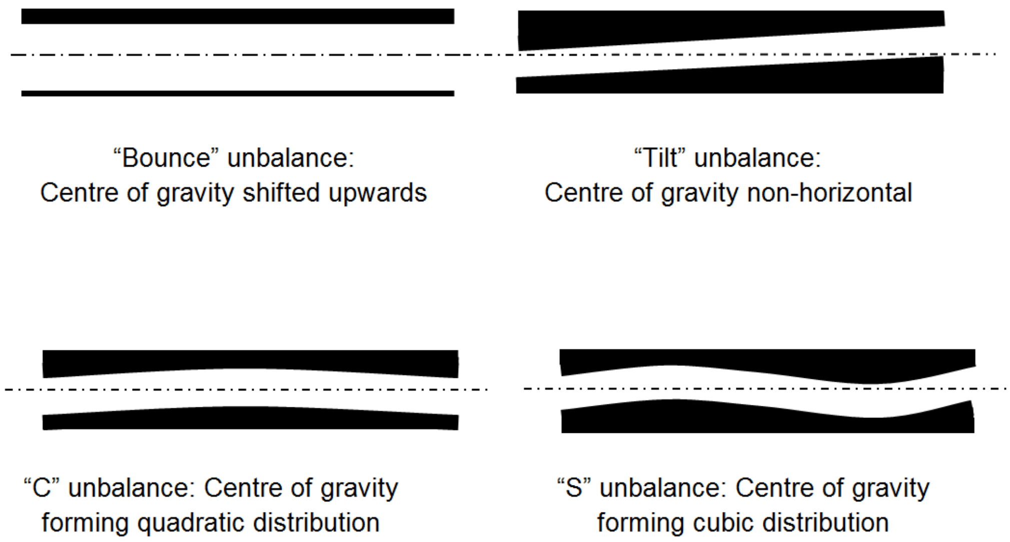

Figure 53: Typical patterns of unbalance

A batch of 1000 such rotors is modelled – nominally of the example rotor configuration. A right handed coordinate system with x along the rotor axis positive to the right and y vertically upward is applied. Each rotor has a different bore trajectory whose y and z coordinates, $u(x)$ and $v(x)$ respectively, are given by:

$$u(x) = 0.005\left(\rho_{uB} + \rho_{uT}\left(\frac{2x}{L}\right) + 0.1\rho_{uC}\left(\frac{1}{2} - \frac{3}{2}\left(\frac{2x}{L}\right)^2\right) + 0.001\rho_{uS}\left(\left(\frac{2x}{L}\right) - 2\left(\frac{2x}{L}\right)^3\right)\right) + 10^{-6}\nu_u(x)$$

$$v(x) = 0.005\left(\rho_{vB} + \rho_{vT}\left(\frac{2x}{L}\right) + 0.1\rho_{vC}\left(\frac{1}{2} - \frac{3}{2}\left(\frac{2x}{L}\right)^2\right) + 0.001\rho_{vS}\left(\left(\frac{2x}{L}\right) - 2\left(\frac{2x}{L}\right)^3\right)\right) + 10^{-6}\nu_v(x)$$

where each of $\{\rho_{uB}, \rho_{vB}, \rho_{uT}, \rho_{vT}, \rho_{uC}, \rho_{vC}, \rho_{uS}, \rho_{vS}\}$ are random variables following a standard normal distribution and where $\{\nu_u(x), \nu_v(x)\}$

are random functions of x (represented by 13 individual nodal values and having a root-mean square value of unity) . L is the length of the rotor. Evidently, each rotor will have a random pattern of unbalance on it.

The co-variance between the nodal unbalances of all rotors can now be computed and arranged to form the co-variance matrix, as per eq. 8.3. The process may be summarised as follows:

$$\underbrace{\begin{Bmatrix} u_{1,1}\\ u_{1,2}\\ u_{1,3}\\ \cdots\\ u_{1,26}\end{Bmatrix}, \begin{Bmatrix} u_{2,1}\\ u_{2,2}\\ u_{2,3}\\ \cdots\\ u_{2,26}\end{Bmatrix}, \ldots\ldots, \begin{Bmatrix} u_{1000,1}\\ u_{1000,2}\\ u_{1000,3}\\ \cdots\\ u_{1000,26}\end{Bmatrix}}_{\text{Unbalance vectors, for all 1000 rotors}} \quad \boldsymbol{\rightarrow} \quad \underbrace{\begin{Bmatrix} u_{m,1}\\ u_{m,2}\\ u_{m,3}\\ \cdots\\ u_{m,26}\end{Bmatrix}}_{\text{Sample mean of unbalance}} \quad \boldsymbol{\rightarrow} \quad \underbrace{\begin{bmatrix} \sigma_{u1u1} & \sigma_{u1u2} & \sigma_{u1u3} & \cdots & \sigma_{u1u26}\\ \sigma_{u2u1} & \sigma_{u2u2} & \sigma_{u2u3} & \cdots & \sigma_{u2u26}\\ \sigma_{u3u1} & \sigma_{u3u2} & \sigma_{u3u3} & \cdots & \sigma_{u3u26}\\ \cdots & \cdots & \cdots & \cdots & \cdots\\ \sigma_{u26u1} & \sigma_{u26u2} & \sigma_{u26u3} & \cdots & \sigma_{u26u26}\end{bmatrix}}_{\text{Co-variance Matrix}}$$

Recall that the beam elements used in the example rotor have two translational DOFs per node. Therefore, for this 13-node system the unbalance vectors will be (26×1).

The sample mean unbalance column is obtained as per eq. 8.4. In the above representation of the co-variance matrix, the notation is such that $\sigma_{up\,uq}$ is the co-variance between the entry up and the entry uq of the 1000 unbalance vectors.

The following figures show the significant eigenvectors and all of the eigenvalues of the co-variance matrix.

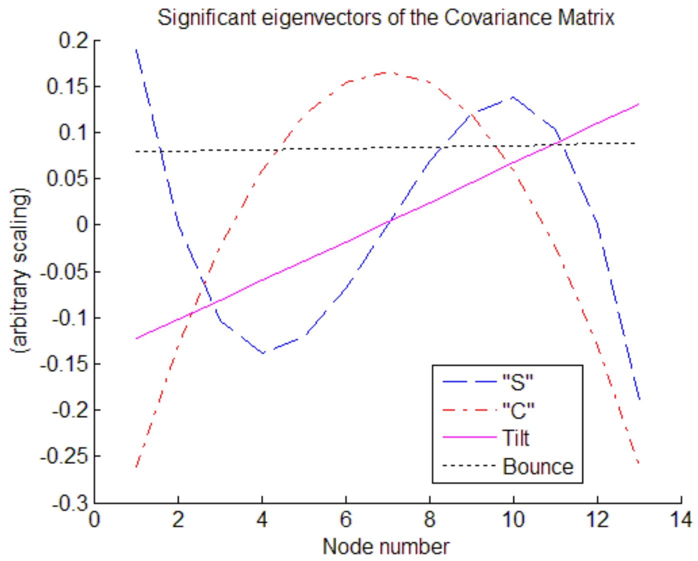

Figure 54: Significant eigenvectors of the co-variance matrix

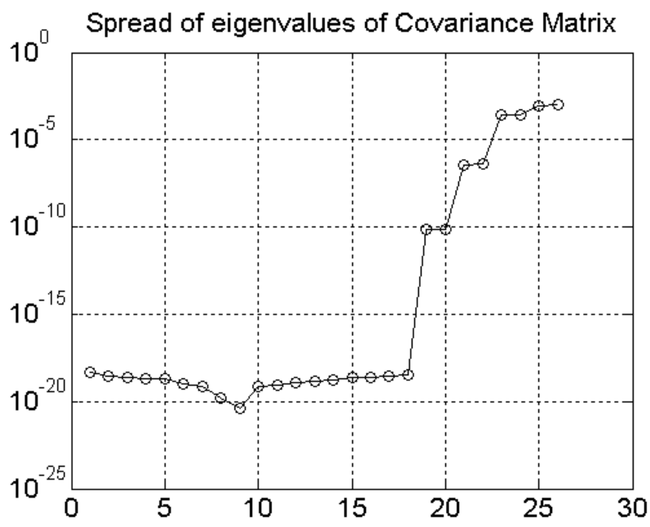

Figure 55: Eigenvalues of the co-variance matrix

The largest four eigenvalues correspond to the two rigid body unbalance shapes, i.e. the tilt and bounce unbalances, in both mutually perpendicular planes. The two below that correspond to the "C" shape flexural unbalance, and the two below that (near the 10^{-10} level) correspond to the "S" shape flexural unbalance. All other eigenvalues are virtually zero, meaning that all other eigenvectors of the co-variance matrix occur in negligible quantities. Notice that the magnitude of the eigenvalue of each respective unbalance pattern reflects the amount of this unbalance simulated initially.

A robust balancing operation will now be performed on all 1000 rotors in the batch, using the procedure that has been presented. Three discs on the rotor are designated as balancing planes. These are the ones shaded dark in *Figure 51*, located at nodes 4, 8 and 11.

- The co-variance matrix is expressed in terms of the reconstructed eigenvalues and original eigenvectors, such that the eigenvalue matrix is invertible. This has been achieved by adding 10^{-10} times the maximum eigenvalue, to all eigenvalues. A sensitivity study has been performed to ensure that this value is acceptable.

- The $\mathbf{M}$, $\mathbf{D}$ and $\mathbf{K}$ system matrices are computed (all these have dimension (52×52), and are identical for all rotors in the batch).

- A balancing speed of 5000 rpm is chosen, and response readings are set to be taken at the bearings (nodes 2 and 12). Since measurements are taken at 2 nodes, the output vector $\mathbf{y}$ will contain 4 entries (i.e. two readings per node). Some noise is incorporated into the values of $\mathbf{y}$.

- $\mathbf{C}^{\mathbf{T}}$ (4×26) is computed and rearranged into the expanded, real form. In this example, the outputs are assumed to be the nodal translations only, for simplicity.

- A separate version of $\mathbf{C}_{\mathbf{X}}^{\mathbf{T}}$ is calculated, with $\mathbf{S}_{\mathbf{R}}^{\mathbf{T}}$ chosen to be the identity matrix. This is required for calculation of the cost function based on all nodal translations, which will be performed later on.

- Singular value decomposition is performed on $\mathbf{C_X}$, and the $\mathbf{U_{C2}}$, $\mathbf{S_{C2}}$ and $\mathbf{V_{C2}^T}$ SVD Matrices are obtained (see equations 8.10 and 8.11).

- The $\mathbf{T}$ matrix is computed.

- Each rotor in turn is taken from the batch and run in a balancing machine at the chosen speed. The response at the mentioned locations is recorded.

- $\mathbf{y}$ is rearranged into the expanded, real form.

- $\mathbf{u}_k$ is now calculated from eq. 8.17.

- $\mathbf{u}_u$ is calculated using eq. 8.22.

- The next step is to compare the cost function in 2 cases, at a very high running speed.

1. The cost of the rotor balanced only with knowledge of $\mathbf{u}_k$
2. The cost of the rotor balanced with knowledge of $\mathbf{u}_k$ and the most likely value of $\mathbf{u}_u$

It is found that in all 1000 cases, the balancing operation that takes into account the most likely estimate of $\mathbf{u}_u$ results in a lower cost than when it is ignored. Furthermore, when the program is re-run with readings taken at nodes 5, 6, 8 and 11 in addition to the two bearings, yet again a lower cost is obtained in all cases when $\mathbf{u}_u$ is taken into account. The usefulness of the procedure in spite of the inclusion of additional readings reflects the enduring lack of information in the measurements, which may be explained as arising from the presence of measurement noise. The evident value of including $\mathbf{u}_u$ in the balancing procedure indicates the robustness of the method.

In a slight variation of this example where higher quantities of initial “C” and “S” unbalance patterns were specified and readings were taken at the bearings only, it transpired that in most, but not all cases, a lower cost had resulted after balancing. This may be explained as follows. If there are as many readings as unbalance patterns, then the system of equations is a fully determined one, and a unique value for $\mathbf{u}_k$ may be found. This will result in a more accurate value of $\mathbf{u}_u$. If there are more unbalance patterns present than readings, the system of equations is an under-determined one, and the best numerically conditioned value of $\mathbf{u}_k$ is found; this is not unique. In the initial simulation, the quantities of the two higher-mode patterns of unbalance were so small that the net unbalance was virtually a combination of bounce and tilt only. Therefore a unique value of $\mathbf{u}_k$ was found. In the second simulation, as there were much larger quantities of “C” and “S” unbalance patterns present, and yet only two readings, the system was under-determined. Therefore the best numerically conditioned value of $\mathbf{u}_k$ was found.

There is another conclusion to be drawn from the above. The maximum number of response readings required is equal to the number of existing independent unbalance patterns. Any excess readings will not provide information that is already not known, as the system of equations is already fully determined.

The above is merely an example to illustrate how the co-variance matrix can be used in the method presented in this paper. In reality, the co-variance matrix should be obtained through modelling of the manufacturing processes and conditions under which the rotors are made. It is only after this that an analysis of the like presented here is possible.

8.2.9 The best possible corrective unbalance

Hitherto, it has been shown that the balancing procedure is more robust when the most likely value of the undetectable component of unbalance is taken into account. However, attention has not been given to the influence of the cost function thus far. It remains to be seen whether balancing simply based on the most likely state of unbalance results in the absolute minimum cost that can ever be achieved.

The following procedure is demonstrated through an example. The unbalance is expressed in a two dimensional space, each dimension representing $\mathbf{u}_k$ and $\mathbf{u}_u$. These shall be named u and v respectively. Viz.,

$$\mathbf{u}_k =: \begin{Bmatrix} u \\ 0 \end{Bmatrix} \qquad \mathbf{u}_u =: \begin{Bmatrix} 0 \\ v \end{Bmatrix} \tag{8.37}$$

A (2×2) co-variance matrix is defined as

$$\begin{bmatrix} 9 & 12 \\ 12 & 25 \end{bmatrix} \tag{8.38}$$

This can be used to generate the conditional probability density contour plot between u and v. This plot is shown below:

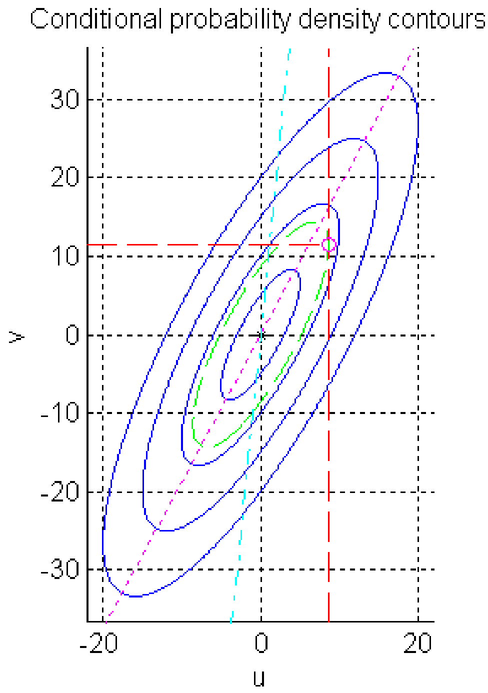

Figure 56: Conditional probability density contours

The ellipses are contours of equal probability density. Those closer to the centre of the distribution correspond to a smaller standard deviation and thus have a high probability density. Those further away correspond to a larger standard deviation and thus have a low probability density. The four solid ellipses shown here correspond to one, two, three and four standard deviations respectively, going outward from the centre.

For a given value of u, there is an entire distribution of possible values of v. The most likely value of v in this case is found by locating the point where the smallest possible ellipse is tangential to the given value of u. This is shown by the dashed ellipse in the above figure and the tangential point is located at the crossing between the horizontal and vertical dashed lines.

The conditional distribution of v can be obtained by plotting many ellipses of the like shown here, finding the corresponding probability density and plotting these against v. Thus, the number of data points obtained will be equal to the number of ellipses. The distribution is characterised by a mean and standard deviation, which can be found by fitting a normal distribution through the data points. The fitted, continuous function will be used in subsequent calculations.

It is now required to incorporate the cost function in some manner. A (2×2) matrix $\mathbf{A}$ is defined, where this has the same meaning as in equation 8.26. This should be a symmetric positive definite matrix. Furthermore, this matrix shall be constructed such that its two eigenvalues are substantially different (signifying a more elliptical shape of the conditional probability density contours) and its eigenvectors bear a substantial angle with those of the co-variance matrix. The latter results in the 'equal cost' ellipses of the cost function being at a different orientation to the equal conditional probability density ellipses between u and v.

The following integral is now evaluated:

$$\int_{-\infty}^{\infty} p(v)\, J\left(\begin{Bmatrix} u \\ v \end{Bmatrix} + \begin{Bmatrix} u_c \\ v_c \end{Bmatrix}\right) dv \tag{8.39}$$

which is the integral with respect to v of a product between the conditional probability density of v and the residual cost after applying a given set of balance corrections. From the definition of cost in eq. 8.26,

$$J\left(\begin{Bmatrix} u \\ v \end{Bmatrix} + \begin{Bmatrix} u_c \\ v_c \end{Bmatrix}\right) = \begin{bmatrix} u+u_c & v+v_c \end{bmatrix} \mathbf{A} \begin{Bmatrix} u+u_c \\ v+v_c \end{Bmatrix} \tag{8.40}$$

which results in a quadratic, scalar expression. For a given correction u_c and v_c, this integral is the sum of residual cost, weighted by the conditional probability density of the respective value of v across the entire distribution. Therefore it is a quantity that should be minimised by choosing the appropriate corrective unbalances.

As u corresponds to the known component, it would seem reasonable to balance this component with $u_c = -u$. Now, the above integral is evaluated for many different values of v_c, and the resulting values of the integral are plotted against v_c, under the conditional distribution plot for v. This plot is shown below.

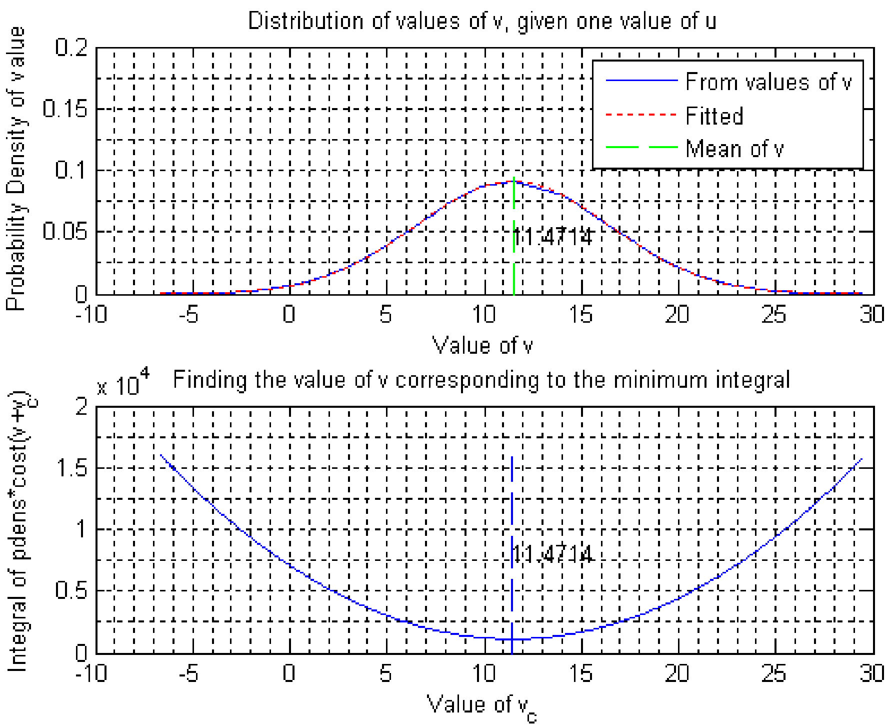

Figure 57: Comparison of the integral with the probability density plot

It can be seen from this plot that when the value of v_c is chosen to be equal to the mean of v – i.e. the most likely value of v – the integral takes its minimum value.

It may be concluded from this observation that if the known component is balanced by exactly its negative, then the best correction to be applied to v is its most likely value.

It is still not clear whether a value of the integral lower than this minimum can be obtained. Suppose u is balanced not exactly by its negative, but by slightly lower and higher values than this. It is found that when a slightly lower value of the negative of u is used to balance u, the respective minimum integral occurs at a value of v_c which is slightly higher than the mean of v and vice versa. However, the minimum value of the integral in both cases is higher than the minimum obtained when $u_c = -u$ and v_c equals the mean of v.

The conclusion to be drawn from this demonstration is that the best possible results are obtained when the balancing is performed based on the most likely value of the unknown component of unbalance.

8.2.10 Unbalance Co-variance Matrix Conclusions

This section has presented a novel, robust balancing method for rotors from high speed rotating machinery that are balanced in a balancing machine. A technique has been developed for estimating the most likely state of unbalance on a given rotor from a batch based on the unbalance co-variance matrix of the batch and experimental readings from the rotor. The merits of performing balancing via this approach have been demonstrated through a Matlab example.

Furthermore, it has been shown that the best possible balance correction - i.e. that which would bring the residual vibration down to its absolute minimum – is one that is based on the most likely value of the component of unbalance that is undetectable at lower rotational speeds.

8.3 Using Modular Balancing Methods to Inform the Balance Distribution of a Complex Rotor

Modular balancing is normal industry practice due to the requirements outlined in section 1.3. As designs have progressed and requirements become more challenging, an improvement in the outcome of low-speed modular balancing is required for rotors where some appreciable flexibility is present. With some small adaptations, it is possible to gain a much greater insight into the distribution of unbalance within a modular rotor. Using this data, it is possible to perform corrections to produce a low-speed balancing correction that will correct a rotor bend mode as well as the rigid body modes of the rotor.

8.3.1 The Use of Multiple Mass Simulators

The ideal situation in balancing rotors that experience appreciable flexibility during their operation is to correct all unbalances in the same axial locations that they arise. If this was possible, the limiting factor for the accuracy of balancing would be the resolution of the balancing machine. However, in low-speed balancing very little information is gained about the distribution of unbalance in a rotor; only the sum of unbalances in two planes is available. Because of this limitation, the low-speed balancing process often inadvertently builds-in large internal bending moments. The largest bending moment that is typically generated is when balancing simulators are used to simulate axially displaced components. This situation and bending moment diagram is illustrated in *Figure 28* where a typical HP compressor is balanced with a turbine mass simulator.

In the papers (Schneider, Balancing of Jet Engine Modules, 1988) and (Schneider, Exchangeability of rotor modules - a new balancing procedure for rotors in a flexible state, 2000) using a short mandrel followed by a balancing mass simulator is recommended as an option to gain more information about the unbalance distribution in a rotor. This method is also commonly followed in industry to identify the “high side” of a swashed joint face to facilitate a straight build alignment process. In the latter paper, Schneider outlines the following process for balancing:

8.3.2 Schneider’s Approach[3]

Step One: Short Mandrel Balancing

A short mandrel is a piece tooling that connects the rotor to the balancing machine in the shortest distance possible. This configuration is shown in *Figure 58* where it can be seen that the module joint alignment error labelled as ‘θ’, has a minimal effect on the eccentricity of the module “e”. This step therefore corrects for unbalances within the module and aligns them to a centreline that only exists on a short mandrel. The static unbalances that arise due to errors within the module in this configuration are denoted $\tilde{u}_{s,m(i)}$, they are defined collectively as a column vector $\tilde{\mathbf{u}}_{s,m} = \{\tilde{u}_{s,m(1)}, \tilde{u}_{s,m(2)}, \tilde{u}_{s,m(...)}\}$. Similarly, every point radial unbalance can have a point couple unbalance associated with it, defined by $\tilde{u}_{c,m(i)}$ and, collectively in the column vector, by $\tilde{\mathbf{u}}_{c,m}$ (note that only two are shown in the picture for clarity). For all of these unbalances, e is considered to be sufficiently small that it has no effect on the unbalances. Note that the paper does not mention the effect of an eccentricity error at the joint. It is instructed that balance correction should be applied to the module in this configuration, although it is optional whether it is temporary correction that is removed later in the balancing process, or permanent correction that remains with the module.

[3] Schneider’s equations have been adapted to use consistent notation with this thesis. Complex variables are used to represent vector quantities and are denoted with a tilde.

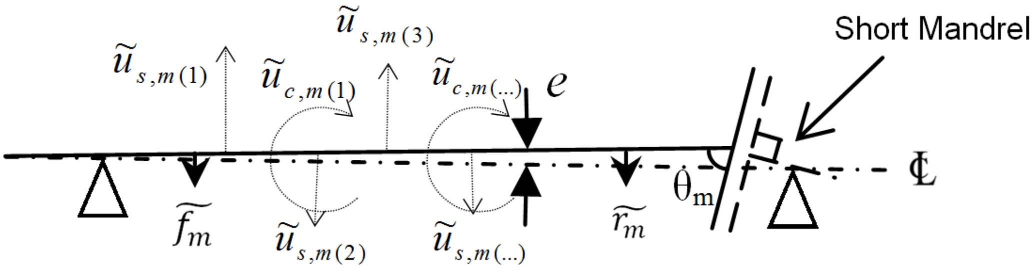

Figure 58: Module balance on a "Short Mandrel"

Step 2: Full Mass Simulator Balancing

Following the short mandrel correction, Schneider explains that the rotor should be assembled with the full mass simulator (as shown in *Figure 59*). It can be seen that two more distinct sets of unbalance data are now represented, these are the unbalances due to the joint face error angle θ_m associated with the module mass and what in the simulator (tooling) mass denoted $\tilde{u}_{s,m,\theta(i)}$ and $\tilde{u}_{s,t,\theta(i)}$. Similarly to the $\tilde{u}_{s,m(i)}$ unbalances, these are also collectively represented by column vectors $\tilde{\mathbf{u}}_{s,m,\theta}$ and $\tilde{\mathbf{u}}_{s,t,\theta}$, and have associated sets of unbalance couples $\tilde{\mathbf{u}}_{c,m,\theta}$ and $\tilde{\mathbf{u}}_{c,t,\theta}$.

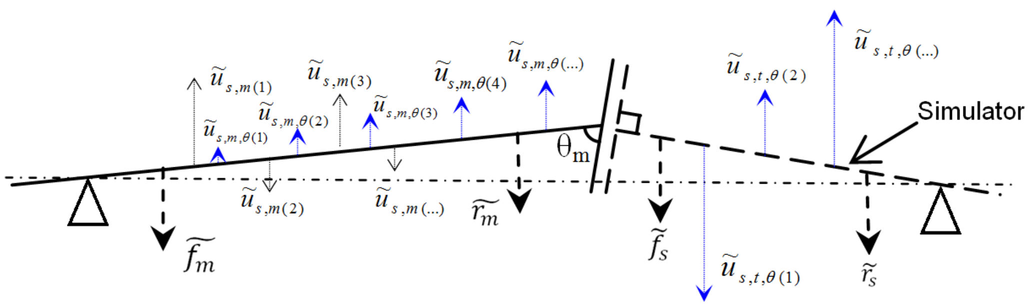

Figure 59: Module assembled with full mass simulator

Figure 60 is given to summarise the situation of the different sources of unbalance now present on the balancing machine:

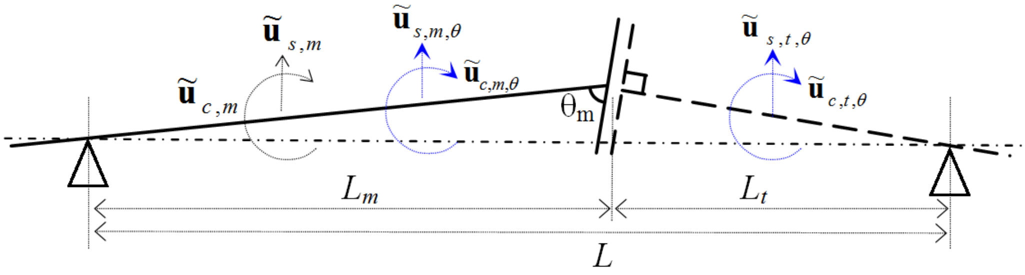

Figure 60: Module assembled with full mass simulator with unbalance vectors defined

Due to balancing corrections applied on the short mandrel in step 1, $\tilde{\mathbf{u}}_{s,m}$ and $\tilde{\mathbf{u}}_{c,m}$ have been nulled. Therefore, the unbalance detectable on the low-speed balancing machine in the two bearing planes $\tilde{f}_{m+t}$ and $\tilde{r}_{m+t}$, is a combination of the unbalances arising in the module ($\tilde{\mathbf{u}}_{s,m,\theta}$ and $\tilde{\mathbf{u}}_{c,m,\theta}$) and the simulator tooling ($\tilde{\mathbf{u}}_{s,t,\theta}$ and $\tilde{\mathbf{u}}_{c,t,\theta}$).

The purpose of this exercise is to gain knowledge of the unbalance distribution along the rotor, therefore it is necessary to be able to separate what unbalance arises in the module and simulator. The paper recommends calculating θ_m from the balancing machine results, (although it is noted that it could be directly measured), using the following equations that assume small angles:

$$\theta_m = (\tilde{f}_{m+t} + \tilde{r}_{m+t}) \frac{L}{L_m m_m x_m + L_t m_t (L - x_t)} \qquad (8.41)$$

Where the L values are the lengths of the rotor and modules as shown in *Figure 60*, x_m and x_t are the coordinates of the centres of masses of the module and simulator tooling respectively. The paper also gives an equation to calculate θ_m from the measured couple unbalance from the rotor which has not been reproduced here.

Now that θ_m is known, it is a relatively simple task to use knowledge of the geometric and mass properties of the rotor to calculate the static and couple unbalance that is arising from each significant mass along the rotor; fully populating the unbalance distribution vectors $\tilde{\mathbf{u}}_{s,m,\theta}$, $\tilde{\mathbf{u}}_{c,m,\theta}$, $\tilde{\mathbf{u}}_{s,t,\theta}$ and $\tilde{\mathbf{u}}_{c,t,\theta}$ which are then collectively defined as full rotor length unbalance and couple vectors by concatenation into column vectors $\tilde{\mathbf{u}}_{s,r,\theta}$ and $\tilde{\mathbf{u}}_{c,r,\theta}$:

$$\tilde{\mathbf{u}}_{s,r,\theta} = \begin{bmatrix} \tilde{\mathbf{u}}_{s,m,\theta} \\ \tilde{\mathbf{u}}_{s,t,\theta} \end{bmatrix} \tag{8.42}$$

$$\tilde{\mathbf{u}}_{c,r,\theta} = \begin{bmatrix} \tilde{\mathbf{u}}_{c,m,\theta} \\ \tilde{\mathbf{u}}_{c,t,\theta} \end{bmatrix} \tag{8.43}$$

Equation 8.44 gives the modal unbalance $\tilde{u}_{\omega}$ (as defined by (ISO11342, 1998)) of a rotor with q elements (i.e. significant masses)

$$\tilde{u}_{\omega} = \sum_{i=1}^{q} \left(\tilde{\mathbf{u}}_{s,r,\theta(i)} \tilde{\varphi}_{\omega(i)} + \tilde{\mathbf{u}}_{c,r,\theta(i)} \frac{d\tilde{\varphi}_{\omega(i)}}{dx} \right) \tag{8.44}$$

where $\varphi_{\omega(n)}$ denotes the "mode function" of mode ω as a function of axial location $x_{(n)}$. Schneider does not describe the source of this mode function.

Step 3: Calculation of unbalance corrections

Three planes of balancing corrections are assumed to be available in each module being balanced. These are denoted $\tilde{u}_{\kappa(n)}$ where n=1,2,3, as shown in *Figure 61*.

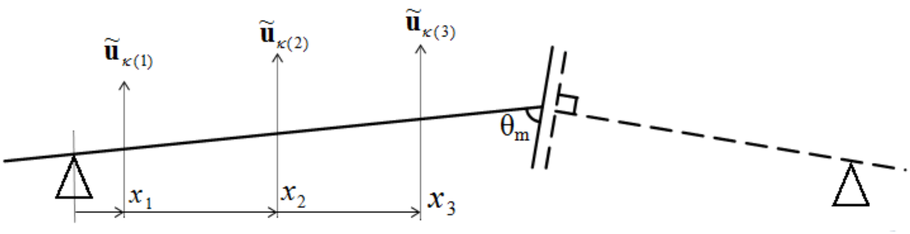

Figure 61: Three unbalance corrections planes in the module.

The three equations defined to calculate these corrections are given below:

$$\sum_{n=1}^{3} \tilde{u}_{\kappa(n)} = 0 \tag{8.45}$$

$$\sum_{n=1}^{3} \tilde{u}_{\kappa(n)} x_{(n)} = 0 \tag{8.46}$$

$$\sum_{n=1}^{3} \tilde{u}_{\kappa(n)} \tilde{\varphi}_{\omega(n)} = -\tilde{u}_{\omega} \tag{8.47}$$

This determinate set of equations is solved simultaneously for the three unbalance correction planes.

Step 4: Repeat for other modules

This process is repeated on the adjoining module if the module has sufficient dynamic bending in the mode shape for practical unbalance correction levels to be determined.

Discussion

This method works very well to achieve a satisfactory balancing result on modular rotors with some flexibility. However the disadvantage of this method is that it uses two mandrels which make it extremely time consuming in a production environment. For each mandrel the standard balancing indexing procedure has to be performed[4]. Disassembly/assembly of the rotor joint between the modules, which has to be performed at least twice for a standard balancing indexing process (normally three times if a joint repeatability test is needed) is very time consuming; one indexing process can take several hours for the following reasons:

- On many aerospace rotors the weight of the rotors is very large, so hoisting equipment is required for a joint disassembly/assembly.
- The best orientation to assemble a rotor is vertically to load the joint evenly, therefore a rotating assembly stand is required.
- The joints are very sensitive to the torque tightening methods used so a strict tightening sequence is used with multiple incremental torque steps.
- There are often a large number of bolts at the joint.
- Sometimes a heat treatment is needed to make or break the joint.
- Unless the build is performed in a clean-room, before each reassembly the rotor joint must be cleaned using solvents and compressed air to ensure that no debris has entered the joint (debris the thickness of a human hair can cause significant influence on the balancing result).
- The difference in bearing support locations between the short mandrel and the mass simulator means that the balancing machine setup has to be altered and sometimes the rotor drive method changed.

[4] In balancing, if tooling is used it must be possible to attach the tooling to the module being balanced at two relative angles, ideally 180° apart. This allows for any geometric or unbalance errors in the tooling to be eliminated from the balancing process mathematically. This allows for the assumption of the perfectly right angled joint face shown on the tooling in *Figure 58* and *Figure 59*.

8.3.3 The Dual Mass Simulator Approach

The following description illustrates the “dual mass simulator” proposal, which produces a very similar result to the method proposed by Schneider above, but only requires one indexing procedure, and one set-up of the balancing machine.

The general principle of the dual mass simulator is pictured in *Figure 62*, where an example of a turbine dual mass simulator can be seen is both heavyweight (a) and lightweight (b) configurations. The removable mass is located with a quick release mechanism that locates it very accurately and repeatably. The actual mechanism is not described as part of this study but many options are available because this mechanism has to carry very little load compared to the engine flange joint, so it can be very simple with few fasteners and contact points.

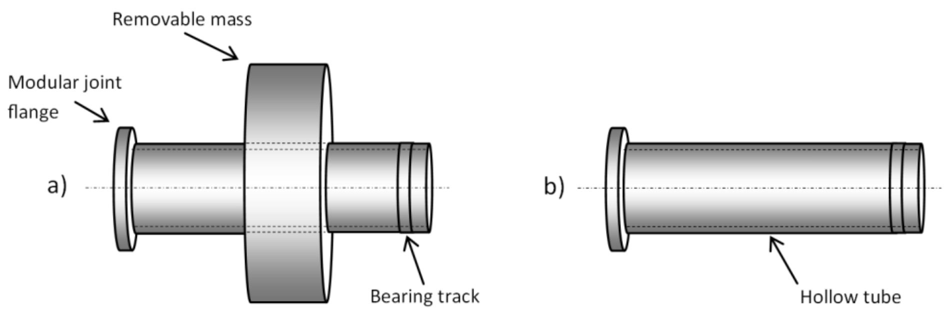

Figure 62: a) Example design of the “dual” mass simulator for a typical turbine. b) The simulator in lightweight configuration.

The process of using the dual mass simulator is very similar to Schneider’s method but the key details are outlined below:

Step One: Measure Unbalance on a Long Mandrel

The module is balanced using a balancing tooling mandrel that is intended to have zero mass but maintain the engine stator bearing location, which has been named a “long mandrel” for the purposes of this study. Obviously zero mass is not achievable, but it is considered negligible for the purposes of this explanation.

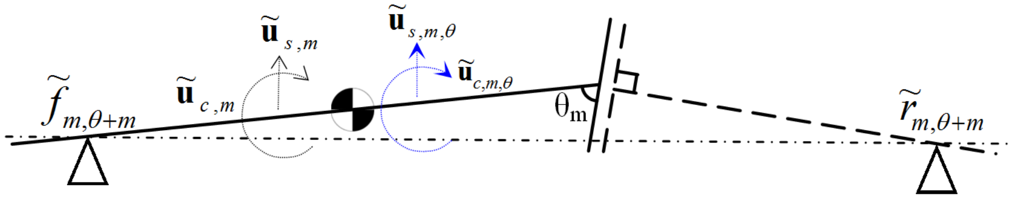

Figure 63: Balancing a module with a long mandrel of negligible mass

This situation is pictured in *Figure 63* where it can be seen that the unbalance distribution within the module due to the misalignment within the module is present (denoted $\tilde{\mathbf{u}}_{s,m}$ where $\tilde{\mathbf{u}}_{s,m(i)} = \{\tilde{\mathbf{u}}_{s,m(1)}, \tilde{\mathbf{u}}_{s,m(2)}, \tilde{\mathbf{u}}_{s,m(...)}\}^T$) together with the unbalance distribution arising from the angular joint error (denoted $\tilde{\mathbf{u}}_{s,m,\theta}$ where $\tilde{\mathbf{u}}_{s,m,\theta} = \{\tilde{\mathbf{u}}_{s,m,\theta(1)}, \tilde{\mathbf{u}}_{s,m,\theta(2)}, \tilde{\mathbf{u}}_{s,m,\theta(...)}\}$)). As previously, each static unbalance defined as $\tilde{u}_{s,m(i)}$ or $\tilde{u}_{s,m,\theta(i)}$ will have an associated point couple unbalance denoted $\tilde{u}_{c,m(i)}$ or $\tilde{u}_{c,m,\theta(i)}$ respectively (not pictured). The unbalance is measured on the balancing machine in this configuration at the bearings, and the complex readings are denoted $\tilde{f}_{m,\theta+m}$ and $\tilde{r}_{m,\theta+m}$.

Step Two: Measure Unbalance on a Long Mandrel with Mass Added

The next step in the process is to assemble the removable mass onto the long mandrel, as pictured in *Figure 62* a). The distribution of unbalances that now arises is identical to the situation pictured in *Figure 59* with three sets of unbalance present on the balancing machine, it is also summarised in *Figure 60* with the unbalances in vectors. The appropriate notation for the unbalance measured at the bearings in this case however would be $\tilde{f}_{m,\theta+m+t,\theta}$ and $\tilde{r}_{m,\theta+m+t,\theta}$.

In a variation of eq. 8.41, the angle of the joint at the mating face θ_m can now be calculated from the following:

$$\theta_m = \frac{(\tilde{f}_{m,\theta+m+t,\theta} + \tilde{r}_{m,\theta+m+t,\theta} - \tilde{f}_{m+t} - \tilde{r}_{m+t})}{m_t(L - x_t)} \tag{8.48}$$

Where L is the length of the rotor, m_t is the mass of the simulator tooling, and x_t is the coordinate of the centre of mass of the simulator (measured from the left hand bearing). The full situation is pictured in *Figure 64* below.

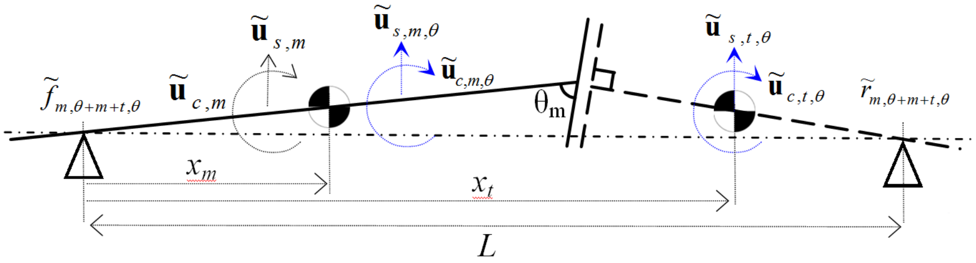

Figure 64: Balancing a module with a long mandrel plus mass

In the same way as Schneider recommended in step 2, now that θ_m is known, it is a relatively simple task to use knowledge of the geometric and mass properties of the rotor to calculate the static and couple unbalance that is arising from each significant mass along the rotor; fully populating the unbalance distribution vectors $\tilde{\mathbf{u}}_{s,m,\theta}$, $\tilde{\mathbf{u}}_{c,m,\theta}$, $\tilde{\mathbf{u}}_{s,t,\theta}$ and $\tilde{\mathbf{u}}_{c,t,\theta}$. However, there is another piece of information here that is not being exploited. Equating $\tilde{\mathbf{u}}_{s,m,\theta}$, $\tilde{\mathbf{u}}_{c,m,\theta}$ from θ_m assumes no unbalance distribution within the module itself ($\tilde{\mathbf{u}}_m$, $\tilde{\mathbf{c}}_m$) which will not actually be the case. The resultant of these unbalances measured at the two bearings can be calculated from

$$\left|\tilde{\mathbf{u}}_{s,m}\right| = \tilde{f}_{m,\theta+m} + \tilde{r}_{m,\theta+m} - \left|\tilde{\mathbf{u}}_{s,m,\theta}\right| \tag{8.49}$$

and

$$\left|\tilde{\mathbf{u}}_{c,m}\right| = \tilde{f}_{m,\theta+m} x_f + \tilde{r}_{m,\theta+m} x_r - \left|\tilde{\mathbf{u}}_{s,m,\theta}\right| x_m \tag{8.50}$$

where x_f , x_r and x_m are the axial coordinates of the front bearing, the rear bearing, and the module centre of mass respectively. These values clearly represent the sum of the unbalances within the module, but do not reflect the distribution of that unbalance. It is recommended that some other data be used to the most likely distribution. Build alignment measurements can be used, or if some other knowledge of the module manufacture is known, the covariance method (section 8.2) can be used to determine the most likely distribution. In Schneider's method, it is suggested to correct this unbalance on the short mandrel, therefore the distribution will not be taken into account. This may not be a concern if the unbalance levels are small or the mode shape within the module is relatively straight (stiff). However if this is not the case, then this distribution must be considered. In a footnote, Schneider suggests that it may be appropriate to make this correction temporary, which would mean the module unbalance could be detected by its removal and some kind of unbalance distribution assumed.

Similarly to equations 8.42 and 8.43, the unbalance distributions are collectively defined as full rotor length unbalance and couple vectors by concatenation into column vectors $\tilde{\mathbf{u}}_{s,r,\theta}$ and $\tilde{\mathbf{u}}_{c,r,\theta}$ but with the inclusion of the unbalance distribution in the module ($\tilde{\mathbf{u}}_{s,m}$, $\tilde{\mathbf{u}}_{c,m}$) :

$$\tilde{\mathbf{u}}_{s,r,\theta} = \begin{bmatrix} \tilde{\mathbf{u}}_{s,m,\theta} + \tilde{\mathbf{u}}_{s,m} \\ \tilde{\mathbf{u}}_{s,t,\theta} \end{bmatrix} \tag{8.51}$$

$$\tilde{\mathbf{u}}_{c,r,\theta} = \begin{bmatrix} \tilde{\mathbf{u}}_{c,m,\theta} + \tilde{\mathbf{u}}_{c,m} \\ \tilde{\mathbf{u}}_{c,t,\theta} \end{bmatrix} \tag{8.52}$$

These unbalance distributions are then used in eq. 8.44, which gives the modal unbalance $\tilde{u}_{\omega}$ as before, but now with some account taken of the unbalance distribution within the module itself.

Step Three: Calculation of unbalance corrections

Balancing correction can be carried out in an identical fashion to that described in Schneider's method providing that no more than three planes of balancing corrections are assumed to be available in each module being balanced.

Step Four: Correction other modules

As with Schneider's method, the other modules are corrected in the same fashion.

8.3.4 Simulation of the 3 Plane Modular Balance / Dual Mass Simulator.

In the following demonstration a real engine WEM is used, where a pass off vibration issue has been identified. The engine rotor in question always fails the vibration test at a particular speed, so the optimisation is performed using a URF response at that speed. The rotor is a typical HP rotor as pictured in *Figure 15*. The unbalance response to a swashed rotor unbalance caused by a swash in the compressor joint face, with balance corrections applied using the normal full mass simulator correction method (As described in section 3.6.1), is shown below in *Figure 65*.

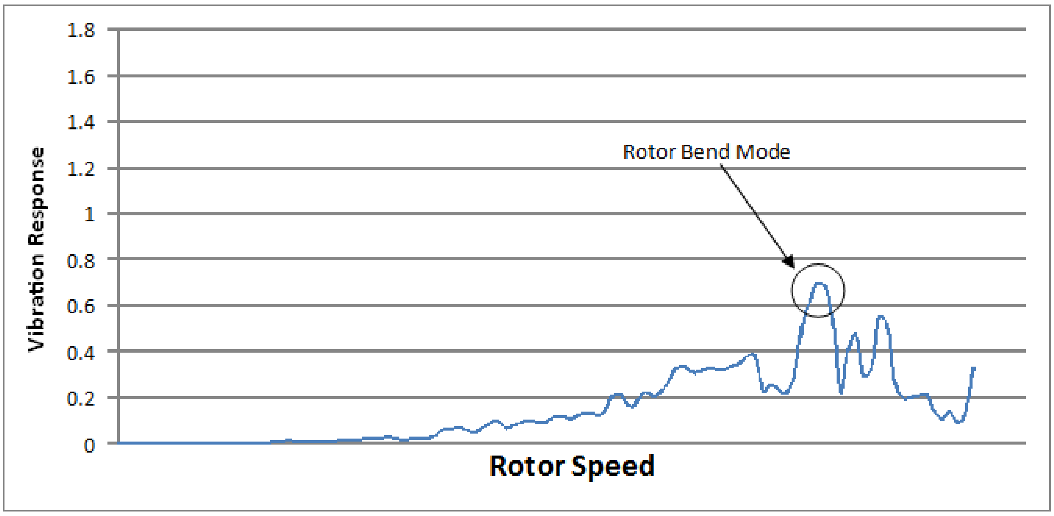

Figure 65: Engine response with rotor balanced using full mass simulator.

The vibration pass-off test failures are occurring at the speed of the first bend mode as indicated in the figure. The URF graph for this mode was generated and is shown in *Figure 66* below:

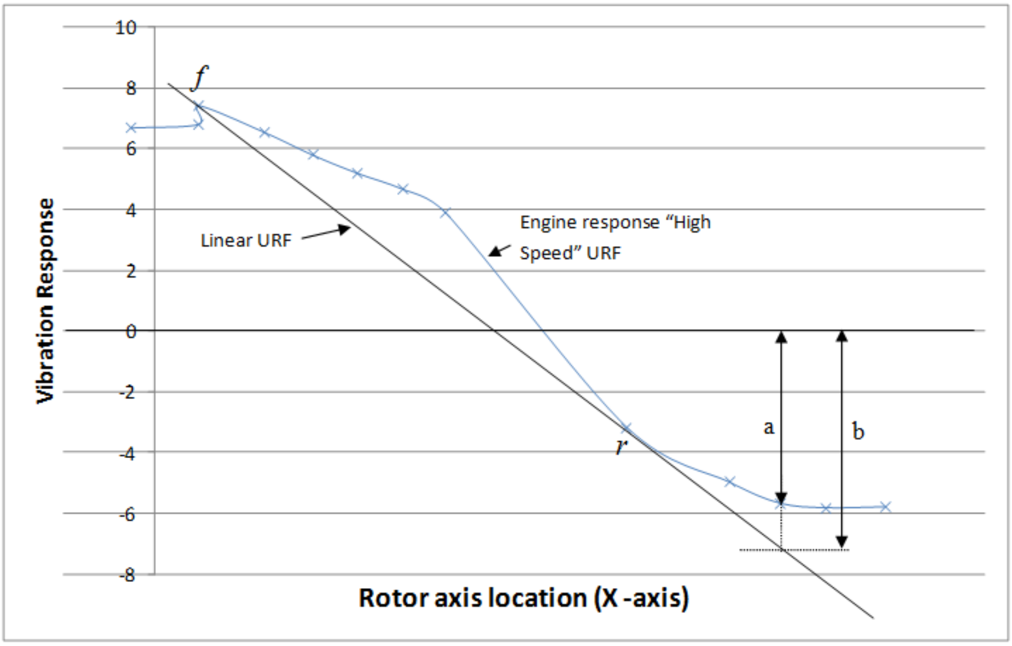

Figure 66: Unbalance Response Function (URF) graph for 1st bend mode at vibration sensor.

The topic of interpreting the URF graph is covered in detail in section 5.6. The front and rear correction lands for the compressor are labelled f and r. Initially the suitability of a scaled mass simulator was assessed from the graph. It can be seen from the graph that *b/a**100=120%. This indicates that the balancing machine will under predict the influence of unbalance at the centre of unbalance of the turbine at this rotor speed, so the appropriate turbine simulator would be approximately 120% mass. Prediction of scaled simulator properties is covered in more detail in section 5.9.

The balancing of the compressor was modelled using the WEM. The results are shown in Figure 67 below.

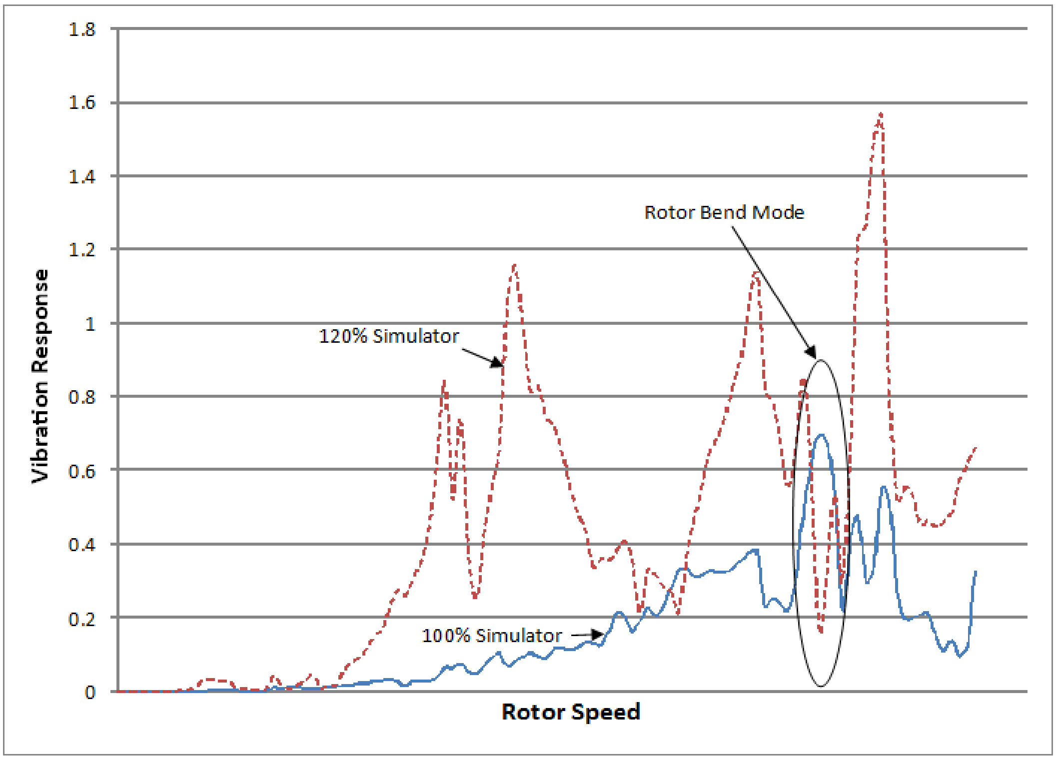

Figure 67: Compressor Balanced with 120% Mass Simulator vs 100% Mass Simulator

Here the red dashed line is the 120% simulator result and the blue solid line is the 100% simulator result. It can be seen that the 120% simulator has been beneficial at the speed where the URF was generated, but the benefits are outweighed by the increased vibration at the other speeds. Therefore a dual mass simulator approach with a three plane correction was modelled, and the results are presented in *Figure 68*:

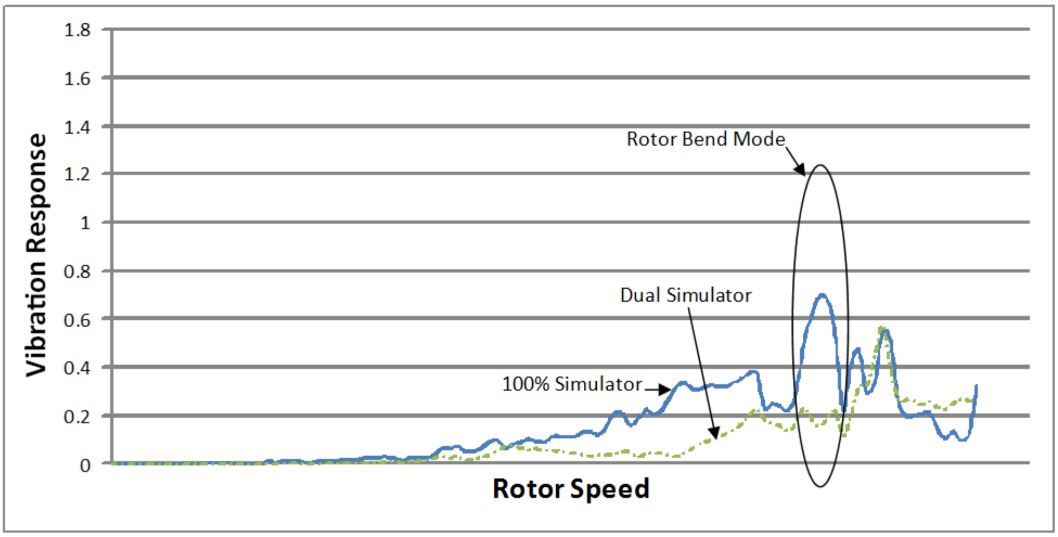

Figure 68: Compressor Balanced with 100% Mass Simulator vs Dual Mass Simulator

Here the blue solid line is the 100% simulator result and the green dash-dot line is the dual mass simulator with balancing in 3 planes. Clearly the approach was beneficial for the rotor bend mode and preserved the balancing of the lower speed rigid body rotor modes.

8.3.5 Modular Balancing Methods Conclusions

Using multiple balancing mass simulators during the low-speed modular balancing process can provide information on the distribution of unbalance in the rotor. This information can be utilised to significantly improve the balancing process vibration result in the engine. However, the use of multiple simulators can make the balancing process very time consuming, therefore the use of a “dual mass simulator” is proposed that will minimise the time impact of this more complex process. The dual mass simulator method takes into account the unbalance distribution within a module due to offsets of the modules component masses. A small enhancement to Schneider’s methodology can be performed to produce the equivalent effect. Therefore the outcome of the two methods with respect to balancing effectiveness is the same.

9 Thesis Conclusions and Further Work

9.1 Thesis Conclusions

The direction of customer requirements and the competitive marketplace for aerospace gas turbine engines have made the engineering challenge progressively greater for each new product. Little progress has been made in the subject area of low-speed balancing technology in recent years, however low-speed balancing is still necessary for turbomachinery in the aerospace industry.

An area that has moved on significantly in this period is the ability to create accessible finite element models of whole engines, however the capability of these models has not been significantly utilised in the areas of build and balancing and the related rotor design issues.

The focus of these studies has been on the development of a methodology for the reduction of the vibration response through making better use of the information practically (and inexpensively) available from the build and balance process and bring it together with the whole engine model. The Robust Rotordynamics Design System which was developed during these studies comprises a *design process* and set of *analytical tools* to facilitate this task.

The Robust Rotordynamics Design Process provides a rapid approach to evaluating the interdependent parameters of the rotor components, balancing methods and build methods to arrive at the optimum solution in terms of vibration performance and cost. Also introduced to facilitate this process is a set of rotordynamic design criteria that consider the duty of the rotor more widely and in greater depth than has previously been achieved in the early design stages of an engine. This is a critical requirement for an aero engine business to both avoid the cost of major redesigns, or the in-service costs of managing a non-robust engine.

The analytical methods developed here comprise two innovative tools, the unbalance response function (URF) graph and the rotor unbalance distribution Monte-Carlo dynamic simulation software. The URF graph is a design tool that can be used to very quickly inform the analyst of the most appropriate balancing, build and rotor design solutions that are likely to be successful. The Monte-Carlo software is used to test, investigate, and refine those solutions identified to determine the optimum method considering both cost and vibration performance. Demonstrations of these methods on whole engine models of real engine architectures were presented.

Although the Robust Rotordynamics Design System is primarily aimed at engine design, the process and analytical tools can be very effectively employed on existing products by focussing on build and balance methods which are relatively easy to change, even on production engines.

Because low-speed balancing is a cost-effective incumbent constraint on gas turbine turbomachinery, and low-speed balancing technology has not advanced significantly in recent years, methods to improve the performance of build and low-speed balance solutions have been explored extensively in this study. The “Unbalance Covariance Matrix” is a co-authored method introduced here where knowledge of the manufacturing/build process is combined with low-speed balancing information to compute the most probable unbalance distribution in the rotor. This information can then be used to guide the balancing process.

A “Dual Mass Simulator” invention relating to balancing tooling is also proposed as a fast and cost-effective method to gain information about a rotor’s unbalance distribution. A method of using the information gained to perform a modally effective low-speed three balance plane correction on a rotor module is described and modelled.

This thesis also introduced a theoretical mechanism by which a rolling element ball bearing under an axial “thrust” load might cause coupling between the 1st and 2nd integer harmonics of the rotor. Simplistic mathematical comparisons with some known data points was undertaken to quantify the magnitude of the effect in a real engine, which was shown significant.

9.2 Further Work

Much of the work in this thesis has focussed on the unbalance generated due to manufacturing tolerances and bolted joint alignment performance in gas turbine rotors. Particularly in respect of rotor joints, very little measured or predicted quantitative data is available to aid in the physical detailed design choices of joint with respect to alignment, such as the type (e.g. curvic coupling vs spigoted flange), fits that should be used, use of dowels, etc. A very significant area for future study is the alignment performance of rotor joints.

The generic topic of extracting “extra” information from the low-speed balancing process is worthy of further work. One area within this should be the exploration of perturbed boundary conditions on the balancing machine.

For modular balancing in particular, further work is recommended looking into the possibility of the application of slave weights to adjoining modules to enable balancing on adjoining modules that are not present during the balancing process.

The rotordynamic acceptance criteria proposed in this study will require benchmarking on real engines with known vibration performance histories before they can be fully utilised in industry.

In the use of the unbalance covariance matrix, further work is recommended to formally test (or prove) whether the best correction unbalance is always the one which negates the most likely unbalance distribution.

The hypothesised mechanical coupling between the 1st and 2nd integer harmonics of the rotor via a swashed thrust loaded bearing is worthy of further work to model the real mechanism in the bearing to prove or disprove the theory.

A space saving shaft mechanical fusing mechanism was also proposed during the course of this study and is presented in the Appendix. A significant area of further study would be to optimise the concept for particular engine architecture and perform a detailed design study/demonstration.

References

American Petroleum Institute. (1998). *API Specification 616: Gas Turbines for the Petroleum, Chemical and Gas Industry.* Washington, D.C.: American Petroleum Institute.

Birch, L. (2004). *Corporate Review of Gas Turbine Integral Vibration.* Derby: Rolls-Royce Internal Document.

Edwards, S., Lees, A. W., & Friswell, M. I. (2000). Experimental identification of excitation and support parameters of a flexible rotor-bearings-foundation system from a single run-down. *Journal of Sound and Vibriaton, 232(5)*, 963-992.

Ehrich, F. F. (1990). Pseudo-High Speed Balancing. *Transactions of the ASME, Journal of Engineering*, 418-426.

Foiles, W. C., Allaire, P. E., & Gunter, E. J. (1998). Review: Rotor Balancing. *Journal of Shock and Vibration*, pp. 325-336.

Friswell, M. I., Penny, J. E., Garvey, S. D., & Lees, A. W. (2010). *Dynamics of Rotating Machines.* New York: Cambridge University Press.

Garvey, S. D., Friswell, M. I., Williams, E. J., Lees, A. W., & Care, I. D. (2001). Robust Balancing for Rotoating Machines. *Proc. Instn Mech. Engrs, Part C, Journal of Mechanical Engineering*, (pp. 1117-1130).

Garvey, S. D., Williams, E. J., Cotter, G., Davies, C., & Grum, N. (2005). Reduction of Noise Effects for In Situ Balancing of Rotors. *Journal of Vibration and Acoustics*.

Gneilka, P. (1983). Modal balancing of flexible rotors without test runs – an experimental investigation. *Journal of Sound and Vibration, 90(2)*, 157-172.

Goodman, T. P. (1964). A Least-Squares Method for Computing Balance Corrections. *Transactions of the ASME, Journal of Engineering for Industry*, (pp. 273-279).

Gunter, E. J., Allaire, P. E., & Foiles, W. C. (2000). Balancing a 1150 MW turbine-generator. *Seventh International Conference on Vibrations in Rotating Machinery* (pp. 149-157). Nottingham: IMechE.

Herbert, R. G. (2000). When to high-speed balance large turbine generator rotors. *Seventh International Conference on Vibrtations in Rotating Machinery* (pp. 93-99). Nottinhgam: IMechE.

ISO11342. (1998). Mechanical vibration — Methods and criteria for the mechanical balancing of flexible rotors.

ISO1925. (2001). *Mechanical Vibration - Balancing - Vocabulary.* London: Bristish Standards.

ISO1940-1. (2003). *Mechanical vibration - Balance quality requirements for rotors in a constant (rigid) state - Part 1: Specification and verification of balance tolerances.* British Standards (BSi).

ISO1940-2. (1997). Mechanical vibration - Balance quality requirements of rigid rotors - Part 2: Balance errors.

Jiffri, S., Garvey, S. D., & Rix, A. I. (2009). Enriching balancing information using the unbalance covariance matrix. *Proceedings of the Institution of Mechanical Engineers, Part C: Journal of Mechanical Engineering Science* (pp. 1815-1826). London: Professional Engineering Publishing.

Kang, Y., Sheen, G. J., & Wang, S. M. (1997). evelopment and modification of a unified balancing method for unsymmetrical rotor-bearing systems. *Journal of Sound and Vibration, 199(3)*, 349-368.

Kumar, B. V. (2005). Correlation Pattern Recognition. p. 119.

Lees, A. W., & Friswell, M. I. (1997). The evaluation of rotor unbalance in flexibly mounted machines. *Journal of Sound and Vibration, 208(5)*, 671-683.

Liu, S. (2005). A modified low-speed balancing method for flexible rotors based on holospectrum. *21 (2007)*, pp. 348-364. Mechanical Systems and Signal Processing.

Lund, J. W., & Tonnesen, J. (1972). Analysis and Experiments on Multi-Plane Balancing of a Flexible Rotor. *Transactions of the ASME, Journal of Engineering for Industry*, (pp. 233-242).

Mahalanobis, P. (1936). On the Generalized Distance in Statistics. *National Institute of Sciences of India*, (pp. 49-55).

Parkinson, A. G. (1991). Balancing of Rotating Machinery. *Proc. Instn. MEch. Engrs, PArt C, Journal of Mechanical Engineering Science*, (pp. 53-66).

Richardson, M. H. (2000, January). *Modal Mass, Stiffness and Damping.* Retrieved 01 02, 2015, from www.systemplus.co.jp: www.systemplus.co.jp

Schneider, H. (1988). Balancing of Jet Engine Modules. *Vibrations in Rotating Machinery* (pp. 523-530). London: IMechE.

Schneider, H. (1991). *Balancing Technology.* Heppenheim: Schenck.

Schneider, H. (2000). Exchangeability of rotor modules - a new balancing procedure for rotors in a flexible state. *Seventh International Conference on Vibrations in Rotating Machinery* (pp. 101-108). IMechE.

Schwartz, B. J., & Richardson, M. H. (1999, October). Introduction to Operating Deflection Shapes. *CSI Reliability Week, Orlando, Florida*. Jamestown, California, USA: Vibrant Technology Inc.

Smith, S. P. (2000). 'The balancing act' - balance for design, or design for balance? *Seventh International Conference on Vibrations in Rotating Machinery* (pp. 109-119). Nottingham: IMechE.

Stephenson, W. J., Grogan, T. A., Rost, R. W., Alleman, R. J., & Brown, D. L. (1992). Neural nets in rotor balancing. *Intelligent Engineering Systems through Artificaial Neural Networks*, pp. 791-796.

Tonnesen, J. (2003). Jorgen W. Lund: Theories Versus Tests, Part 1: Balancing and Response of Flexible Rotors. *Transactions of the ASME, Journal of Engineering for Industry*, (pp. 482-488).

Wang, X., Zhang, B., Zhang, D., & Ma, X. (1998). Application of artifical neural networks in rotor balancing. *Society of Electrical Engineering*, *18(4)*, pp. 262-266.

Watson, S. H. (2000). *Whole Engine Mechanical Model Group (Civil) Analysis Guidelines*

Critical Speed & Steady State Forced Response Calculations. Derby: Rolls-Royce Internal Document.

Werner, U. (2011). *Optimized rotor design for rigid balancing of large flexible induction rotors.* Institute of Electrical and Electronics Engineers.

Xu, B., & Qu, L. (2001). A New Practical Modal Method for Rotor Balancing. *Proc. Instn. Mech. Engrs., Part C, Journal of Mechanical Engineering Science*, (pp. 179-189).

Xu, B., Qu, L., & Sun, R. (200). Optimisation Technique-Based Balancing of Flexible Rotors Without Test Runs. *Journal of Sound and Vibration, 232*, 963-992.

Zhu, X., & Wang, X. (1995). Method of balancing largescale flexible rotors without test runs. *ASME International Gas Turbine and Aeroengine Congress and Exposition, 5–8 June.*, (pp. Paper 95-GT-363). Houston, Texas.

Appendix:

Management of Fan Blade-Off Loads – A Novel Fusing Method

Summary

During the investigations carried out as part of this study, a related invention for the management of unbalance loads due to fan blade loss was conceived and developed to the point presented here.

Fan Blade-Off Background

A fan blade-off (FBO) event at high engine speeds is one of the most severe mechanical tests of an engine. If a fan blade is released, it must be contained within the engine structure and the engine must run down without hazard to the aircraft or releasing any large mass components. Loss of a fan blade creates a very large out-of-balance force that causes excessive vibration which would lead to rapid mechanical failure of the engine structure and mounts if unmanaged. The current practice is to place radial mechanical fuses in the bearing structural load paths, such that the loads from the fan blade release break the fuses and release the shaft from the bearings. After fusing, the rotor is effectively supported by very low radial stiffness and has a large radial clearance. The new stiffness moves the first rigid body mode of the rotor to a very low frequency which allows the rotor to behave super-critically (above resonance) and rotate around its mass centre (rather than its geometric centre) during run-down. Without the driving force from combustion, the kinetic energy of the shaft is dissipated through contact with the casing and friction, coming down to windmill speed in typically around 10 seconds. Windmilling occurs once aerodynamic loads driving fan rotation equal the frictional loads, causing steady speed operation that may need to be sustained over several hours of flight. The engine is often operating at or near 100% speed when FBO occurs, and must pass through several resonances to slow down to windmill speed. A slow deceleration allows time for resonances to build.

Description and Effects of Proposed Mechanism

It is proposed that instead of radial fuses, the fuse could be incorporated into the shaft, such that the breaking of the fuse leads to the shaft being converted into a universal coupling. Torsion of the fan relative to the shaft would be restrained by a splined feature of the universal coupling. This mechanism would allow the fan and fusing shaft to precess about the main shaft axis, possibly allowing it to come into contact with the structures behind (possibly vanes or purpose built snubbers) and causing more rapid deceleration. The faster deceleration gives the resonances less time to build, reducing run-down loads due to resonances; however, this must be balanced against the torque transferred into the structure due to high deceleration which could fail engine mounts. The invention allows run-down blade meshing[5] to be tuned through a combination of the position of the “hinge” point on the fuse, a bump stop, and a facility for the fuse to allow some forward movement of the fan. Furthermore, the mechanism would allow significantly more scope for tuning resonances to the less vital operation speeds (i.e. away from windmilling speed) due to the ability to choose the position of the coupling hinge point axially, allowing variability of gyroscopic stiffening effects, as well as the stiffness of the supporting spring. It also caters for architectures of engines where traditional fusing may not be possible, such as geared turbofans.

---

[5] Blade meshing is where the blades are allowed to contact the stator vanes as a method of aiding deceleration of the rotor.

Windmilling is a significant design case that causes considerable design issues. The aircraft will have to endure windmill loads for many hours, making it the defining fatigue case for many components. The traditional arrangement with the slow fan speed combined with the rotor now resting on “broken” fuses means that after run-down the system becomes sub-critical and transmits significant vibration. Smoother windmilling should be possible with the proposed configuration. Because of the geometry proposed in the shaft, the fuse-released mass is significantly smaller. This may allow springs that are stiff enough to support the rotor mass under gravity, while still being soft enough to allow the supercritical behaviour that reduces run-down resonances. There may be a weight saving associated with having a single fuse rather than fuses at multiple bearings. This fuse is also expected to be more predictable than the existing bearing fuses because the shaft is of uniform stiffness, therefore the fuse shear pins are mounted in a predictable axisymmetric stiffness. This is in contrast to the engine structure which has extremely variable stiffness around its circumference, with spoke structures and asymmetric engine mounting points.

Features

The arrangement, as shown in *Figure 69*, contains a fusing shaft that joins the fan to the main shaft, via a spherical bearing. In normal operation the shear mechanism is fixed and the spherical bearing is inactive. It may however be used to carry torque, using axial fluting (splines) in the spherical bearing. An additional feature is the bump stop at the end of the main shaft. This is used to restrict the angle the fusing shaft and fan can rotate through, as seen in *Figure 70*.

It is proposed to include springs between the main shaft and fusing shaft, as shown in *Figure 69*. These are intended to support the rotor weight at windmill speed, whilst keeping the rotor supercritical during run-down.

In the main design proposed here, any shear fusing mechanism would need to release the spherical bearing to move in all radial directions, not just in the direction that the shear was achieved. Many mechanisms could be created to achieve this. One such mechanism is given in *Figure 71*, where a cross section of *Figure 69* is given at the shear mechanism. Three shear pins are held in place by springs under tension that are connected to each other at the shaft centreline. If one shear pin is sheared the head of the pin would no longer react the tension of the spring and the other two springs would lose tension and their pins would be free to move outward under centrifugal force.

A further modification could be made to allow the fan to pull forwards a short distance at FBO. This would allow greater control over the blade contact points and the dynamics of the precessing fan, and greater clearance around the blade tips.

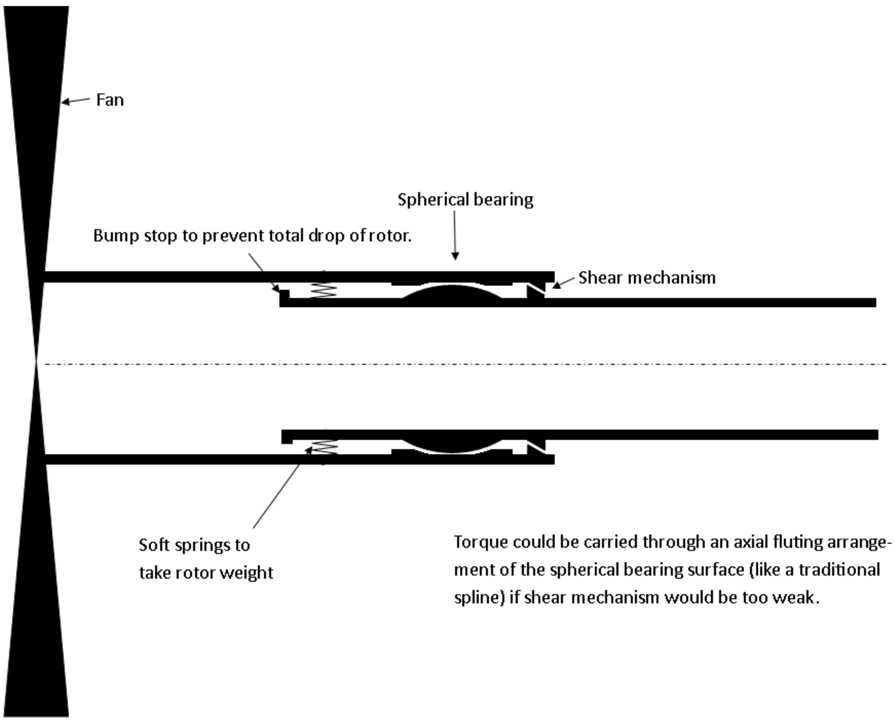

Figure 69: Schematic of proposed fusing mechanism.

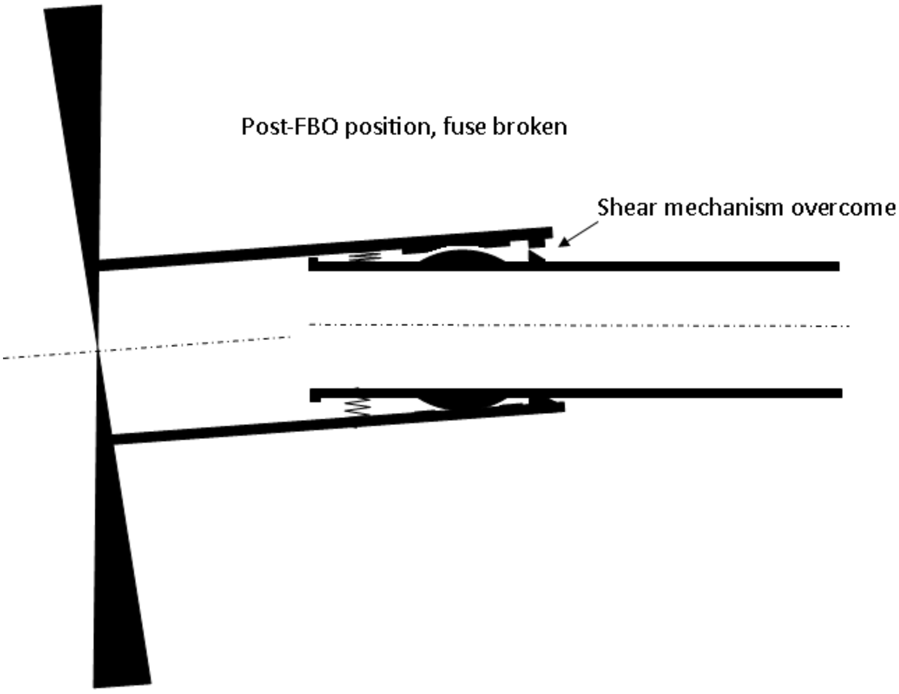

Figure 70: Schematic of mechanism after FBO, with fan and fusing shaft rotated away from the centreline.

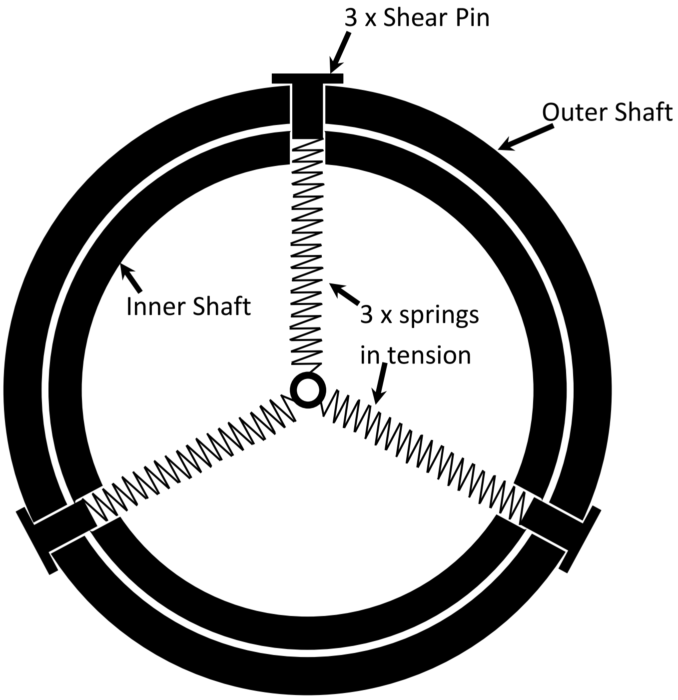

Figure 71: Possible shear fuse mechanism